THE NUCLEAR STRUCTURE OF ^{151}Sm

THE NUCLEAR STRUCTURE OF ^{151}Sm

by

DEWART ERLE NELSON, B.Sc.

A Thesis

Submitted to the Faculty of Graduate Studies

in Partial Fulfilment of the Requirements

for the Degree

Doctor of Philosophy

McMaster University

November 1972

DOCTOR OF PHILOSOPHY (1972)
(Physics)

McMASTER UNIVERSITY
Hamilton, Ontario

TITLE: The Nuclear Structure of ^{151}Sm

AUTHOR: Dewart Erle Nelson, B.Sc. University of Saskatchewan

SUPERVISOR: Dr. D. G. Burke

NUMBER OF PAGES: viii, 132

SCOPE AND CONTENTS:

An experimental study of the low-lying levels of the nucleus ^{151}Sm has been made using the single particle transfer reactions 1) $^{152}Sm(d,t)^{151}Sm$, 2) $^{152}Sm(^{3}He,\alpha)^{151}Sm$, 3) $^{150}Sm(d,p)^{151}Sm$, 4) $^{151}Sm(d,p)^{152}Sm$, 5) $^{151}Sm(d,t)^{150}Sm$ and 6) $^{151}Sm(^{3}He,\alpha)^{150}Sm$. Also, inelastic scattering and Coulomb excitation experiments were performed on targets of ^{151}Sm. The information obtained from these experiments when combined with the results of previous studies of the decay of ^{151}Pm, has allowed definite spin and parity assignments to be made for about 15 levels in ^{151}Sm, and has put limitations on the possible assignments for several others. The level scheme obtained is compared with the predictions of the Nilsson model, including the effects of Coriolis and $\Delta N=2$ mixing.

ACKNOWLEDGEMENTS

I am very grateful to Dennis Burke, my supervisor, for his capable direction of the experimental program which is the subject of this thesis. His continuing interest and his many suggestions and criticisms have been essential to this work.

Jim Waddington has also made a large contribution to this study, particularly in the attempts made to interpret the data within the framework of existing models. Furthermore, the results of his work together with Brian Cook on the decay scheme of ^{151}Pm have been very useful.

I should also like to thank Jack Tippett and Bob O'Neil for providing the DWBA and Coriolis coupling computer programs, and for the many hours of help they have unreservedly given me. Bob Gadsby's help with some of the experiments is also appreciated.

Phil Ashbaugh and his staff deserve much credit for providing excellent experimental facilities and for maintaining a very congenial atmosphere in the laboratory.

Drs. R. Summers-Gill and R. Bell have spent several hours on my behalf as members of my supervisory committee.

Helen Kennelly, Eileen Stewart and Gitte Nelson have managed to put this thesis into its final form. That was no small task.

Finally, I should like to thank the over-burdened Canadian tax-payer who has made this work possible.

TABLE OF CONTENTS

LIST OF FIGURES

LIST OF TABLES

CHAPTER I

INTRODUCTION

1.1 Some general remarks on the problem

Our inability to solve many-body problems and our limited understanding of inter-nucleon forces has meant that theoretical descriptions of nuclei have been restricted to the construction of models. The most successful of these has been the shell model, in which nucleons are considered to move independently in orbits defined by some common average potential. In other words, the force on a nucleon as derived from this average potential approximates its interaction with all other nucleons in the nucleus.

In some regions of the periodic table (in particular those nuclei with nucleon numbers at or near the so-called magic numbers), the nuclei appear to be spherical in shape and the potential used in these shell model calculations is isotropic. On the other hand, nuclei with proton or neutron numbers far from the magic numbers, in particular those in the rare earth and actinide regions of the periodic table, have large permanent deformations. Evidence for this is found in the appearance of rotational bands in their low-lying level spectra, and the large measured quadrupole moments of these levels.

In adapting the shell model to nuclei with such large

deformations, one may make the approximation that the shape is stable, and that rotations of the nucleus as a whole are sufficiently slow that they do not disturb the orbital motions of the individual nucleons in the nucleus. When this adiabatic approximation has been made, the nucleon orbits may be calculated in the same manner as for the spherical cases, except that the potential used is non-isotropic. This model (generally known as the Nilsson model) has given good descriptions of an impressive number of nuclear properties; its successes are so well known they need not be further discussed here.

For nuclei in which the deformation is less well developed, it is not clear that the intrinsic particle motions will be independent of the rotational motions, and one might expect very complicated nuclear spectra to result. Behaviour of this sort would be most evident in the case of nuclei with odd numbers of neutrons and/or protons, as these nuclei have low-lying particle states at about the same energies as the rotational states.

The onset of deformation may occur very rapidly as one adds nucleons to a nucleus. A prime example of this occurs at neutron number N = 89. Figure 1 shows the low-lying spectra of the N = 88 and N = 90 isotopes $^{150}_{62}Sm_{88}$ and $^{152}_{62}Sm_{90}$, as taken from the compilation of Lederer et al (1968). For ^{150}Sm, the 0^+, 2^+, 4^+ triplet at twice the first 2^+ energy typify the vibrational excitations of a spherical nucleus, while

Figure 1.

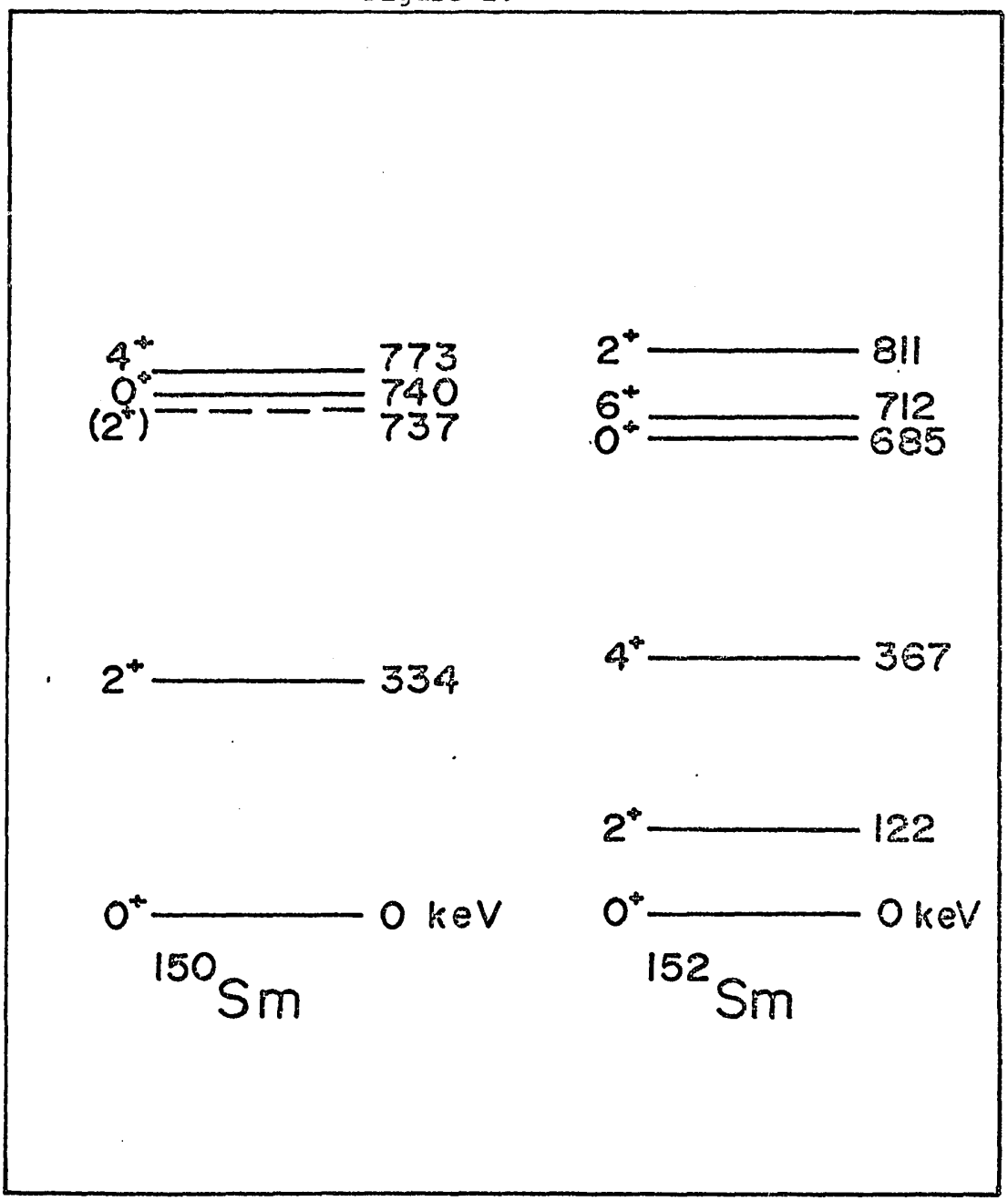

Low-lying level spectra of ^{150}Sm and ^{152}Sm.

in ^{152}Sm, the low lying 0, 2, 4, 6^+ levels form the ground state rotational band characteristic of a well deformed nucleus. One might then expect that the nucleus ^{151}Sm, lying between these two, will exhibit characteristics of a semi-deformed nucleus and will perhaps not be well described by the adiabatic Nilsson model.

Recently, the applicability of the Nilsson model to nuclei in this shape-transition region has been tested by various researchers. For example, Borggreen et al. (1969) have shown that the positive parity levels in ^{155}Gd are well described by the adiabatic Nilsson model if the calculations include Coriolis and $\Delta N = 2$ mixing. (These effects are described in a following section.) A similar study of an isotone of ^{151}Sm, namely ^{153}Gd, has shown that the positive parity levels in this nucleus may be qualitatively described by the Nilsson model, but quantitatively the agreement is not as good as for ^{155}Gd (Løvhøiden et al. (1972)). In this work, it was postulated that deviations from a pure rotational model were present. It would be of interest to determine whether the Nilsson model with $\Delta N = 2$ and Coriolis effects included is capable of describing the spectrum of levels of ^{151}Sm.

The experimental information that is available on ^{151}Sm comes mostly from studies of the decay of ^{151}Sm (e.g. Burke et al. (1963), Bertelsen et al. (1964)). While a great number of low-lying energy levels have been established in ^{151}Sm, until recently spins and parities for none of the levels had been

established. Two single-particle reactions had been performed leading into this nucleus: 1) $^{150}Sm(d,p)^{151}Sm$ (Kenefick et al. (1965) and 2) $^{152}Sm(d,t)^{151}Sm$ (Tjøm, 1968), but not too much detailed information was obtained from these.

The experimental program that is the subject of this thesis was centered around a series of single particle transfer reactions, inelastic scattering experiments and Coulomb excitation experiments. A list of the experiments performed, and the reasons for doing these experiments is as follows:

1) $^{151}Sm(d,d')^{151}Sm$ and ^{151}Sm Coulomb excitation

In general, inelastic scattering and Coulomb excitation processes tend to populate levels closely resembling the ground state of a target nucleus. In odd mass deformed nuclei, the first two excited members of the rotational band based on the ground state are populated strongly. If ^{151}Sm were deformed, these experiments would be expected to indicate which of the many low-lying excited states in this nucleus belong to the ground state rotational band.

2) The reactions $^{150}Sm(d,p)^{151}Sm$, $^{152}Sm(d,t)^{151}Sm$ and $^{152}Sm(^3He,\alpha)^{151}Sm$

These single particle reactions transfer a neutron into or out of the target nucleus. The (d,p) reaction therefore tends to populate low-lying particle states in the final nucleus, while the (d,t) and (^{3}He,α) reactions tend to populate the hole

states. For the case of single neutron transfer reactions leading into ^{151}Sm, a further differentiation between the states populated in the stripping and pick-up reactions must be considered. It has been suggested (Kenefick et al. (1965)) that the level spectrum of ^{151}Sm may contain levels due to both spherical and deformed nuclear configurations. The (d,p) reaction (on the spherical nucleus ^{150}Sm) would, according to this suggestion, tend to populate the spherical levels in ^{151}Sm, while the (d,t) reaction on the deformed nucleus ^{152}Sm would populate the deformed levels. As mentioned above, reports on these two reactions have been published. It was decided to repeat these experiments as targets of exceptionally high purity were available, and it was also possible that better resolution would be achieved. Also, angular distributions could be obtained for the (d,t) experiment. These distributions are often sufficiently distinctive as to yield the ℓ-value of the transferred particle, therefore determining the parity of the level and restricting the possible spin values to either $\ell+1/2$ or $\ell-1/2$.

The reaction $^{152}Sm(^{3}He,\alpha)^{151}Sm$ also removes a neutron from the target nucleus, and in this respect is no different than the corresponding (d,t) reaction. But $(^{3}He,\alpha)$ reactions favour population of states in which large ℓ-transfers are involved, contrary to (d,t) reactions, which favour low ℓ-transfers. The two reactions thus complement each other nicely,

as one will populate levels of high spin and the other levels of low spin. Also, the ratio of the intensity of a level populated in the (^{3}He,α) reaction to that of the same level populated in the (d,t) reaction gives a second, independent means of determining the ℓ-transfer to that level.

3) The reactions ^{151}Sm(d,t)^{150}Sm, ^{151}Sm(^{3}He,α)^{150}Sm and ^{151}Sm(d,p)^{152}Sm

These reactions on the target nucleus ^{151}Sm may yield information on the ground state wave function for ^{151}Sm. The predicted cross-sections for states of known configuration in the final nuclei depend on the wave function of the target nucleus.

During the course of this work, two other groups of researchers at this laboratory undertook experiments on ^{151}Sm. Robertson et al. (1971) have measured the ground state spin using a paramagnetic resonance technique. A second group has undertaken a complete re-examination of the decay scheme of ^{151}Pm, using very high resolution Ge(Li) detectors and coincidence techniques (Cook et al., private communication). This same group has also studied the decay of an isomeric state in ^{151}Sm. The information available from these other researchers has been most useful, and reference is made to their studies throughout this report.

CHAPTER II

THEORETICAL BACKGROUND

2.1 Nilsson model

In the shell model description of spherical nuclei, the force on a nucleon is derived from an average isotropic potential. The orbitals of a particle in such a potential well are calculated, and nucleons filled into these orbitals. In the extreme single particle model, it is assumed that the properties of an odd mass nucleus are given by the characteristics of the orbit of the last nucleon; that is to say, the first A-1 nucleons form an inert core to which the last nucleon is coupled. This model is extended to greater degrees of complexity by putting fewer of the A particles into the inert core and considering the effects of "residual" interactions between the valence nucleons that are coupled to this core. These residual interactions tend to distribute the actual nuclear wave function over many of the calculated single particle orbitals; nuclear states so described are said to be "configuration mixed".

For a deformed nucleus, rotations of the nucleus as a whole can take place. The intrinsic orbitals in such a deformed nucleus are calculated in much the same manner as for spherical nuclei, except that the potential from which the force on a nucleon is derived is non-isotropic. In this case,

the intrinsic spin J of the nucleus (ie. the spin of the nucleus as measured in a system of axes fixed to the nucleus) is not constant, and the total nuclear spin I (which is of course conserved) consists of a vector sum of the intrinsic spin and the rotational spin. For a nucleus with one axis of symmetry (defined as the 3-axis) the diagram below gives the angular momentum coupling scheme

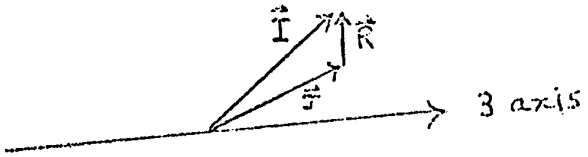

The vector $\vec{R}$ describes the rotation of the nucleus as a whole (which has no component along the axis of symmetry) and the total spin $\vec{I}$ is given by

$$\vec{I} = \vec{J} + \vec{R} \ .$$

The projections of $\vec{I}$ and $\vec{J}$ on the 3-axis are constants of the motion and are equal, if the nucleus has an axis of symmetry, and are labelled K.

The Hamiltonian for the system may be written

$$H = T_r + H_{int} + H_c$$

where T_r describes the rotational energy of the system, H_{int} gives the intrinsic energy, and H_c in some way describes the influence of the rotations on the intrinsic orbits. (There is much confusion about the nature of H_c as the rotational kinetic

energy T_r also contains a term which in effect couples the rotation of the nucleus and the intrinsic states, as is shown below). If one is to calculate intrinsic orbitals using a potential of given deformation, then it follows that the particle orbital motion must be very rapid compared to the rotational motion of the nucleus itself. If this adiabatic condition holds, then one may use the shell model approach with a fixed potential; H_c is small and may be neglected.

The term T_r may be written as

$$T_r = \frac{1}{2}\hbar^2 \sum_{x=1}^{3} \frac{R_x^2}{\mathcal{I}_x}$$

where $\mathcal{I}_x$ is the moment of inertia of the system along the x axis. For a nucleus with one axis of symmetry, and using the relation $\vec{R} = \vec{I}-\vec{J}$, this becomes

$$T_r = \frac{\hbar^2}{2\mathcal{I}} \{I^2+J^2-2I_3^2 - 2(\vec{I}\cdot\vec{J}-I_3J_3)\} .$$

The last term couples the rotational and intrinsic spins in a manner analogous to the classical mechanical Coriolis force, and is given the name Coriolis coupling.

The term J^2 involves only intrinsic coordinates and may be conveniently buried in the intrinsic part of the Hamiltonian. The total Hamiltonian may then be written

$$H = \frac{\hbar^2}{2\mathcal{I}} \{I^2-2I_3^2-2(\vec{I}\cdot\vec{J}-I_3J_3)\} + H'_{int} \quad (H_c=0)$$

Apart from the Coriolis term, an eigenfunction of this Hamiltonian is

$$\psi^I_{MK} = D^I_{MK}\ \phi^K_{int}$$

where D^I_{MK} (the standard rotational D function) and ϕ^K_{int} are defined by

$$I^2 D^I_{MK} = I(I+1) D^I_{MK};\ I_3 D^I_{MK} = K D^I_{MK} \quad \text{and} \quad H'_{int}\ \phi^K_{int} = E_{int} \phi^K_{int} .$$

The total energy of a nuclear state, neglecting the Coriolis term, is then

$$E_T = E_{int} + \frac{\hbar^2}{2\mathcal{J}} [I(I+1) - 2K^2] .$$

If the total intrinsic energy E_{int} may be subdivided into the energy of the nucleus in its ground state plus the energy of the excited state .

$$E_{int} = E_{g.s.} + \varepsilon_i$$

then one may write an expression for the energy of a member of a rotational band as measured with respect to the ground state, which is in practise what is measured in experiments

$$E^I_K = \varepsilon_i + \frac{\hbar^2}{2\mathcal{J}} \{I(I+1) - 2K^2\}.$$

In the shell model formulation, excited states may result from the transfer of a nucleon from one orbital to another, and thus in these cases the excited state energy ε_i above may be calculated from the Nilsson model.

Following the original calculations of Nilsson (1955) the intrinsic orbitals in this model are determined as follows: the nuclear radius is given by the expansion

$$r = r_o (1 + \beta_2 Y_{20})$$

where β_2 gives the deformation and Y_{20} is a spherical harmonic If one assumes that the equipotential surfaces are deformed in the same way as the nuclear surface itself, and one chooses the harmonic oscillator for the form of the potential, the particle Hamiltonian is given by

$$H_i = \frac{p^2}{2m} + \frac{1}{2} m\omega_o^2 r^2 (1-2\beta_2 Y_{20}) + C\vec{\ell}\cdot\vec{s} + D\vec{\ell}\cdot\vec{\ell}$$

where the last two terms are introduced to reproduce the spherical shell model calculations in the limit $\beta_2 = 0$.

The eigenstates are calculated using as basis vectors the set of eigenvectors of the isotropic harmonic oscillator

$$\psi_K = \sum_{j\ell} C_{j\ell}\, \phi_{N\ell j}$$

where ψ_K is the deformed intrinsic orbital and $\phi_{N\ell j}$ the set of basis vectors. The expansion coefficients $C_{j\ell}$ characterize the individual orbitals thus calculated. These orbitals are labelled by the quantum numbers which describe the system at an asymptotically large deformation. These labels are written $K\pi[Nn_3\Lambda]$. Here π and N are the parity and major oscillator number, while K and Λ are the projections on the 3-axis of I and the orbital angular momentum ℓ, respectively. The quantum number n_3 refers to the number of oscillator quanta along the symmetry axis.

Lists of wave functions and energies for these orbitals have been tabulated in convenient form (eg. Chi (1967)) and include diagrams of the energies of the orbitals as a function

of deformation (the so-called Nilsson diagram). An example of such a diagram is given in Figure 2. This is the appropriate diagram for Nilsson model neutron orbitals for $82<N<126$, and thus is applicable to a study of ^{151}Sm. The original calculations (Nilsson (1955)) did not include the effects of mixing between orbitals of major quantum numbers N differing by two units, as these effects were shown to be small, even for certain N = 4 and N = 6 orbitals which were expected to lie very close in energy. It has since been found that the interaction between these orbitals can indeed be significant (c.f. Kanestrøm et al. (1971)).

The single particle energies calculated from this model must be modified to include the effects of pair correlations of the nucleons. (The application of pairing theory to nuclei is reviewed by Nathan and Nilsson (1965). Here, just the results which are of importance to this work are mentioned.) The pairing theory defines a definite probability V^2 that a given orbital will be occupied by a pair of nucleons. The probability of finding the orbital empty is U^2, and, of course $U^2+V^2 = 1$. Unpaired nucleons occupy definite orbitals (ie. the probability of finding the odd nucleon in a given orbital is unity). The observed single particle excitation energy relative to the energy of the ground state is given by

$$\varepsilon_{q.p} = \sqrt{(\varepsilon_i-\lambda)^2+\Delta^2} - \sqrt{(\varepsilon_{g.s.}-\lambda)^2+\Delta^2}$$

Figure 2

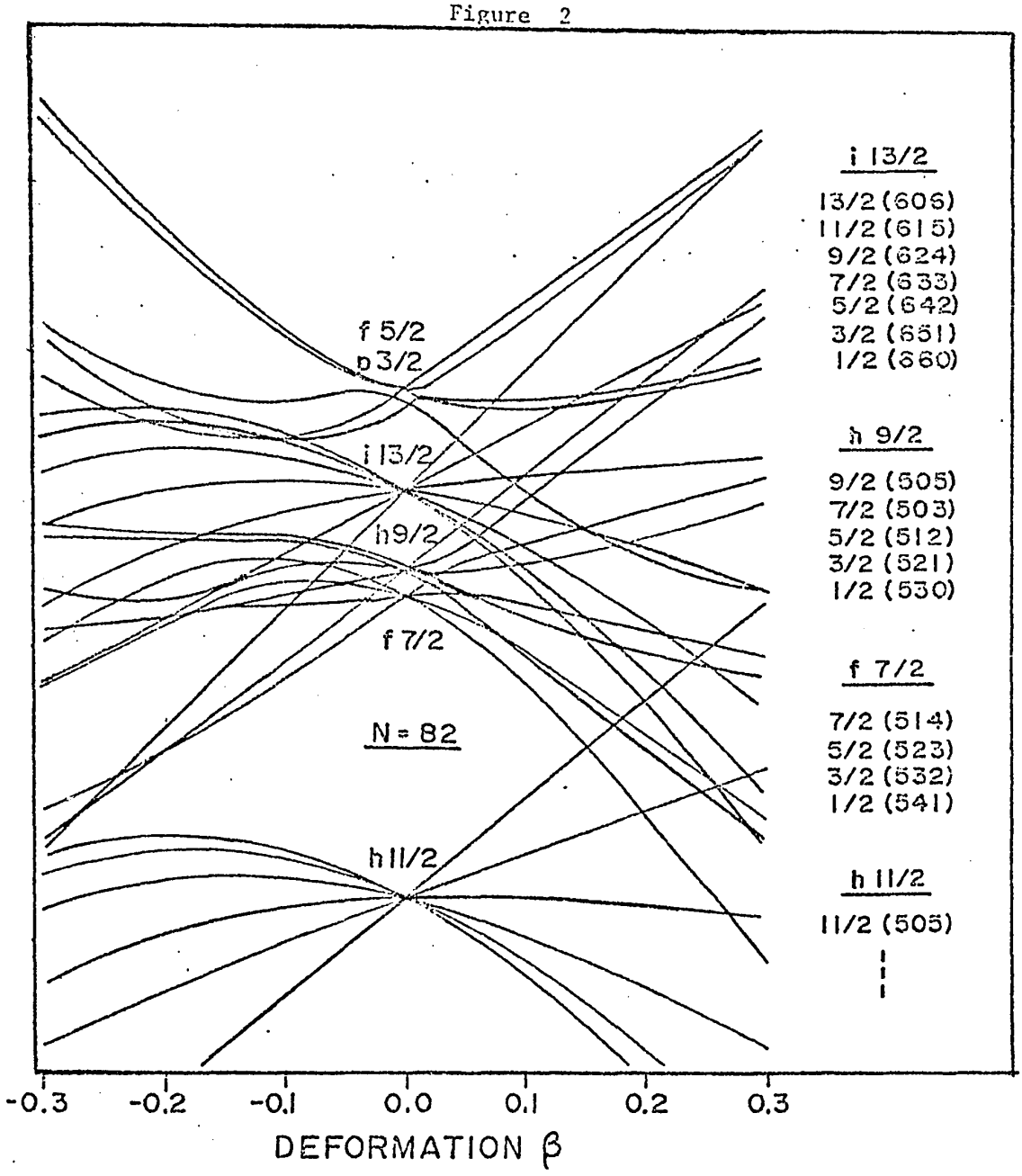

Nilsson diagram for neutrons in the N = 89 region.
The orbitals of interest to this study are listed on the right.

where ε_i and $\varepsilon_{g.s}$ are the Nilsson single particle energies for the excited state and ground state. The parameter λ gives the Fermi energy of the nucleus, and Δ is a measure of the pairing strength. The effect of the pairing force is to lower the energies of the single particle levels with respect to the ground state.

The Coriolis term, which has been neglected up to now, may be shown to mix states for which the K numbers differ by one unit (eg. Kerman (1956)). The eigenfunctions of the complete Hamiltonian may be written as sums of the functions ψ_K.

The effects of both the Coriolis term and the $\Delta N=2$ coupling may be determined by constructing and diagonalizing a new energy matrix, in which the diagonal terms are

$$E = \varepsilon_{q.p.} + \frac{\hbar^2}{2\mathcal{J}} \{I(I+1)-2K^2+\delta_{K\frac{1}{2}}\, a(-1)^{I+\frac{1}{2}}(I+\tfrac{1}{2})\} .$$

The off-diagonal Coriolis terms are given by

$$\langle \psi_I^K | V_{Coriolis} | \psi_I^{K+1} \rangle = \frac{\hbar^2}{4\mathcal{J}} \sqrt{(I-K)(I+K+1)}\ \ (U_K U_{K+1}+V_K V_{K+1}) \times$$

$$\sum_j C_{j\ell}^K C_{j\ell}^{K+1} \sqrt{(j-K)(j+K+1)} .$$

It turns out that the calculation of the $\Delta N=2$ elements is extremely sensitive to the form of the potential used, and the usual procedure is to use empirical values for these elements.

The Nilsson model has given very good predictions for

the properties of a large number of nuclei, and one must conclude that in such cases the adiabatic assumption made at the outset is certainly valid. Complete Nilsson calculations which include Coriolis and $\Delta N=2$ mixing have shown that this model can also describe levels in nuclei near the shape transition region even though these levels do not exhibit the $I(I+1)$ rotational spacings characteristic of deformed nuclei, (eg. the positive parity levels in ^{153,155}Gd).

An empirical modification to the rotational model has been proposed which to a certain extent provides a smooth transition between the spherical and deformed nuclear models (Mariscotti et al. (1969)). In this model, the moment of inertia of the nucleus is considered variable, and the energy of an excited band member is given by

$$E_I = \frac{\hbar^2}{2} C(\mathcal{J}_I - \mathcal{J}_o)^2 + \frac{\hbar^2}{2\mathcal{J}_I} I(I+1).$$

Here, the moment of inertia $\mathcal{J}_I$ is a function of the total spin I, and C is a "restoring force constant". A "softness parameter σ is defined as

$$\sigma = \frac{1}{\mathcal{J}_I} \frac{\partial \mathcal{J}_I}{\partial I}$$

and in effect is a measure of the extent to which the rotational motion is adiabatic, ie. for $\sigma = 0$, $\mathcal{J}_I = \mathcal{J}_o$ and the motion is completely adiabatic. In this model, when $\sigma > 0$, the rotational and intrinsic motions would not be independent.

This model has been shown to give extremely accurate predictions for the energies of the excited levels of not only

well deformed nuclei, but even for nuclei previously believed to be spherical. It is not too clear how one would obtain the equations above from fundamental considerations, but it is perhaps possible that it gives an approximate solution to the problem in which the assumption of adiabatic motion is invalid and the term H_c may not be neglected. One would expect that the intrinsic states in the nucleus would be profoundly affected by large changes in the moment of inertia, as this in effect is a change in the deformation of the potential well. No theoretical information on this problem is yet available.

2.2 Single particle transfer reactions

Nuclear reactions which directly transfer a single nucleon into or out of a nucleus can yield a great deal of information on the intrinsic states in that nucleus, since the probability for transfer of a nucleon is directly dependent on the wave function of the orbital which gains (or loses) the nucleon. In this section, a very qualitative description is given of the theory which relates measured cross sections to nuclear structure. No attempt will be made to be rigorous. Exhaustive treatments of this theory have been given by Macfarlane and French (1960) and by Satchler (1958,1964) and the reader may refer to those articles for the details. Here, the general approach is given in outline form, and the main assumptions and approximations in the theory are mentioned.

Following Satchler, the differential cross section is written as

$$\frac{d\sigma}{d\Omega} = \frac{\mu_i \mu_f}{(2\pi\hbar^2)^2} \left(\frac{k_f}{k_i}\right) \Sigma |S_{fi}|^2$$

where μ_i and μ_f are the reduced masses of the incident and outgoing particles, k_i and k_f are the corresponding linear momenta and S_{fi} is the transition amplitude. The summation includes an average over the initial spins and a sum over the final spins. The transition amplitude S_{fi} is given by

$$S_{fi} = \langle \Phi_f | V_p | \Phi_i \rangle$$

where Φ_f and Φ_i are complete wave functions describing the initial and final systems, and V_p is the perturbing interaction causing the transition. The assumption is made that this transition amplitude may be written for the reaction T(A,B)F as

$$S_{fi} = \int \psi^*_{in} \chi^*_A \chi^*_T V_p \psi_{out} \chi_B \chi_F d\tau_1 \ldots d\tau_n$$

where ψ_{in} and ψ_{out} describe the motion of the incoming and outgoing particles with respect to the nucleus, χ_A and χ_B are the internal motions of the incoming and outgoing particles, and χ_T, χ_F are the wave functions of the target and final nuclei, respectively. In the laboratory system of coordinates, the individual particles are transferred with a definite ℓ-value. If it is assumed that the transferred particle enters into a single particle orbital in a spherical nucleus without

appreciably disturbing the "core" of the nucleus, then one may write the wave function for the final nucleus as a product function

$$\psi_F = \phi_{N\ell j}\chi_{F'}$$

where $\phi_{N\ell j}$ is a spherical particle orbit and $\chi_{F'}$ describes the rest of the nucleus. The approximation is then made that the product of V_p and the internal wave function of the incoming particle may be replaced by a delta function

$$V_p\chi_A = D_o\delta(r_{A-B}-r_B).$$

This requires the outgoing particle to be emitted at the point at which the incident particle is absorbed. The size of the constant D_o depends on the wave functions used for χ_A. This factor determines the absolute magnitude of the calculated cross-sections; for some reactions (eg. (d,p)), the size of D_o may be calculated accurately, for others, empirical values are used. The expression for the transition amplitude may then be written (omitting vector coupling coefficients) as

$$S_{f_i} = D_o \int \psi_T\psi_{F'}d\tau_{\text{nucleus}} \int \psi_{in}\phi_{N\ell j}\psi_{out}d\tau .$$

In this expression, the term

$$\int \psi_T\psi_{F'}d\tau_{\text{nucleus}}$$

contains most of the nuclear information. Apart from the factor $\phi_{N\ell j}$, the rest contains details of the mechanical transfer process. The expression for the differential cross section may

then be re-written as a product of the terms

$$\frac{d\sigma}{d\Omega} = \frac{2I_f+1}{2I_i+1} \sum_{\ell} S_{\ell}\ \sigma_{\ell}(\theta)$$

where $S_{\ell} = \left|\int \psi_T \psi_F, d\tau\right|^2$ and all other terms including vector coupling coefficients are lumped into the factor $\sigma_{\ell}(\theta)$. In the expression above, I_i and I_f are the initial and final spins; the ratio $(2\ I_f+1)/(2\ I_i+1)$ results from the average of initial spins and sums over final spins. This formula gives the cross sections for single particle transfer reactions on a spherical nucleus.

For a deformed nucleus, the single particle orbits are given by the Nilsson model as a sum of spherical states. In the body-fixed coordinates of the nucleus

$$\phi'_{\text{Nilsson}} = \sum_{j\ell} C_{j\ell}\ \phi_{N\ell j}$$

where the prime indicates the body-fixed coordinate system. In order to get this function into the laboratory system, one makes use of a rotation operator, and

$$\phi'_{\text{Nilsson}} = \sum_{m'} \sum_{j\ell} C_{j\ell}\ D^{j}_{m'm}\ \phi_{N\ell j}\ .$$

For the deformed nucleus, the initial and final wave functions for the rotating core are also described by D functions; the expression for S_{fi} may then be written for the deformed nucleus as

$$S_{fi} = D_o \int \sum_{m'j\ell} C_{j\ell}\ D^{j}_{m'm}(\theta) D^{I_i}_{MK_i}(\theta) D^{I_f}_{M_fK_f}(\theta)\, d\tau_{\text{nucleus}}$$
$$\times \int \psi_{in} \phi_{N\ell j}\ \psi_{out}\, d\tau.$$

The integral over the 3 D-functions may be shown to be equal to the product of two Clebsch-Gordan coefficients, one of which refers to vector coupling in the laboratory system, and is then included in the factor $\sigma_\ell(\theta)$. Taking full account of the various sums over initial and final spins, the differential cross section is then written

$$\frac{d\sigma}{d\Omega} = \sum_{j\ell} g^2 \langle I_i j K_i \Delta K | I_f K_f \rangle^2 C_{j\ell}^2 \sigma_\ell(\theta)$$

where g^2 is a normalization factor which for the purposes of this report is equal to 2 if $K_i = 0$ or $K_f = 0$; otherwise $g^2 = 1$. The sum over ℓ is defined by the angular momentum coupling selection rule

$$|(|I_i - \ell| - 1/2)| \leq I_f \leq I_i + \ell + 1/2$$

The mechanical transfer cross section $\sigma_\ell(\theta)$ is

$$\sigma_\ell(\theta) = P\, D_o \int \psi_{in}\, \phi_{N\ell j}\, \psi_{out}\, d\tau$$

where P includes all the factors not given explicitly, such as the reduced masses, linear momenta, vector coupling coefficients, etc.

If one is to consider the effects of the pairing theory, then this cross section formula should be multiplied by the probability V^2 for finding a pair of particles in the orbitals in question, or U^2, the probability for finding the orbital empty, as the case may be. Also, the $C_{j\ell}$ expansion coefficients are those of a single Nilsson orbital. For nuclear states best described by mixtures of Nilsson orbitals, the contri-

bution from each must be added coherently to form the total cross-section.

For example, in the case of a target nucleus with a mixed ground state, the cross-section formula is

$$\frac{d\sigma}{d\Omega} = \sum_{j\ell} \left(\sum_{n} g_n \langle I_i j K_i^{(n)} \Delta K | I_f K_f \rangle a_n C_{j\ell}^{(n)} \begin{Bmatrix} U_n \\ \text{or} \\ V_n \end{Bmatrix} \right)^2 \sigma_\ell(\theta)$$

where the index n runs over all the Nilsson states in the mixture and a_n is the admixture coefficient for the n^{th} Nilsson orbital.

For the case of a single nucleon transfer on an even-even deformed nucleus (such as ^{152}Sm) where $I_i = K_i = 0$, the cross section formula simplifies considerably, as the final nuclear spin is necessarily equal to the j-value of the transferred particle. Then,

$$\frac{d\sigma}{d\Omega} = 2\left(\sum_{n} a_n C_{j\ell}^{(n)} \begin{Bmatrix} U_n \\ \text{or} \\ V_n \end{Bmatrix} \right)^2 \sigma_\ell(\theta).$$

If the reaction populates a rotational band with members whose spins are I_f, $I_f + 1$, $I_f + 2$, --- , one sees that the cross section for each of these rotational band members is proportional to the appropriate wave function coefficient $(a_n C_{j\ell}^{(n)})^2$, and thus, by measuring the intensities of the members of a rotational band, one may directly determine the wave function of the intrinsic state if the $\sigma_\ell(\theta)$ functions are known. These intensity patterns thus characterize

the wave function, and have appropriately been dubbed "fingerprint patterns". Measurement of these patterns has resulted in the identification of a large number of Nilsson orbitals in the rare-earth region, and is an extremely powerful spectroscopic tool. For reactions on odd targets, transfers involve mixtures of ℓ-values, and the intensity patterns are sometimes not sufficiently characteristic to allow identification of the orbitals involved.

To calculate $\sigma_\ell(\theta)$, use is made of the distorted wave Born approximation (DWBA) model. At McMaster, the computer code DWUCK is available to do these calculations. In this model, the assumption is made that the incoming and outgoing waves ψ_{in} and ψ_{out} may be given by the wave functions describing particles scattered elastically from an optical model potential. The function $\phi_{N\ell j}$ is calculated for a spherical Woods-Saxon well, the depth of which is adjusted such that the orbital has the correct binding energy.

The calculated functions $\sigma_\ell(\theta)$ vary, as has been implied till now, as a function of the transferred orbital angular momentum ℓ and the reaction angle θ. A simple-minded, semi-classical argument which illustrates this dependence on ℓ and θ can be made, and gives some physical insight into the mechanics of the reaction process. Let the linear momentum of the incoming particle be designated $\vec{k}_a$, and that for the outgoing particle be $\vec{k}_b$. The assumption is made that the outgoing particle is emitted at the same point at which the incoming particle is absorbed (this is the zero range ap-

proximation made previously); let this reaction take place at some distance R from the centre of the nucleus. Since these reactions are viewed as surface reactions, one can associate R with the nuclear radius.

If the transferred nucleon has momentum $\vec{k}_n = \vec{k}_a - \vec{k}_b$, the transferred angular momentum with respect to the nucleus is $\approx k_n R$. Then, those reactions which fulfill the requirement

$$\sqrt{\ell(\ell+1)}\,\hbar \approx k_n R\hbar$$

will be very much more probable than others. For any given reaction, one may use the cosine rule to solve the equation above for the preferred angle of reaction for various ℓ-transfers, or conversely, for the preferred ℓ-transfer value at any given angle. As examples, this approach indicates that for the reaction $^{152}Sm(d,t)^{151}Sm$, the preferred angle of reaction is small for small ℓ-transfers, and increases as ℓ increases. Also, for most angles, the preferred ℓ-value is $\ell = 1$. For the reaction $^{152}Sm(^3He,\alpha)^{151}Sm$, the opposite holds, due to the large Q-value of the reaction. High ℓ-values are preferred, and the preferred angle increases as the ℓ-value decreases.

While these considerations give only a very crude picture of the reaction process, the DWBA calculations exhibit the features predicted. Figures 3 and 4 give the $\sigma_\ell(\theta)$ angular distributions for the reactions above as calculated

Figure 3.

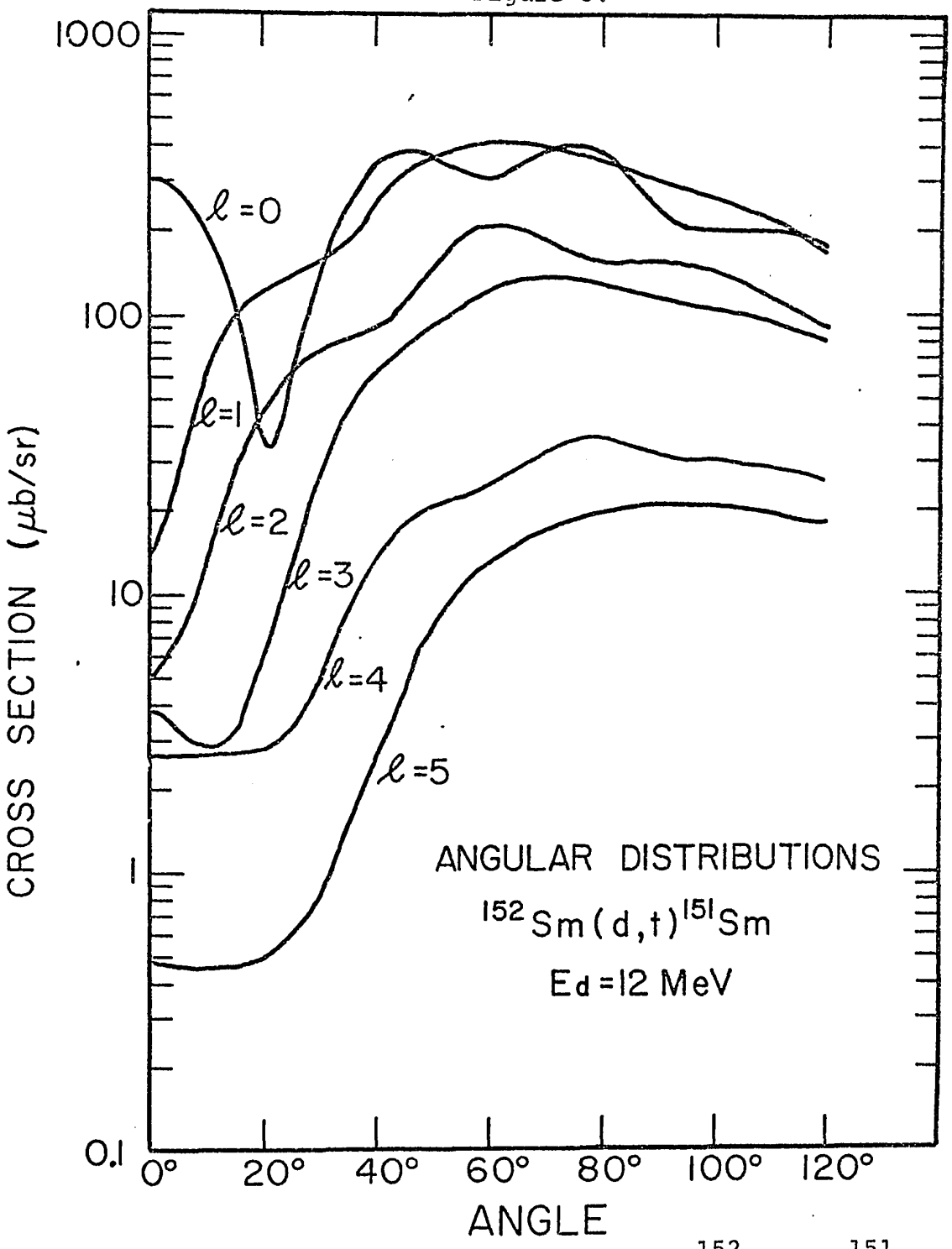

DWUCK calculations for the reaction $^{152}Sm(d,t)^{151}Sm$.

Figure 4.

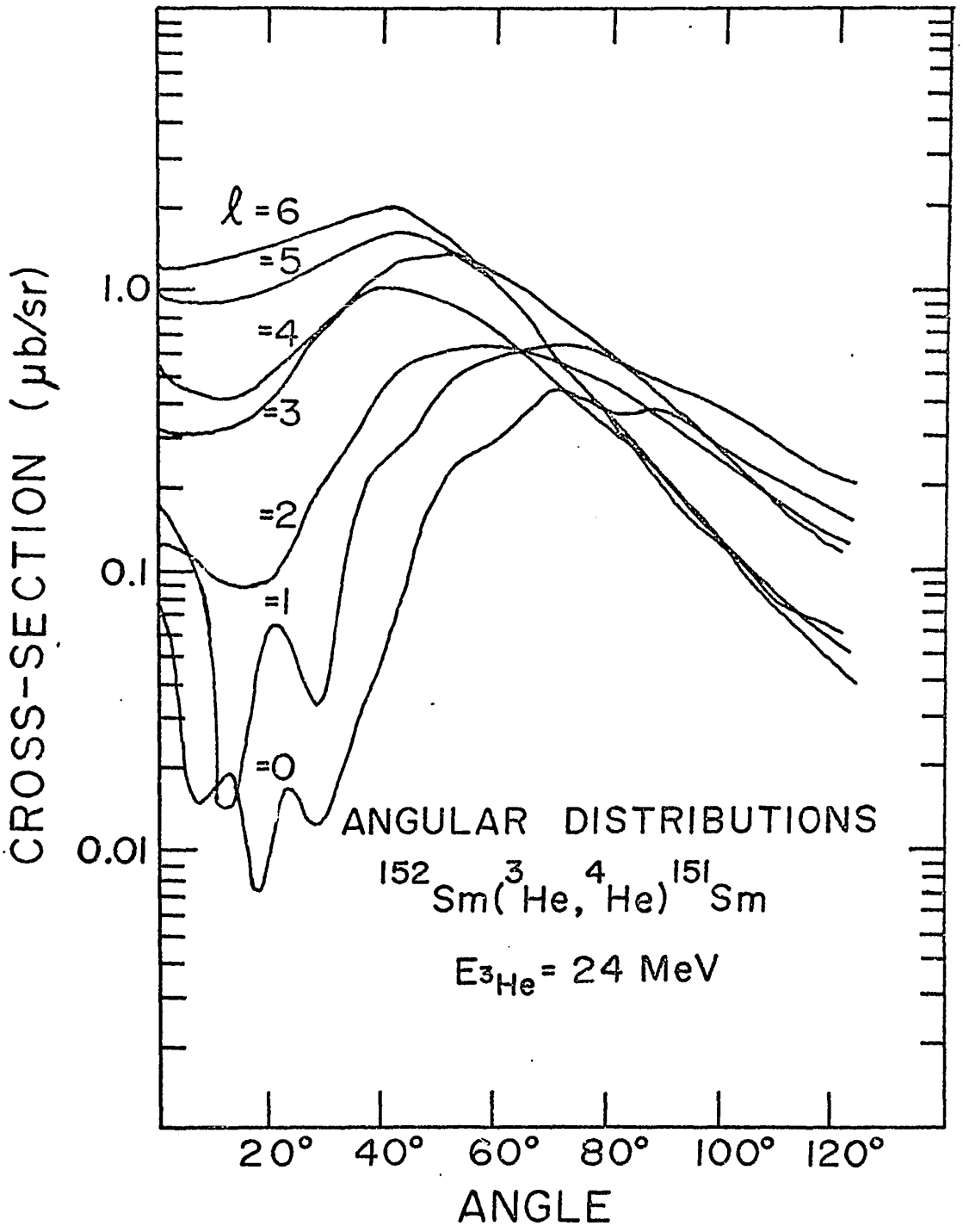

DWUCK calculations for the reaction
$^{152}Sm(^{3}He,\alpha)^{151}Sm$

by the DWUCK computer program. The trends predicted by the simple model are indeed followed.

The DWBA angular distributions for the (d,t) reaction are quite different for different ℓ-transfers. These characteristic angular distributions make the (d,t) reaction a very useful experimental tool. In a (d,t) reaction on an even target, only one ℓ-value is permitted in the population of a level of given spin. Therefore, measuring the angular distribution of the level and comparing this distribution with the results of the DWBA calculations should yield the ℓ-transfer, if the calculations are good. In this case, the parity is given, and the spin of the level determined to be either ℓ+1/2 or ℓ-1/2. For odd targets, various ℓ-transfers may contribute to the final level, and the angular distributions may not characterize the ℓ-values involved.

The (^{3}He,α) reaction can provide a great deal of experimental information to supplement that obtained from a (d,t) reaction. The (d,t) and (^{3}He,α) reactions are identical insofar as they both remove a neutron from a target nucleus. Since (d,t) reactions prefer particle transfers of low ℓ-value , and (^{3}He,α) reactions prefer particle transfers of high ℓ-value,one of these reactions will tend to populate levels of high spin and the other reaction levels of low spin in a given final nucleus. Complementary (^{3}He,α) and (d,t) reactions may also be used to determine ℓ-transfer values. For levels populated in both (^{3}He,α) and (d,t) reactions on an even target ,

the ratio of the intensity of the level in the (^{3}He,α) reaction to the intensity of the level in the (d,t) reaction will simply be the ratio of the $\sigma_\ell(\theta)$ factor for (^{3}He,α) to that for (d,t). These ratios differ by orders of magnitude for the different ℓ-values and are thus a very sensitive test for the ℓ-transfer to a given level. For reactions on odd nuclei, several ℓ-values are involved, and the situation becomes more complicated. The ratios of the factors $\sigma_\ell(\theta)$ may be obtained from DWBA calculations.

In this work, both these techniques for determining ℓ-values, the angular distribution method and the cross section ratio method have been used to great advantage in the study of ^{151}Sm.

2.3 Coulomb excitation and inelastic scattering

Coulomb excitation is a process in which a nucleus interacts with a passing charged particle through the mutual electromagnetic field. For the case in which the energy of the bombarding particle is low enough that it can not approach the nucleus so closely that nuclear forces are involved, then the interaction process can be treated exactly using present theoretical methods, and the probability for excitation of the nucleus can be related directly to nuclear parameters. Those relations which are pertinent to this experimental study are given below. These are taken from the standard reference work on Coulomb excitation (Alder *et al.* (1956)) and from the thesis

of Bent Elbek (1963).

Transitions from one nuclear state to another through emission of a gamma photon (electromagnetic decay) or via absorption of a photon (Coulomb excitation) are similar processes, and the probabilities for these processes are both conveniently discussed in terms of a "reduced transition probability". This is essentially an expression for the transition probability from which the influence of the transition energy has been removed. For the electric transitions, this reduced transition probability is defined as

$$B(E\lambda) = \frac{1}{2I_i+1} \sum_{M_i M_f} \langle \psi_f | \varepsilon_\lambda | \psi_i \rangle$$

where $|\psi_i\rangle$ and $|\psi_f\rangle$ are the initial and final nuclear states and ε_λ is the electric multipole operator for emission of a photon carrying off angular momentum λ. Estimates have been made of the transition strengths that would be expected for the transition of a single proton from one shell model orbital to another. These estimates are not expected to be very accurate, but for reference purposes they make convenient units in which measured transition strengths may be discussed. These units are often referred to as Weisskopf units.

The experimental observation of B(E2) values very much larger than those expected for the transition of a single proton from one nuclear orbit to another is an indication that correlated proton movements are involved. For example, the

measured Coulomb excitation transition probabilities to the first excited states in spherical, even-even nuclei (such as ^{150}Sm) have yielded B(E2) values 10-100 times larger than the single particle estimates. In well-deformed nuclei, the transition rates between members of rotational bands are typically two orders of magnitude larger than the single particle estimates. For a simple rotational band (i.e. no configuration mixing) the collective model relates the B(E2) values between members of the band to the static quadrupole moment Q_o of the nucleus through the equation

$$B(E2) = \frac{5}{16\pi} Q_o^2 \langle I_i 2K0 | I_f K \rangle^2$$

where the factor in brackets is a Clebsch-Gordan coefficient. For a homogeneous charged spheroid, Q_o is related to the deformation parameter β (where $\beta = \Delta R/R_o$) by the approximate equation

$$Q_o = \frac{3}{\sqrt{5\pi}} Z_e R_o^2 \beta(1 + 0.157\beta + 0.20\beta^2)$$

where R_o is the mean nuclear radius.

In first order Coulomb excitation of a deformed nucleus, the enhanced E2 transition rates lead to strong populations of the first member of the ground state band of an even A target, and the first two members of the ground state band of an odd A target. In general, the population intensities of these levels in a Coulomb excitation experiment defined relative to that for pure elastic scattering will be given by

(Elbek (1963))

$$P(\theta)=3.721\times10^{3}\ \frac{A_1}{A_1^{2}Z_2^{2}}\ E^{2}(E-\Delta E')B(E2)\frac{df}{d\Omega}\left(1+2\frac{A_1}{A_2}\cos\theta\right)\left(1+\frac{A_1}{A_2}\right)^{-2}\sin^{4}\frac{\theta}{2}$$

where A and Z are, as usual, the nuclear mass and number of protons, E is the bombarding energy, $\Delta E'$ is an expression for the excitation energy, and $\frac{df}{d\Omega}$ is a function dependent on the kinematics of the process. Values for this function have been calculated and may be obtained from published tables (eg. Alder et al. (1956)).

In a practical experiment, the B(E2) value to a given level may be determined by measuring the intensity of the level relative to the elastic scattering intensity. If this value is large, compared to the single proton estimate, one should consider the possibility that the nucleus may be deformed, and that the level is a member of the ground state band. On the further assumption that this band is unmixed, one can calculate the quadrupole moment and deformation β of the nucleus from the equations above. A great deal of the information available on nuclear shapes has been obtained in this manner.

For those experiments in which the bombarding energy of the projectile is approximately as large as the Coulomb barrier, such that the projectile can approach the nucleus closely enough that nuclear forces may be involved, then the last equation above is no longer valid. In such experiments, the closer penetration of the projectile will also result in

appreciable population of levels through higher order (E3 and E4) transitions, and also through multiple step processes. For the rare earth nuclei, empirical methods have been developed which allow one to determine multipolarities and, for E2 transitions, B(E2) values from these inelastic scattering experiments. For a 12 MeV beam of deuterons, Zeidman et al. (1966), have measured the angular distributions of the deuterons scattered inelastically by various Sm targets. The angular distributions were found to be smooth functions dependent on the transition multipolarity, and it was concluded that the ratio of the intensities of a level at two angles, 90° and 125°, was sufficient to identify the multipolarity of the transition leading to that level. For E2 transitions, empirical conversion factors relating the observed intensities to B(E2) values were obtained by Veje et al. (1968), as the B(E2) values for many transitions had been determined from pure Coulomb excitation experiments. These experiments included work on ^{150}Sm and ^{152}Sm. This method can therefore be applied to ^{151}Sm by interpolating between the conversion factors found for these two neighbouring nuclei. This is discussed more fully in a later section.

CHAPTER III

EXPERIMENTAL DETAILS

3.1 Equipment for studying single particle transfer reactions

The energy level spacings of nuclei in the rare earth region are often as small as a few keV, and therefore the study of single particle transfer reactions on these nuclei requires an accelerator capable of producing beams of particles of well defined energy, and a detection system capable of analyzing the reaction products with sufficient resolution to distinguish between these close-lying energy levels. This is particularly important for the study of ^{151}Sm, where the level density is relatively high.

At McMaster, the equipment available is well suited for these studies. The FN model Tandem Van de Graaff accelerator can provide well defined beams of deuterons and ^{3}He ions of sufficient energy with an energy spread of about 1 keV. These ions are delivered, through a series of quadrupole focussing magnets, to the target chamber of an Enge split-pole broad range magnetic spectrograph. In this instrument, the reaction products are analyzed in the magnetic field, such that rays of particles with the same momentum are focussed at a single position on the focal plane of the system. A plot of the number of detected particles as a function of the distance along the focal plane is thus a plot of the number of particles

versus the momentum of the particles. In those cases in which only a single species of reaction particle has been detected, this plot becomes essentially an energy-level diagram, for the nucleus. A schematic diagram of the paths of the reaction products in the magnetic field is given in Figure 5. The characteristics of this instrument have been described by Spencer and Enge (1967).

The spectrograph as a whole may be easily rotated about the target chamber, such that the reaction products at angles from ≈ 5° to ≈ 150° may be analyzed. At the entrance to the pole gap of the magnet, two sets of slits, one vertical and one horizontal, define the acceptance solid angle of the analyzing system. The horizontal entrance slits are in the primary focussing plane of the instrument, and in reality accept particles scattered into a range of $\theta \pm \Delta\theta$, where $\Delta\theta$ is the difference in reaction angle between that for a particle passing through the slit centre and that for one passing close by the slit edge. Thus, rays of particles emitted at the angle $\theta+\Delta\theta$ will have a slightly lower kinetic energy than those emitted at $\theta-\Delta\theta$ (assuming these two rays of particles correspond to the same nuclear state) due to the difference in recoil energy of the target nucleus. For a given beam this difference in energy is dependent on the mass of the target nucleus. The position of the focal plane of the magnet is also dependent on this difference in the ray energy, and therefore dependent

Figure 5

Schematic diagram of the Enge split-pole magnetic spectrograph.

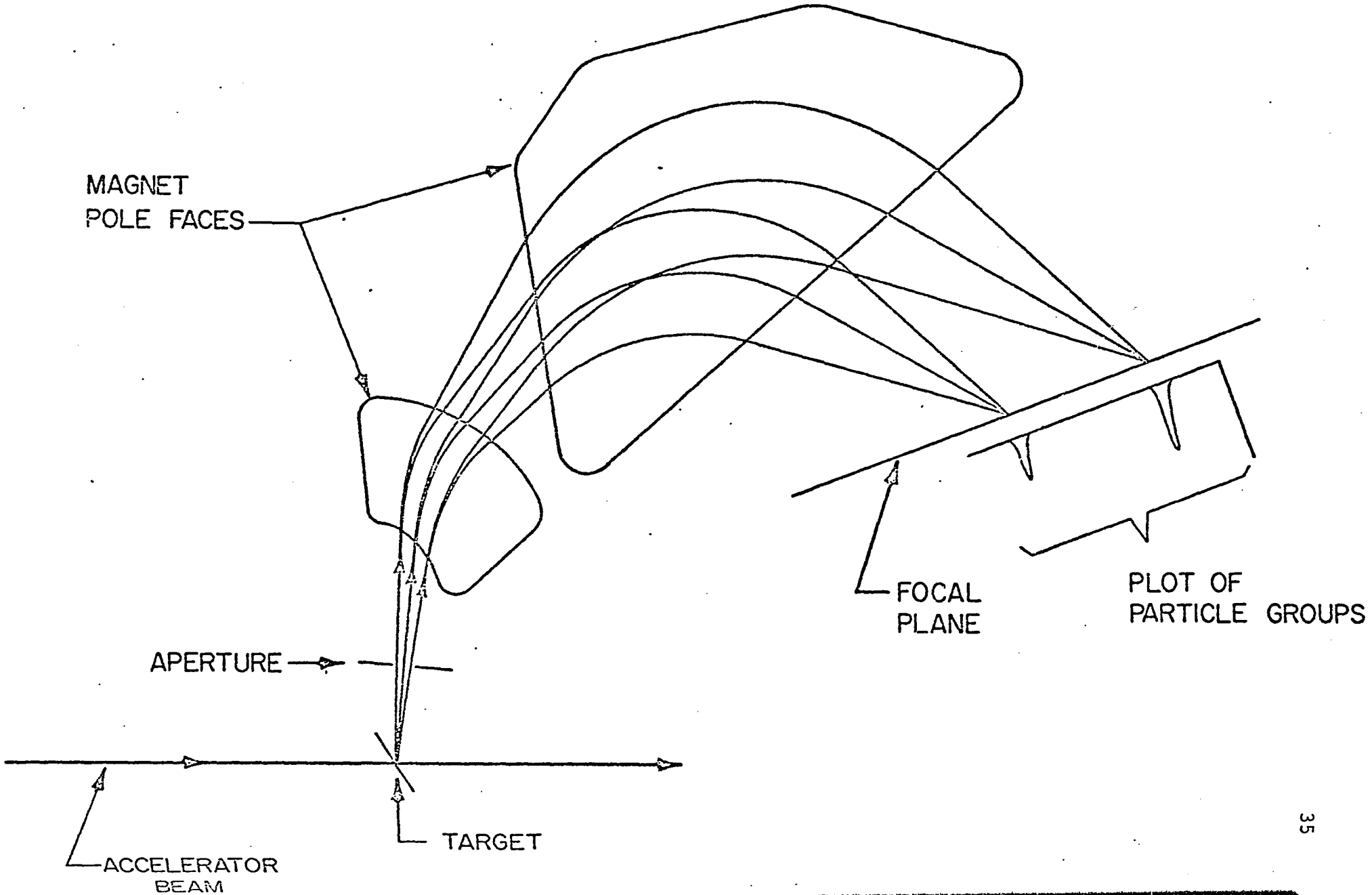

on the mass of the target nucleus. In doing an experiment, the focal plane position for the reaction under consideration is calculated, and the detector carefully placed at that position. (This is known as setting the "kinematic shift".) Should there be any impurities in the target, the peaks due to these impurities will be broader than those due to the target nuclei, as the kinematic shift will not be optimum for the impurity. In many of the spectra in this thesis, peaks due to light impurities (O, Si, Cl) and some due to the carbon backing are seen, and are much broader than the reaction peaks.

The exact identity of these impurity peaks may be established by finding their positions in spectra at different angles, as the difference in recoil loss due to the difference in mass means that the impurity peaks will "march" through the target spectra as one changes angle.

This built-in method of distinguishing peaks due to impurities from those due to the real target is very useful. Only those impurities of mass very similar to the target nucleus may go undetected by this method.

In general, the resolution obtained with this system is determined by the following factors:

1) Beam energy spread and beam spot size on the target

The spread in beam energy provided by the FN accelerator was less than 1 keV. The beam spot size was defined by a set of slits of dimensions 1/2mm by 3 mm with the narrower

dimension being in the primary focussing plane (the horizontal plane) of the instrument. As these slits were about 20 cm in front of the target, the spot width on the target would be slightly larger than 1/2 mm. The magnification of the spectrograph in the horizontal plane is about 1/2, and therefore the spot size by itself would yield a peak width of ≈ 1/4 mm on the focal plane. For a given reaction, the energy resolution corresponding to this width can be determined by the following rule of thumb; the energy dispersion along the focal plane is approximately one keV per mm for each MeV of reaction product energy. As an example, consider the reaction $^{152}Sm(d,t)^{151}Sm$ which is to be discussed in this work. The Q-value for this reaction is about -2 MeV, and the outgoing tritons will therefore have an energy of ∿ 10 MeV. The spot size contribution to the peak width will then be about 2-1/2 keV.

2) The target thickness

Straggling of the incident and resultant particles in the target also contributes to the peak width. The size of this contribution is given by the relation $\Delta E = 18Zt^{\frac{1}{2}}$ (cf Enge (1966) p. 188) where Z is the charge of the particle, t is the target (and target backing) thickness in mg/cm^2 and ΔE is the peak width (full width at half maximum) in keV.

If the stopping power for the outgoing particle is different than that for the incident particle, a further contri-

bution to the peak width will be made, as the reaction can then take place at any depth in the target material. The contribution will be approximately the difference in stopping power, if the target is in transmission geometry. The target used in the $^{152}Sm(d,t)^{151}Sm$ reaction consisted of a 20 $\mu g/cm^2$ layer of ^{152}Sm on a 30 $\mu g/cm^2$ carbon backing. The straggling contribution for this target would be about 4 keV. The differential energy loss for a 12 MeV deuteron is $\sim$ 25 keV/mg/cm^2, and for a 10 MeV triton is 35 keV/mg/cm^2. The stopping contribution for the ^{152}Sm target would be $\sim$ 0.5 keV.

3) Spectrograph aberrations

The contribution of the spectrograph aberration to the peak width in these experiments was not significant. The Enge spectrograph is corrected to second order in aberration. For most of these experiments, the aperture sizes used were $\lesssim$1 msr, compared to the maximum of 9 msr that is available for this instrument, and the aberration effects would be very small, compared to the other contributions.

4) Method of detecting the particles on the focal plane

The reaction products were detected by placing nuclear emulsion plates at the optimum focal plane position for the reaction under consideration. These plates were masked with aluminum foils of suitable thicknesses to exclude unwanted particle groups of lower penetrating range than those being detected. These plates were scanned on a microscope with a

specially constructed stage. The scanning strip size was 1/4 mm, since the contributions from the other effects would be larger than this. This detection method thus makes little contribution to the observed peak width.

The total peak width that may be expected from all these effects may be estimated by adding the individual contributions in quadrature. For the example considered, this gives an expected resolution of ≈ 4-1/2 keV. This is about the resolution obtained in the experiments. A similar calculation for a (^{3}He,α) reaction on the same target would give an expected resolution of approximately 12 or 13 keV. The experimental resolution was somewhat worse than this, about 18-19 keV. Perhaps the ^{3}He beam was not so stable as it was thought to be.

The targets used in these experiments had thicknesses ranging from 20-40 μg/cm^2. The production of these targets was by no means a trivial operation. In particular, the targets of ^{151}Sm were difficult to make, as this material is radioactive, (a weak β-emitter) with a 90 year half-life. For reasons of health safety, it was necessary to construct a target preparation apparatus in a glove box in a radiation laboratory. Furthermore, for reasons of cost (and safety), only a very small amount of ^{151}Sm could be used at one time, and a great deal of preparation was required in order to develop efficient procedures for handing this material. A full description of the equipment and procedures used in making these targets is

given in Appendix A. The separated isotopes used were obtained from Oak Ridge National Laboratories. A list of the isotopic abundances of these materials as determined by the supplier is given in Table 1.

A calibration curve relating the position D of a particle group on the spectrograph focal plane to the radius of curvature R of the particle paths in the magnetic field was established using the 6.0 MeV and 8.8 MeV alpha particles emitted from a ThB radioactive source placed at the target position. The magnetic rigidities BR for these alpha particles have been measured very accurately (Wapstra (1964)). For various magnetic field settings B, the positions of the alpha groups at the focal plane were measured, and a polynomial relating R to D calculated using a least squares fitting computer program. The calibration curve found was

$$R=89.2478-0.40732D+3.8920\times10^{-4}D^2-9.9143\times10^{-6}D^3+9.8126\times10^{-8}D^4.$$

Using this curve and the accurately measured magnetic field strength B, as determined using a nuclear magnetic resonance probe, the magnetic rigidity of a particle group from any reaction could be determined, and hence, the corresponding energy of the particles calculated. If the ground state Q-value of the reaction were known accurately, or one of the peaks in the spectrum could be identified with a level determined from other studies, the excitation energies of the nuclear states could be found. All of these calculations were carried out on the small computers available at the laboratory.

Table 1

Isotopic Composition of the Sm Target Materials, as Determined by the Supplier, ORNL.

	Isotopic Composition (%)		
	^{150}Sm	^{151}Sm	^{152}Sm
^{144}Sm	<0.01	<0.001	<0.01
^{147}Sm	<0.01	0.937	0.08
^{148}Sm	<0.01	0.041	0.07
^{149}Sm	0.017	0.166	0.12
^{150}Sm	99.973	3.090	0.1
^{151}Sm	-	93.11	-
^{152}Sm	0.01	2.390	99.18
^{153}Sm	-	<0.002	-
^{154}Sm	<0.01	0.263	0.45

In order to obtain absolute cross-section measurements for the levels populated in these experiments, a small solid-state detector was placed in the target chamber to monitor the number of beam particles scattered elastically from the target during the exposure. The cross-section for elastic scattering was obtained from DWBA calculations or, in some cases, from other experimental work. The cross-section of a level was then found by multiplying the elastic cross-section by the ratio of the numbers of counts in the reaction peak to the number of elastically scattered particles, suitably corrected for differences in solid angle. This generally gave good results, and in the one experiment which directly reproduced work done in another laboratory, the results were well within experimental error.

As a rule, it is estimated that the cross-section of a strong, well-defined peak may be measured to an accuracy of about 10%, relative to the cross-sections of the other peaks in the spectrum, and to an accuracy of about 25% on an absolute scale. For peaks containing only a few counts or poorly resolved peaks the uncertainties will be larger. In the (d,t) angular distributions, the uncertainties of the intensities of strong peaks relative to those at different angles is estimated at 15%.

The DWBA calculations which are used in this work were carried out with the computer code DWUCK. The parameters used for these calculations have been obtained from published

works on other nuclei; a list of these parameters is given in Table 2. The references from which they were taken are as follows:

Christensen et al.	(1969)	deuteron parameters
Jaskola et al.	(1967)	triton parameters
Burke et al.	(1966)	proton parameters
Burke et al.	(1971)	^{3}He parameters
		α parameters

The output of DWUCK must be multiplied by a normalization factor N to get absolute values for the factors $\sigma_\ell(\theta)$. The values of N for the (d,t) and (d,p) experiments are commonly accepted as 3.33 and 1.53, respectively, and are used here. For the (^{3}He,α) experiments at 24 MeV, no "good" values for N were available, but the value N = 48 was obtained from this experiment in a manner to be described in the following section.

3.2 Experimental details of single particle transfer reactions

A) The ^{152}Sm(d,t)^{151}Sm and ^{152}Sm(^{3}He,α)^{151}Sm reactions

For the reaction ^{152}Sm(d,t)^{151}Sm, an incident beam of 12 MeV deuterons was used and the reaction products were studied at 16 different angles ranging from 5° to 140° in order to obtain complete angular distributions. Figure 6 shows the spectra at 5° and 60°, and Table 3 gives a list of the observed energies and cross-sections at 5°, 60° and 90°. The best resolution obtained for this reaction was somewhat better than

Table 2

Optical Model Parameters for the Dwuck Calculations

		V_o (MeV)	r_o (fm)	a (fm)	ω_o (MeV)	ω_D (MeV)	r_o' (fm)	a' (fm)	r_{oc} (fm)
12 MeV (d,t) and (d,p)	d	91.48	1.15	0.925	0	24.81	1.344	0.579	1.25
	t	154	1.10	0.750	0	12.00	1.400	0.650	1.10
	p	55.0	1.25	0.65	0	15.0	1.250	0.49	1.25
24 MeV (^{3}He,α)	^{3}He	175	1.14	0.723	4.38	0	1.60	0.810	1.40
	α	206.8	1.41	0.519	6.45	0	1.41	0.519	1.30
Bound state neutron		a*	1.25	0.65					

These parameters are defined by the equation

$$V(r) = V_c(r,r_{oc}) - V_o(1+e^x)^{-1} - i(\omega_o - 4\omega_D \frac{d}{dx'})(1 + e^{x'})^{-1}$$

where $x = (r - r_o A^{1/3})/a$ and $x' = (r - r_o' A^{1/3})/a'$

$V_c(r,r_{oc})$ = Coulomb potential of a uniformly charged sphere of radius $R_c = r_{oc}A^{1/3}$

*adjusted to reproduce separation energy

Figure 6.

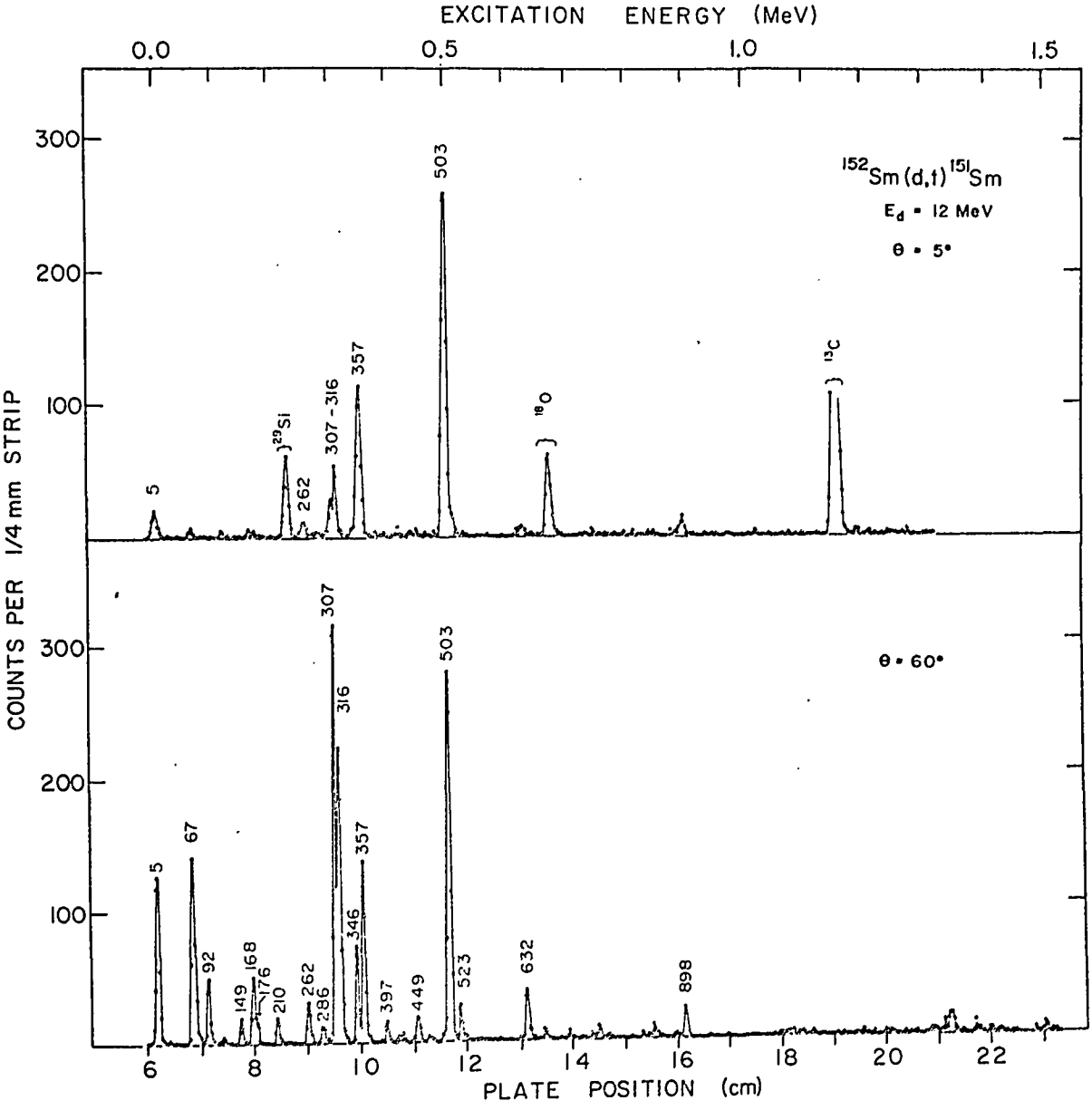

The 5° and 60° spectra of the reaction $^{152}Sm(d,t)^{151}Sm$ The numbers above the peaks are the level energies in keV.

Table 3

Energies and Cross-Sections for the Reactions $^{152}Sm(d,t)^{151}Sm$ and $^{152}Sm(^{3}He,\alpha)^{151}Sm$

Energies from other studies†	$^{152}Sm(d,t)^{151}Sm$ Energy	Cross-Section (μb/sr) 5°	60°	90°	$^{152}Sm(^{3}He,\alpha)^{151}Sm$ Energy	Cross-Section (μb/sr) 10°	45°
4.8	4.8*	23	245	128	∿ 5	< 1	<3
65.8+69.7	67	6	292	199	68	5	30
91.5	92	-	84	62	92	25	14
148	149	-	29	51	150	63	140
167.7+168.4	168	≈ 2	150	55	-	-	-
175.3	176	≈ 1	∿22	42	174	35	47
208.9	210	-	43	34	∿210	∿ 3	∿7
261.1	262	13	56	88	261.1*	75	117
285.0	286	< 4	28	∿20	-	-	-
306.8	307	} 67	550	485	305	-	50
314.9	316		396	264	-	-	-
344.8	346	-	123	118	347	∿12	∿13
-	-	-	-	-	386	14	-
-	357	129	234	172	-	-	-
395.6	∿397	-	33	25	396	-	∿ 3
416.1?	-	-	-	-	420	10	13
448	449	-	47	34	-	-	-
470	∿470	-	6	-	-	-	-
490	-	-	-	-	} ∿496	-	} ∿27
-	503	291	506	451			
520.9	523	-	54	50	-	-	-
	632	∿9	77	85	632	-	∿5
	∿705	-	≈ 6	-	704	15	35
	∿742	-	≈ 5	-	745	∿ 5	12
	898	∿9	34	-	-	-	-
	∿1375	-	≈10	-	1378	46	91

† These energies result from the re-examination of the decay of ^{151}Pm and from the study of the 261.1 keV isomer in ^{151}Sm (Cook et al., private communication).

* The position of this level was used as an energy calibration point.

5 keV,and should be sufficient to resolve the ground state from the first excited state at 4.8 keV. However, only one peak was found in the ground state region. If this peak were identified as the 4.8 keV first excited state the positions of other peaks in the spectrum corresponded to energies which were the same as those of known levels as determined in the decay studies. This correspondence did not occur if the single peak in the 0 keV region was taken to be the ground state. It was therefore concluded that there was little, if any, ground state population in the $^{152}Sm(d,t)^{151}Sm$ reaction, and that the intensity of the peak in that region was due to the first excited level at 4.8 keV.

The angular distributions obtained for the levels populated were compared directly with the theoretical curves calculated using the DWUCK program. Two of these levels, at 357 keV and 503 keV, have unique angular distributions for ℓ=0 transfers. (These levels thus have spin $1/2^+$.) The extremely good fit of the DWUCK calculations for this ℓ-value lent encouragement that the calculated curves for other ℓ-values would also give good fits to the data. Figures 7 to 12 show the empirical data fitted to the calculated curves for all those levels to which ℓ-transfers have been assigned. No attempt at fitting absolute cross sections was made; in each case the calculated line has been adjusted up and down to give the best visual fit to the experimental points.

The spectrum for the complementary reaction

Figure 7.

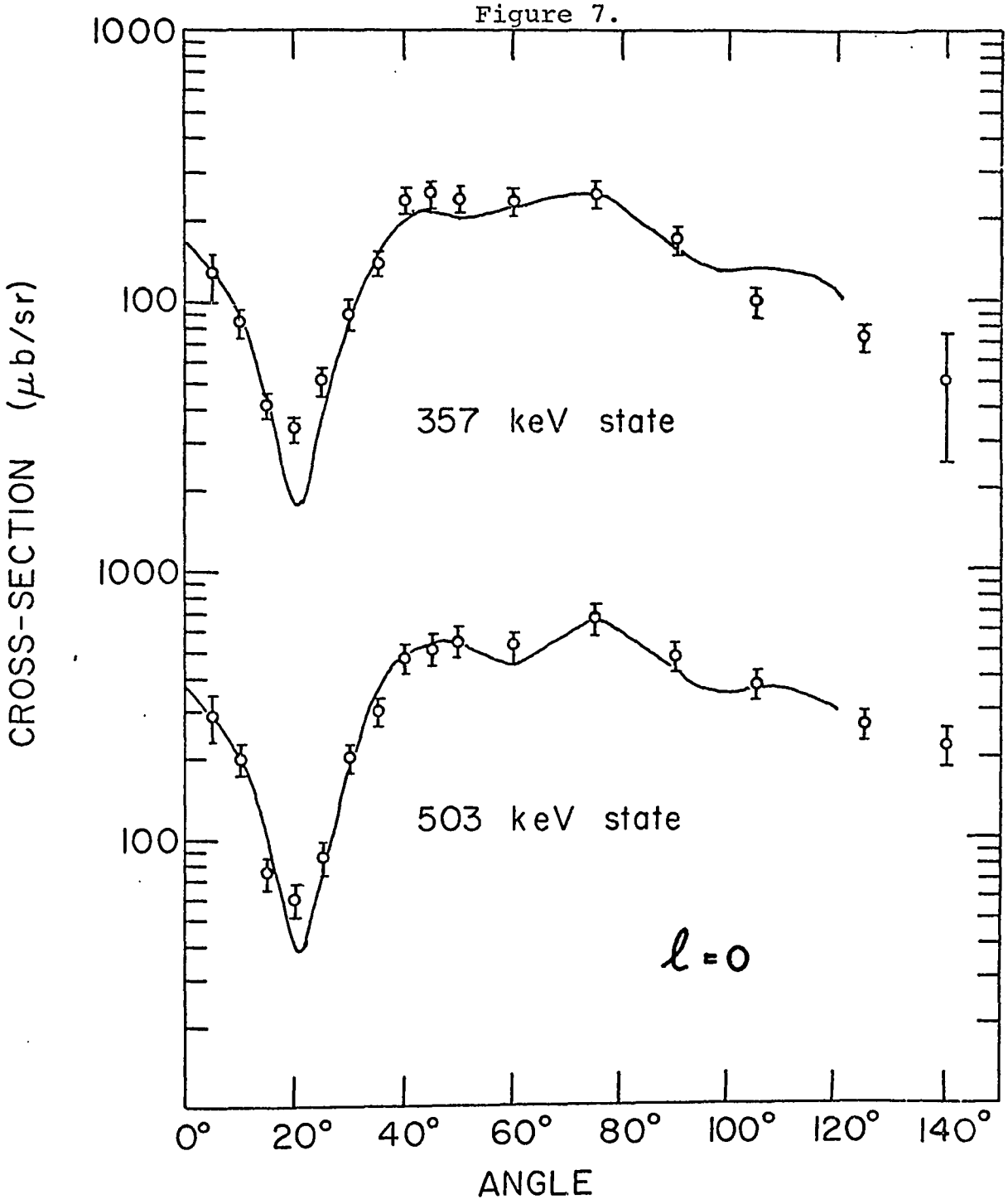

The ℓ=0 angular distributions from the reaction $^{152}Sm(d,t)^{151}Sm$.

Figure 8.

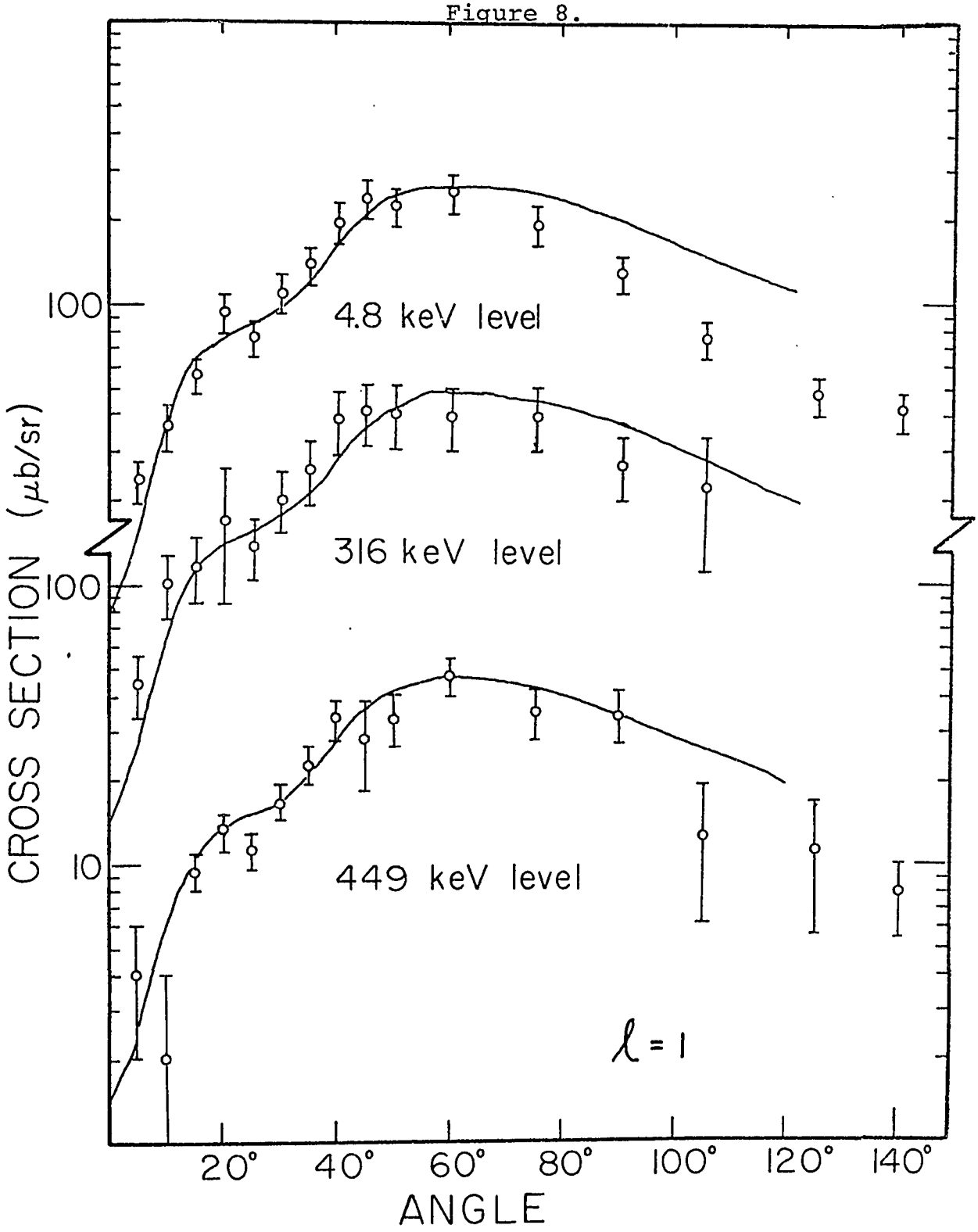

The ℓ=1 angular distributions from the reaction $^{152}Sm(d,t)^{151}Sm$.

Figure 9.

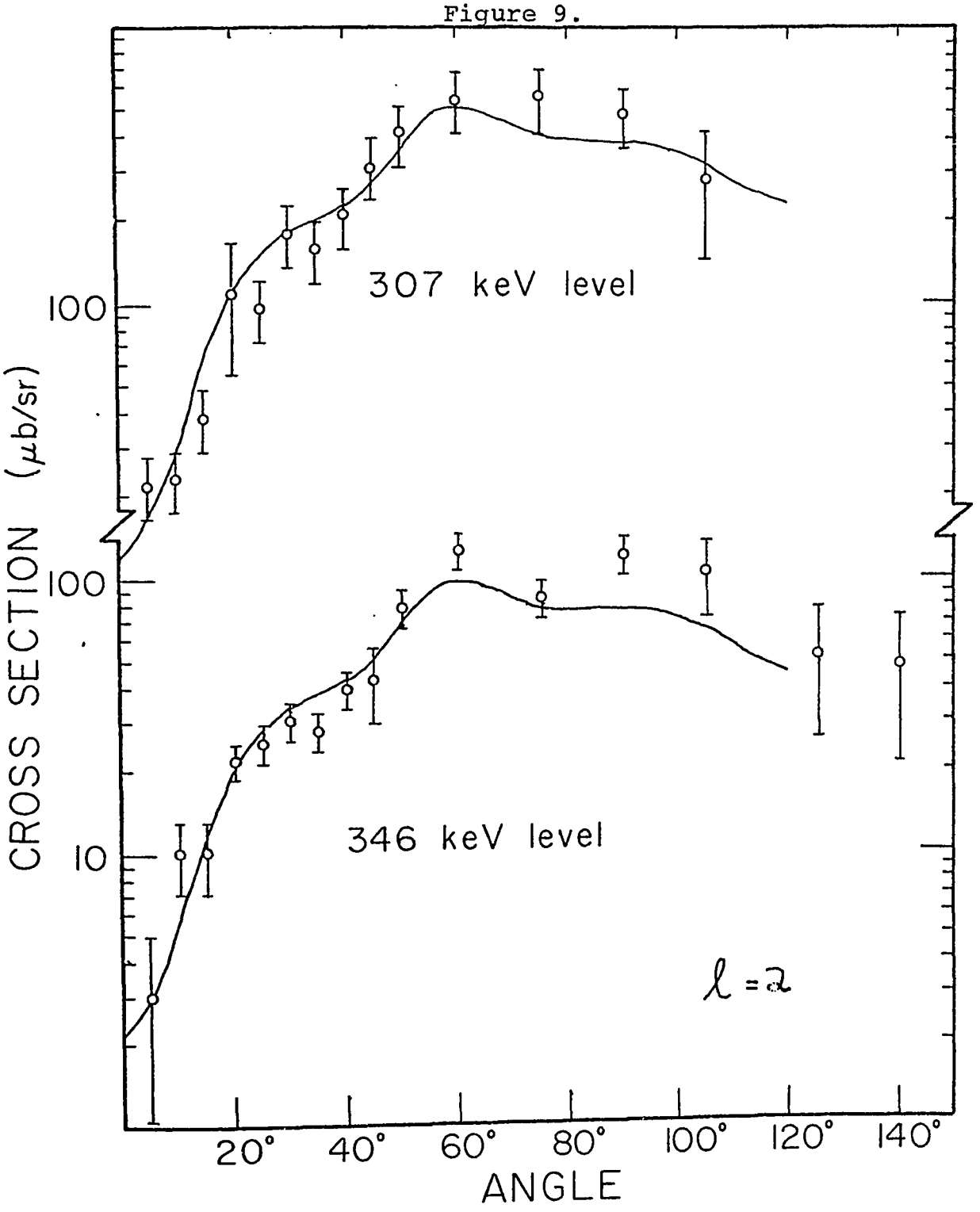

The ℓ=2 angular distributions from the reaction $^{152}Sm(d,t)^{151}Sm$.

Figure 10.

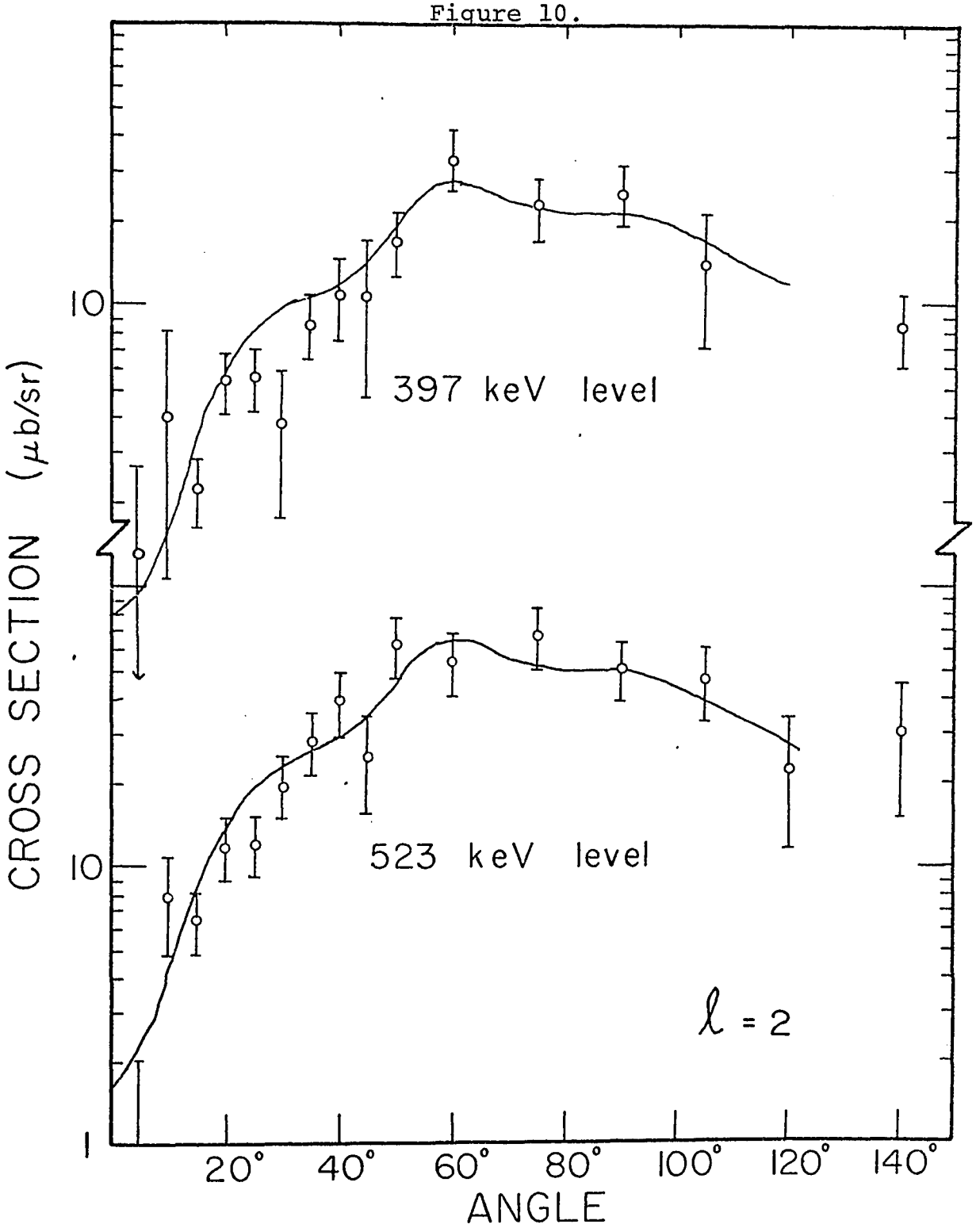

More ℓ=2 angular distributions from the reaction $^{152}Sm(d,t)^{151}Sm$.

Figure 11.

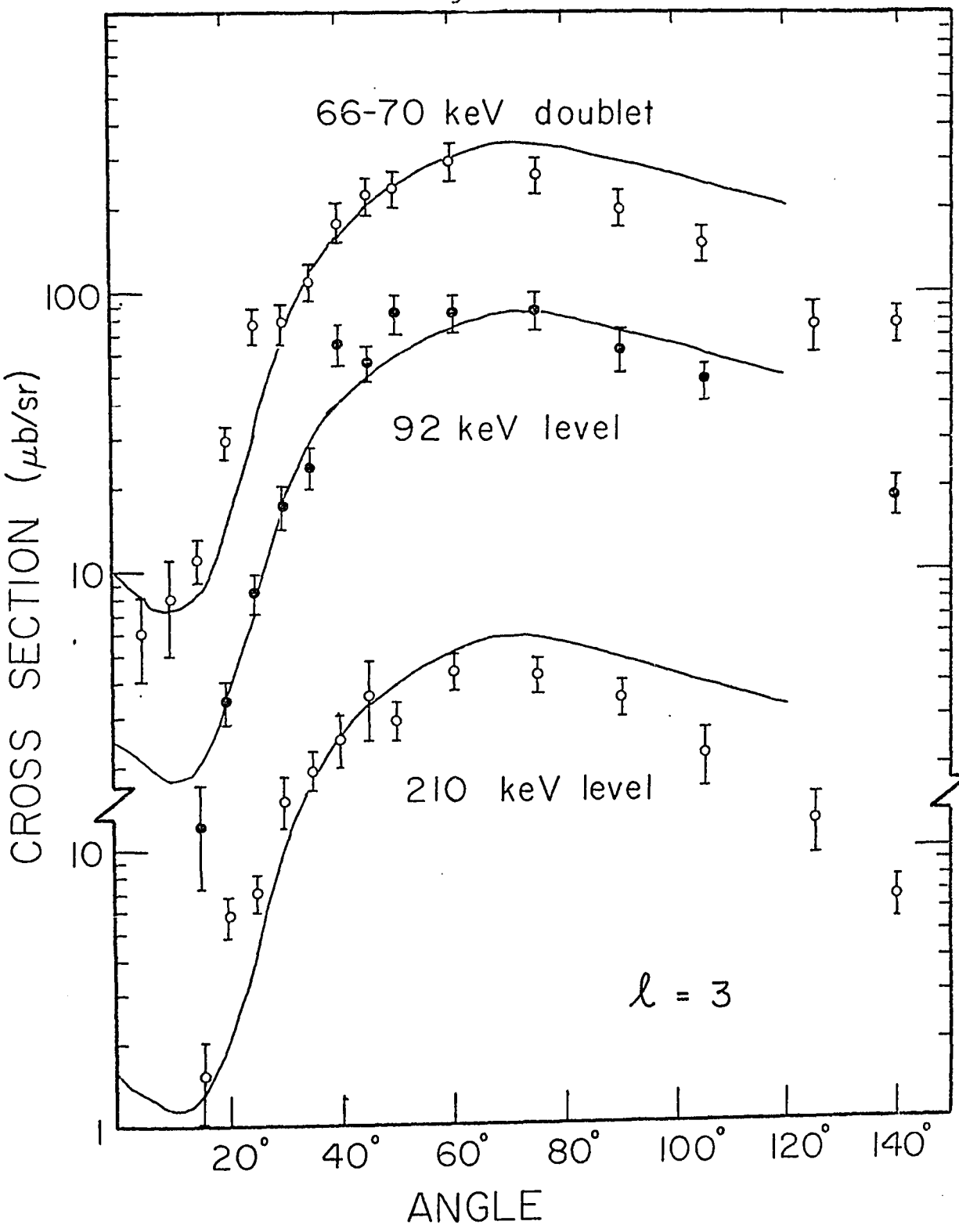

The ℓ=3 angular distributions from the reaction $^{152}Sm(d,t)^{151}Sm$.

Figure 12.

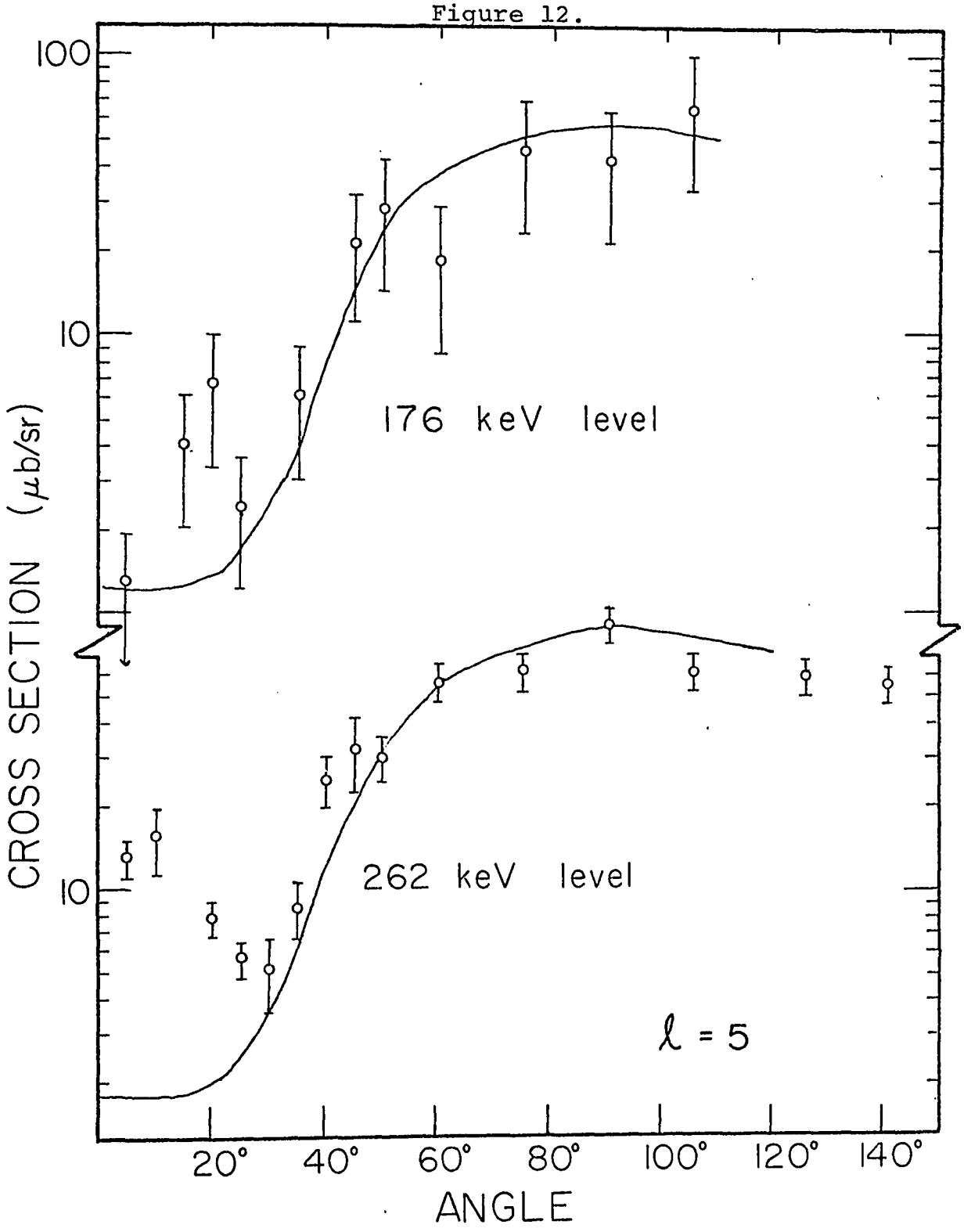

The ℓ=5 angular distributions from the reaction $^{152}Sm(d,t)^{151}Sm$.

$^{152}Sm(^{3}He,\alpha)^{151}Sm$ was originally obtained as a by-product of another experiment. This reaction was performed using 28 MeV beams of ^{3}He particles at the University of Rochester Nuclear Structure Research Laboratory. The reaction products were analyzed at six angles with an Enge-type magnetic spectrograph. This experiment was later repeated with the express interest of obtaining the best possible resolution in order to clear up ambiguities that existed in the first spectra. Spectra at angles 10°, 27.5° and 45° were taken using 24 MeV ^{3}He beams at McMaster. The 24 MeV spectra at 10° and 45° are shown in Figure 13, and the corresponding energies and cross sections are listed in Table 3. The resolution was about 19 keV.

In order to compare the empirical cross section ratios of levels populated in the $(^{3}He,\alpha)$ and (d,t) reactions to the ratios obtained from the DWBA calculations, one must either have accurate values for the normalization factors by which the DWUCK computer output is adjusted to give absolute values, or one must know the ℓ-transfer value for one of the levels so this can be used as a normalization point. The normalization factor 3.33 for (d,t) reactions at 12 MeV is widely accepted, and the value of 23 for 28 MeV $(^{3}He,\alpha)$ data has been used in studies on Yb (Burke et al (1971)) but as some doubt exists about the appropriate normalization factor to use for 24 MeV $(^{3}He,\alpha)$ reactions, the empirical and calculated ratios were normalized by placing the empirical ratio for the level at

Figure 13.

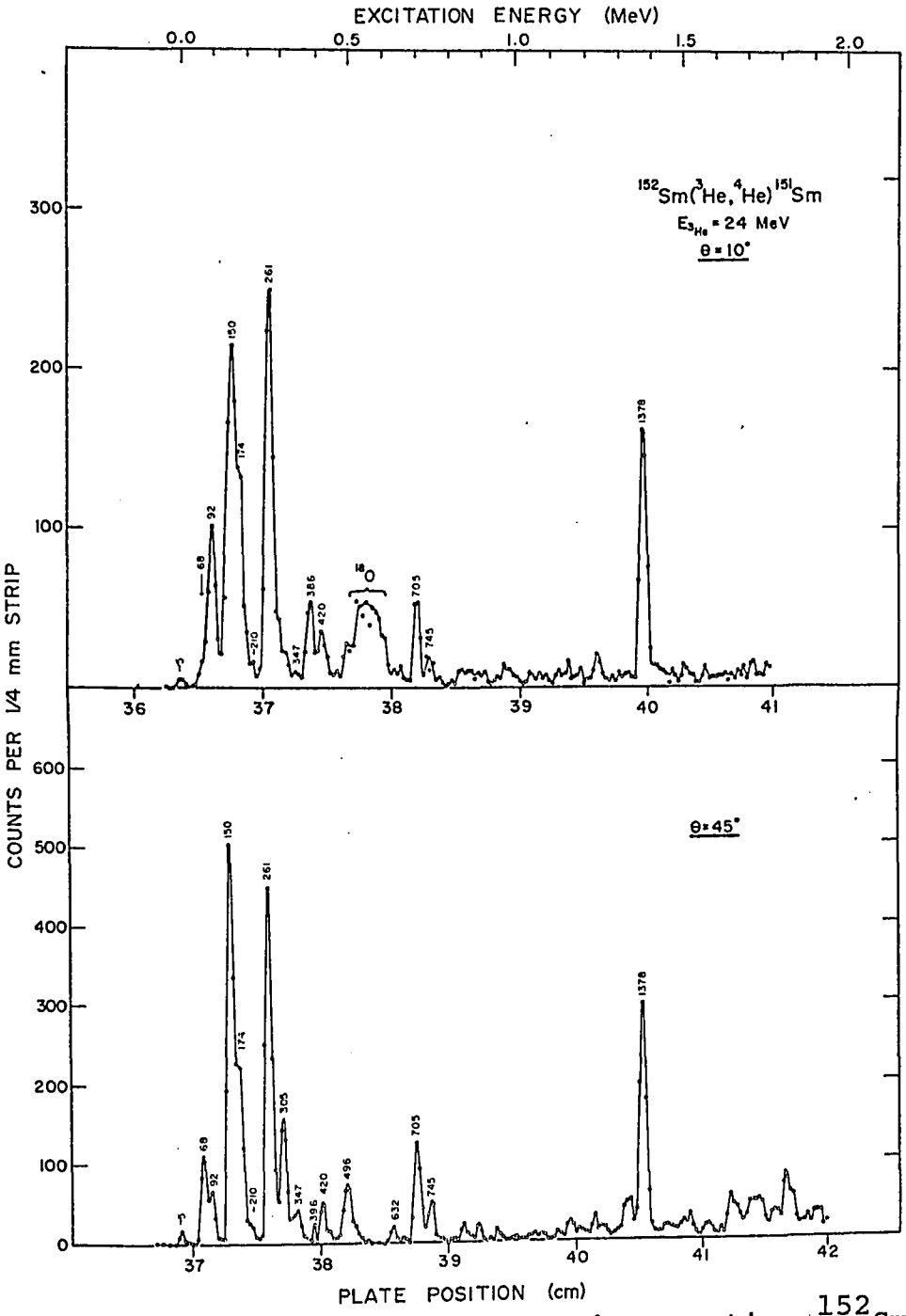

The 10° and 45° spectra of the reaction ^{152}Sm $(^{3}He,\alpha)^{151}Sm$. The numbers above the peaks are the level energies in keV.

261 keV at the calculated position for an ℓ=5 transfer. The (d,t) angular distribution for this level was that for an ℓ=5 transfer, apart from an unexpected forward peaking, (see Figure 12) and the errors on the empirical ratio were small for this level, making it an appropriate choice as a calibration point. In order to check this choice, the theoretical and empirical ratios were calculated for the 28 MeV (^{3}He,α) data using the normalization factor of 23 given for this energy, and indeed, little adjustment was required to put the 261 keV level empirical ratio at the position for an ℓ=5 transfer.

In Figure 14, the results are given for all of the levels populated in both the 12 MeV (d,t) reaction at θ = 60° and the 24 MeV (^{3}He,α) reaction at θ = 45°. In this graph, the solid lines are the corresponding cross-section ratios as calculated by the DWUCK program. The circles give the empirical ratios, adjusted vertically as a group such that the 261 keV level has an ℓ=5 transfer.

Once this calibration has been made, the DWUCK normalization factor for the 24 MeV (^{3}He,α) reaction may be calculated, since the 12 MeV (d,t) value of 3.33 may be assumed accurate. The resulting (^{3}He,α) value is 48. These normalization factors are used in subsequent calculations for which the absolute DWBA cross-sections are required.

Figure 14.

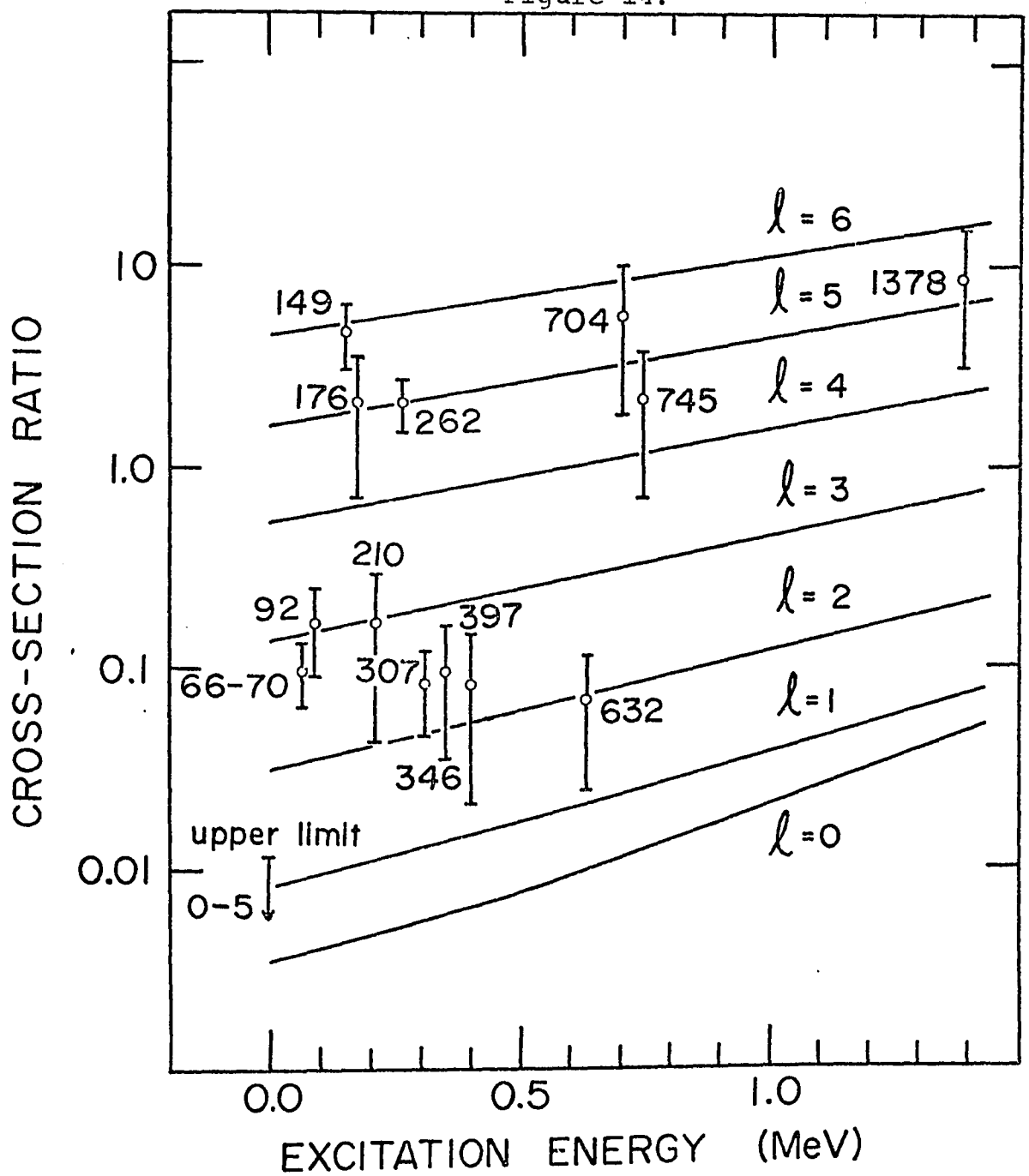

The cross-section ratios for levels populated in both the reactions $^{152}Sm(^{3}He,\alpha)^{151}Sm(\theta=45°)$ and $^{152}Sm(d,t)^{151}Sm(\theta=60°)$. The solid lines are those given by DWUCK calculations. The numbers give the level energies in keV.

B) The $^{150}Sm(d,p)^{151}Sm$ reaction

The reaction $^{150}Sm(d,p)^{151}Sm$ was also performed at McMaster using an incident beam of 12 MeV deuterons. Spectra were taken at only three angles, with no attempt to measure angular distributions. The spectrum at 45° is shown in Figure 15, and a list of energies and cross-sections at 45° and 75° is given in Table 4. The best resolution obtained was about 7 keV.

As in the (d,t) reaction, the position and shape of the peak found in the 0 keV region indicated that it was due almost entirely to the first excited state at 4.8 keV, with at the very most about 30% of the total intensity due to the ground state. Similarly, the position and shape of the strong peak at 66 keV indicate that it is primarily due to the level seen in the decay studies at 65.8 keV, and not that at 69.7 keV. These conclusions differ from those made in the earlier study of this nucleus (Kenefick et al. (1965)) where these two peaks were assigned the energies 0 and 60 keV. Since the resolution obtained in the present study was considerably better than that previously reported (7 keV compared to $\sim$17 keV) it is believed that these conclusions are more accurate.

C) The reactions $^{151}Sm(d,t)^{150}Sm$, $^{151}Sm(d,p)^{152}Sm$ and $^{151}Sm(^{3}He,\alpha)^{150}Sm$

These reactions were performed to try to obtain information on the ground state wave function of ^{151}Sm. The (d,t) and (d,p) reactions were carried out using 12 MeV beams of

Figure 15.

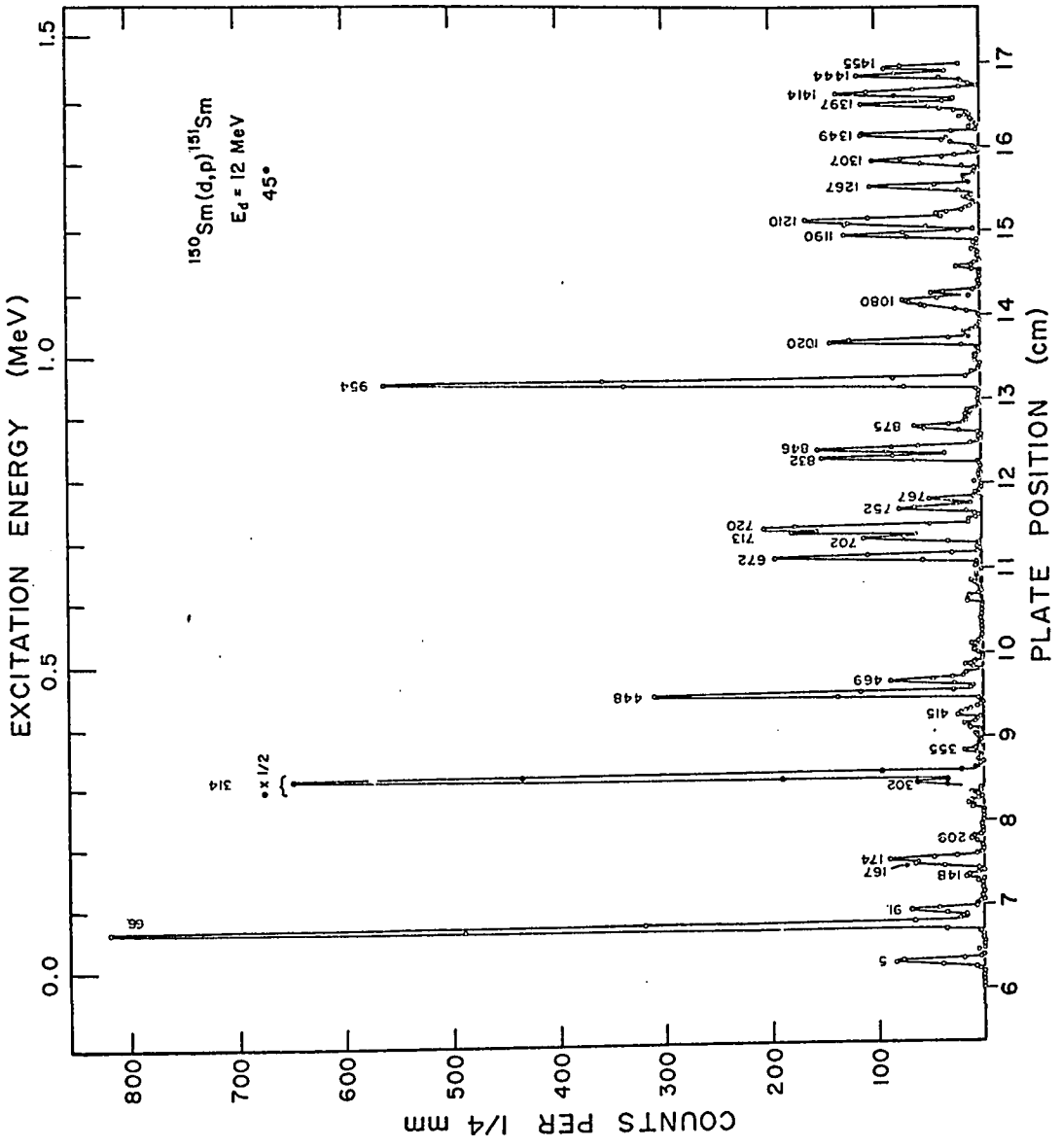

The 45° spectrum of the reaction ^{150}Sm(d,p)^{151}Sm. The numbers above the peaks are the level energies in keV.

Table 4

Energies and Cross-Sections for the Reaction $^{150}Sm(d,p)^{151}Sm$

Energy Other work†	$^{150}Sm(d,p)^{151}Sm$		
	Energy	Cross-Section (μb/sr)	
		45°	75°
4.8	5	124	76
65.8	65.8*	954	664
91.5	91	90	53
148	148	18	65
167.7+168.4	167	76	}165
175.3	174	92	
208.9	209	16	∿8
303	302	132	∿50
313.8+314.9	314	1514	844
	355	18	∿16
416.1	∿415	∿39	∿36
448	448	325	165
470	469	108	54
	672	212	146
	702	∿138	∿77
	713	∿157	∿145
	720	∿270	∿145
	752	102	∿59
	767	44	∿27
	832	171	113
	846	223	200
878?	875	94	66
953.4	954	766	444
	1020	171	124
	∿1080	∿100	∿40
	1190	158	74
	1210	320	212
	1267	124	57
	1307	170	76
	1349	153	100
	1397	138	104
	1414	229	109
	1444	143	80
	1455	110	100

†The energies in this column were determined from a re-examination of the decay of ^{151}Pm and from a study of an isomer in ^{151}Sm (Cook et al, private communication)

*The position of this peak was used as a calibration point.

deuterons. For the (d,t) reaction, spectra were taken at 10 angles. The spectrum at 25° is given in Figure 16 and a list of energies and cross sections for this angle and that at 60° is given in Table 5. For the (d,p) reaction leading into ^{152}Sm, spectra were taken at 4 angles, but in three of these spectra, some members of the ground state band were obscured by impurities in the target. This problem was particularly troublesome in this experiment, due to the similarity in Q-values for the reaction under study and those for the contaminants which tend to be found in most targets. The spectrum taken at 87.5° has a clear ground state band, and is shown in Figure 17. A list of energies and cross sections for the spectra at 50° and at 87.5° is in Table 6.

The reaction $^{151}Sm(^{3}He,\alpha)^{150}Sm$ was performed at an incident energy of 24 MeV. Spectra at 2 angles were taken. Figure 18 and Table 5 give the spectrum, energies and cross sections at 30°. The purpose for taking these spectra was to attempt to determine the relative amounts of $\ell=3$ and $\ell=5$ transfer to the 2^+ level at 334 keV and to the 4^+ level at 774 keV from the cross section ratios for these levels from the $(^{3}He,\alpha)$ and (d,t) reactions. In order to ensure that the calculated cross section ratios were properly normalized, the following procedure was used: After a spectrum for the reaction $^{151}Sm(d,t)^{150}Sm$ had been taken, a short re-run of the reaction $^{152}Sm(d,t)^{151}Sm$ was performed, with no changes in

Figure 16.

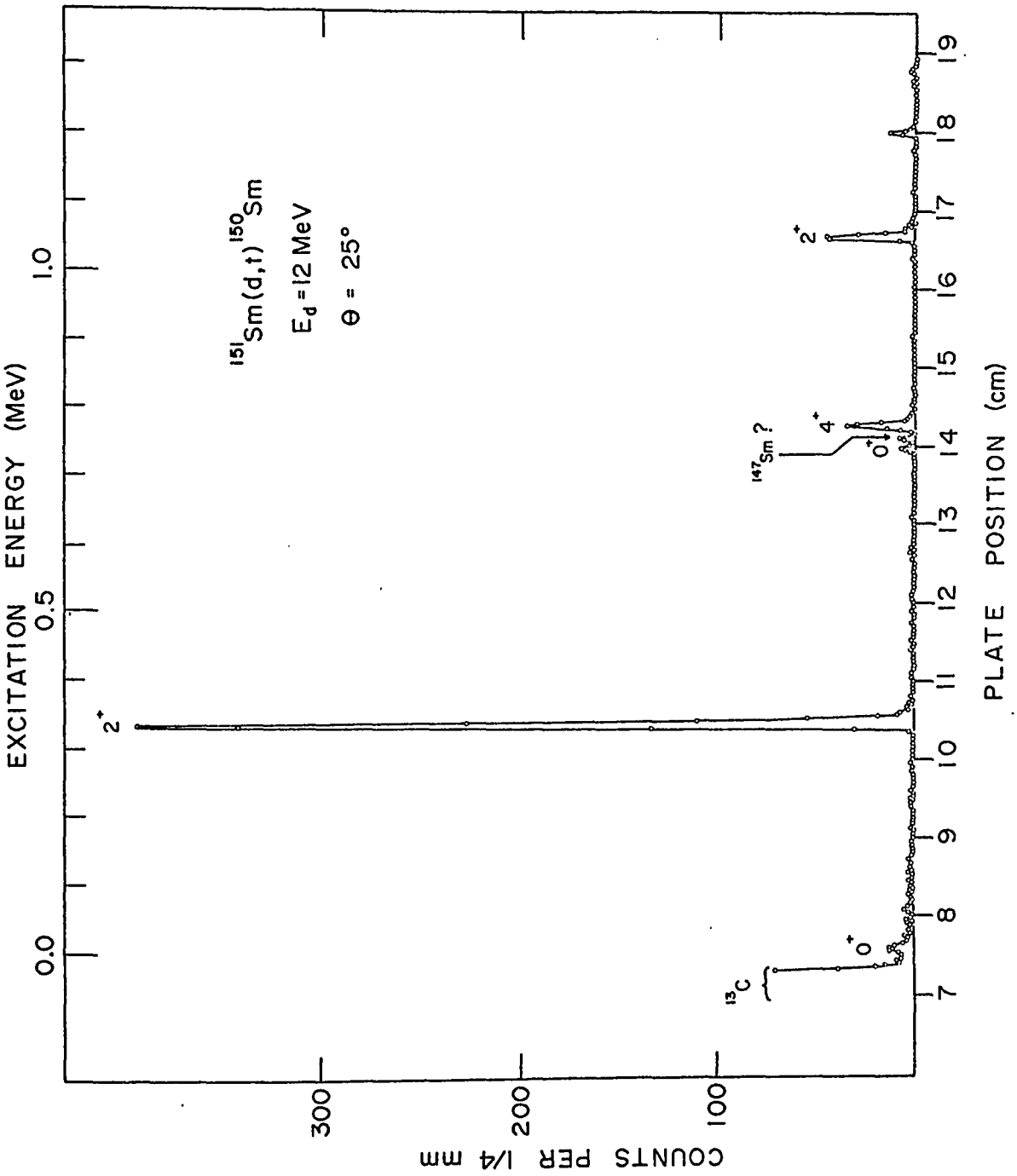

The 25° spectrum of the reaction $^{151}Sm(d,t)^{150}Sm$. The numbers above the peaks are the known spins and parities of the levels.

Table 5

Energies and cross sections for the reactions $^{151}Sm(d,t)^{150}Sm$ and $^{151}Sm(^{3}He,\alpha)^{150}Sm$

$^{151}Sm(d,t)^{150}Sm$			$^{151}Sm(^{3}He,\alpha)^{150}Sm$	
Energy (keV)	Cross Section (μb/sr) 25°	60°	Energy (keV)	Cross Section (μb/sr) 30°
0	† 4	5.8	-	-
334*	86	274	334*	2.3
741	1	∿3	-	-
775	8	33	775	1.2
1049	10	-	-	-
1198	2	-	-	-
			1268	0.5
			1354	0.8
			1683	0.5
			1764	2.5
			1823	2.3

*The position of this peak was used as an energy calibration point.

†The uncertainty in the absolute cross sections listed in this column is larger than that given for other experiments due to difficulties experienced with the monitor counter.

Figure 17.

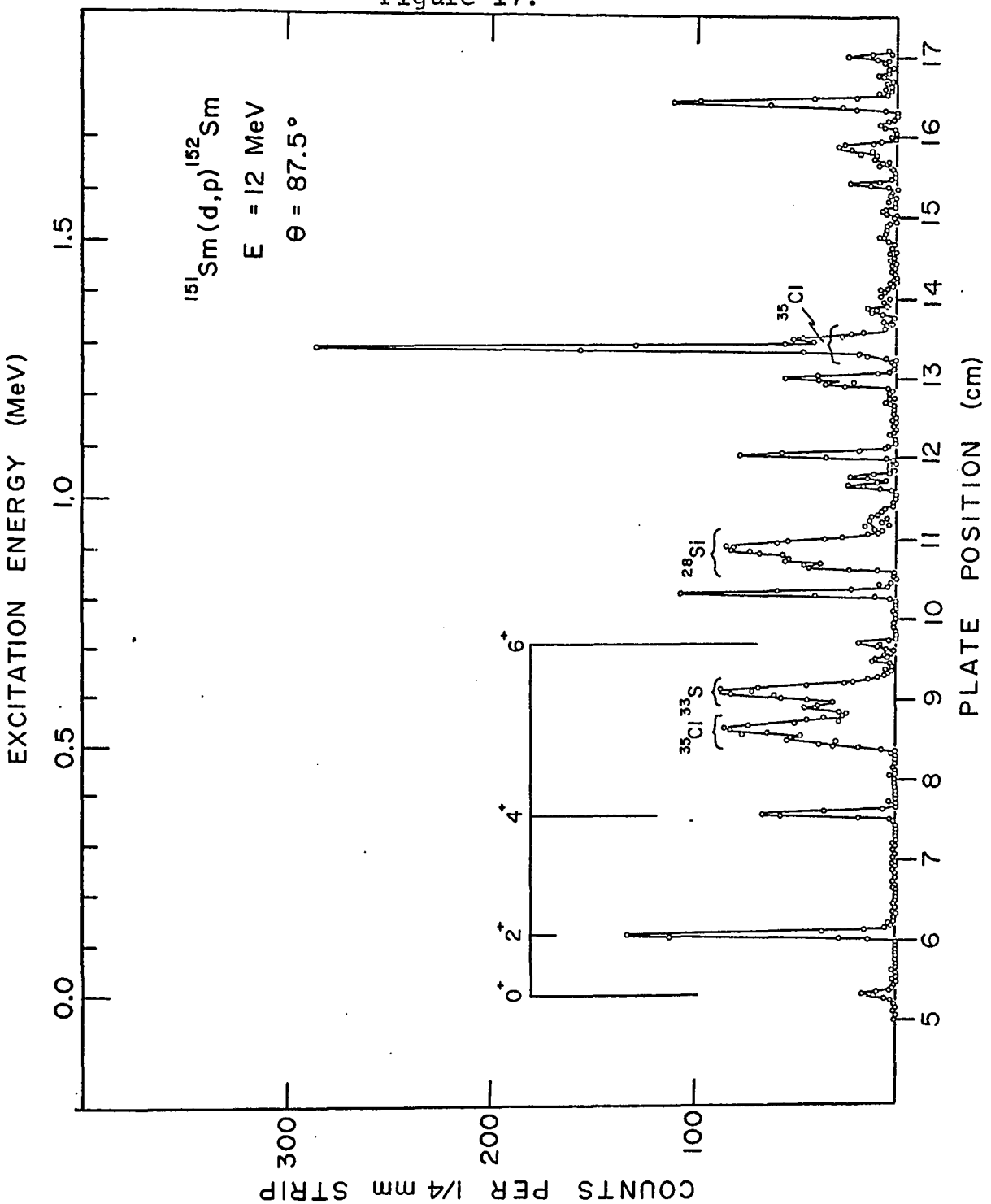

The 87.5° spectrum of the reaction ^{151}Sm(d,p)^{152}Sm. The spins and parities of the peaks due to the ground state rotational band are indicated.

Table 6

Energies and cross sections for the reaction $^{151}Sm(d,p)^{152}Sm$

Energy (keV)	Cross-Section (μb/sr) 50°	87.5°
0	obscured	1.3
122*	21	8.4
366	8.7	4.5
679	1.4	0.9
711	2.2	1.1
812	19	6.0
1025	obscured	1.5
1042	obscured	1.3
1087	obscured	4.9
1223	2.9	1.9
1236	10	3.6
1295	27	16.9
1616	4.1	1.3
1773	21	8.9

*The position of this peak was used as an energy calibration point.

Figure 18.

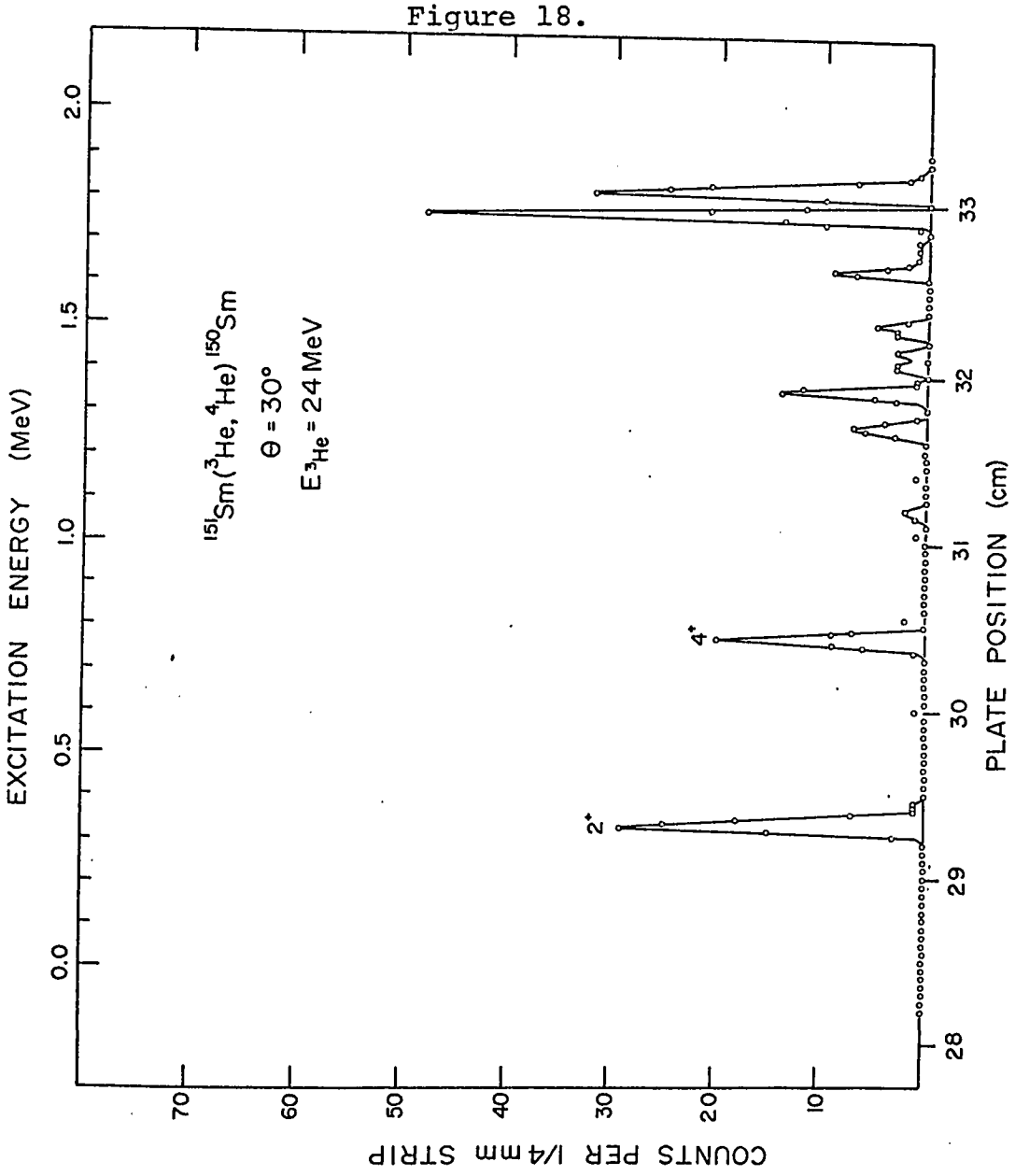

The 30° spectrum for the reaction $^{151}Sm(^{3}He,\alpha)^{150}Sm$.

equipment settings except for the change in target. The same procedure was followed for the corresponding (^{3}He,α) reactions. The calculated cross-section ratio curves were extended over a Q-value range broad enough to include both reactions. In this way, the ℓ=5 transfer ratio to the 261 keV level in ^{151}Sm could be used as a calibration point for the levels in ^{150}Sm. The effective (^{3}He,α) normalization factor obtained from the ratio for the 261 keV level in ^{151}Sm in this experiment was found to be $\sim$ 50, in good agreement with that found in the initial experiment.

The empirical ratios obtained for the 2^+ level at 334 keV and the 4^+ level at 774 keV are given in Figure 19. These ratios are those for the (d,t) reaction at 60° and the (^{3}He,α) reaction at 30°. The solid lines are the calculated DWBA ratios, normalized to the empirical data as discussed above. The other points are the results of theoretical considerations, and will be discussed in a following section.

In the reactions on the ^{151}Sm target, the ground state populations of ^{150}Sm and ^{152}Sm were found to be very weak, indicating that the reverse reactions leading into ^{151}Sm would also result in a weakly populated ground state. This evidence supports the conclusions drawn in the previous two sub-sections concerning the ^{151}Sm ground state intensity.

Figure 19.

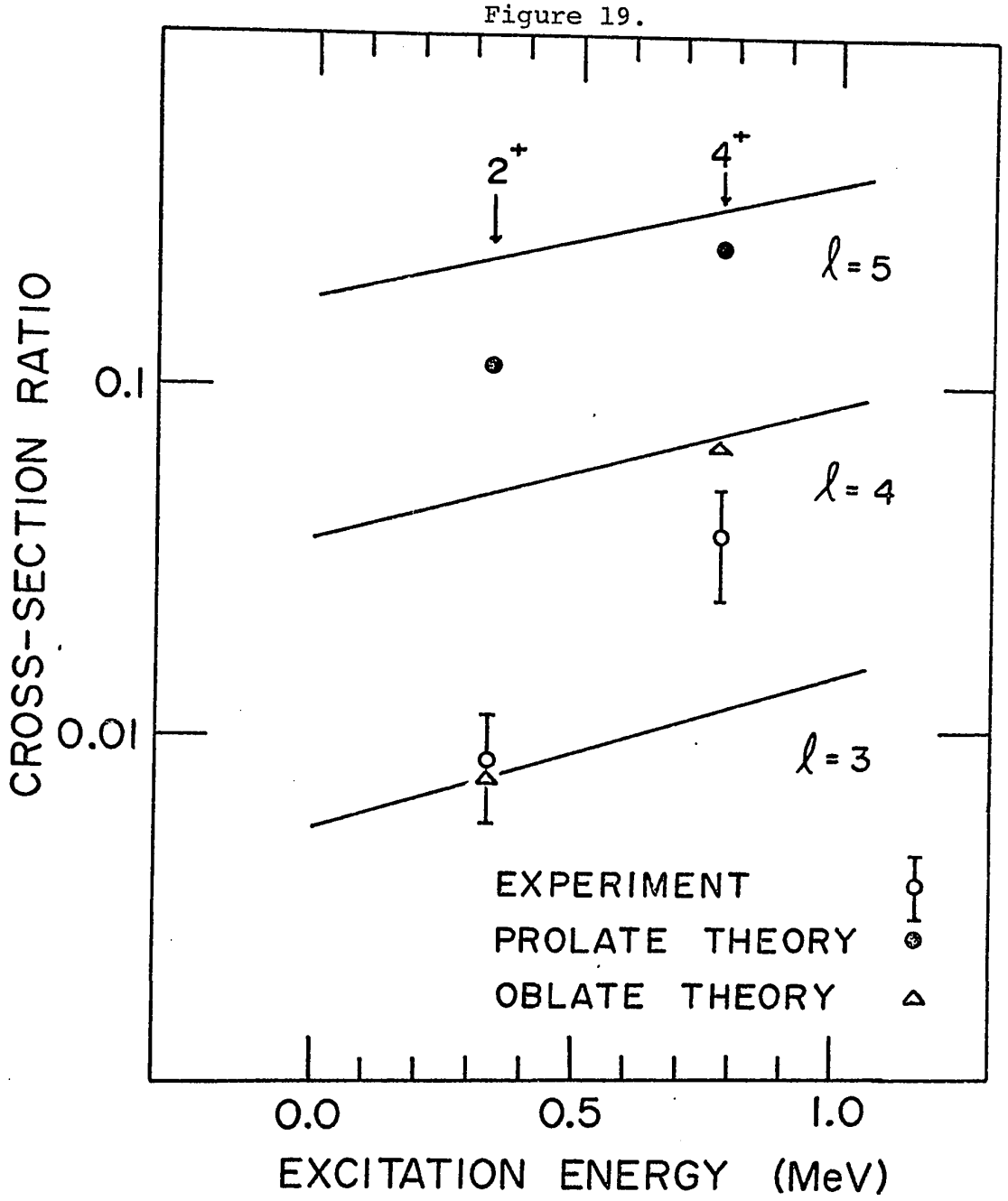

The cross-section ratios for the first 2^+ and 4^+ levels in ^{150}Sm as populated in the reactions $^{151}Sm(^3He,\alpha)^{150}Sm(\theta=30°)$ and $^{151}Sm(d,t)^{150}Sm(\theta=60°)$. The "theoretical" points above are discussed in section 4.4. The solid lines are those given by DWUCk calculations.

3.3 Details of Coulomb excitation and inelastic scattering experiments

The inelastic scattering experiment $^{151}Sm(d,d')^{151}Sm$ was performed at two different beam energies; at 5 MeV, for which nuclear excitation should occur only through the Coulomb interaction, and at 12 MeV, as there exists empirical methods to relate the observed inelastic cross sections to B(E2) values at this bombarding energy (Veje et al. (1968)). The outgoing deuterons scattered from the target were analyzed with the Enge spectrograph, in exactly the same manner as discussed in the previous section on single particle transfer experiments.

The target used was the same as that for the (d,p), (d,t) and (^{3}He,α) reactions on ^{151}Sm. For the inelastic scattering and Coulomb excitation experiments the isotopic impurities in this target accidentally turned out to be rather useful, as they could be used as calibration points, as will be discussed later. While some peaks were obscured by other impurities, these levels were at relatively high excitation energy, and of secondary importance to this investigation.

Spectra were taken at 140° with 5 MeV deuterons and at 90°, 125° and 140° with 12 MeV deuterons. Since the elastic cross section to the ground state is so large compared to the inelastic cross sections, the elastic peaks of the main exposures contained so many tracks as to be completely impossible to count. Therefore a short exposure was taken

after each main exposure, with the length of this short exposure planned such that there would be a reasonable number of tracks in the elastic peak. The short and long exposures were normalized using the ratios of the numbers of elastically scattered particles detected by a small solid state monitor counter placed at 30° from the beam axis. Examples of the spectra obtained at 5 MeV and 12 MeV are given in Figures 20 and 21. The cross sections obtained for all of the spectra are listed in Table 7. The cross section given for the ground state at 5 MeV is that calculated from the Rutherford formula, while those listed for the 12 MeV spectra are values obtained from interpolation of empirical results obtained for ^{150}Sm and ^{152}Sm at this energy. (Christensen et al, (1969)). The inelastic cross sections are determined relative to the elastic cross-sections.

The last column in Table 7 gives the ratio R of the 12 MeV cross-sections at 90° to those at 125°. As discussed in section 2.3, these ratios have been found empirically to give a good indication for the multipolarity of a Coulomb excitation transition. The ratios obtained for the peaks in the spectrum due to the first excited states of the ^{150}Sm and ^{152}Sm isotopic impurities are 2.18 and 2.47 respectively. These values are slightly higher than those reported by Veje et al, (1968) for these E2 transitions in ^{150}Sm and ^{152}Sm. This is not a serious discrepancy, as the uncertainties on

Figure 20.

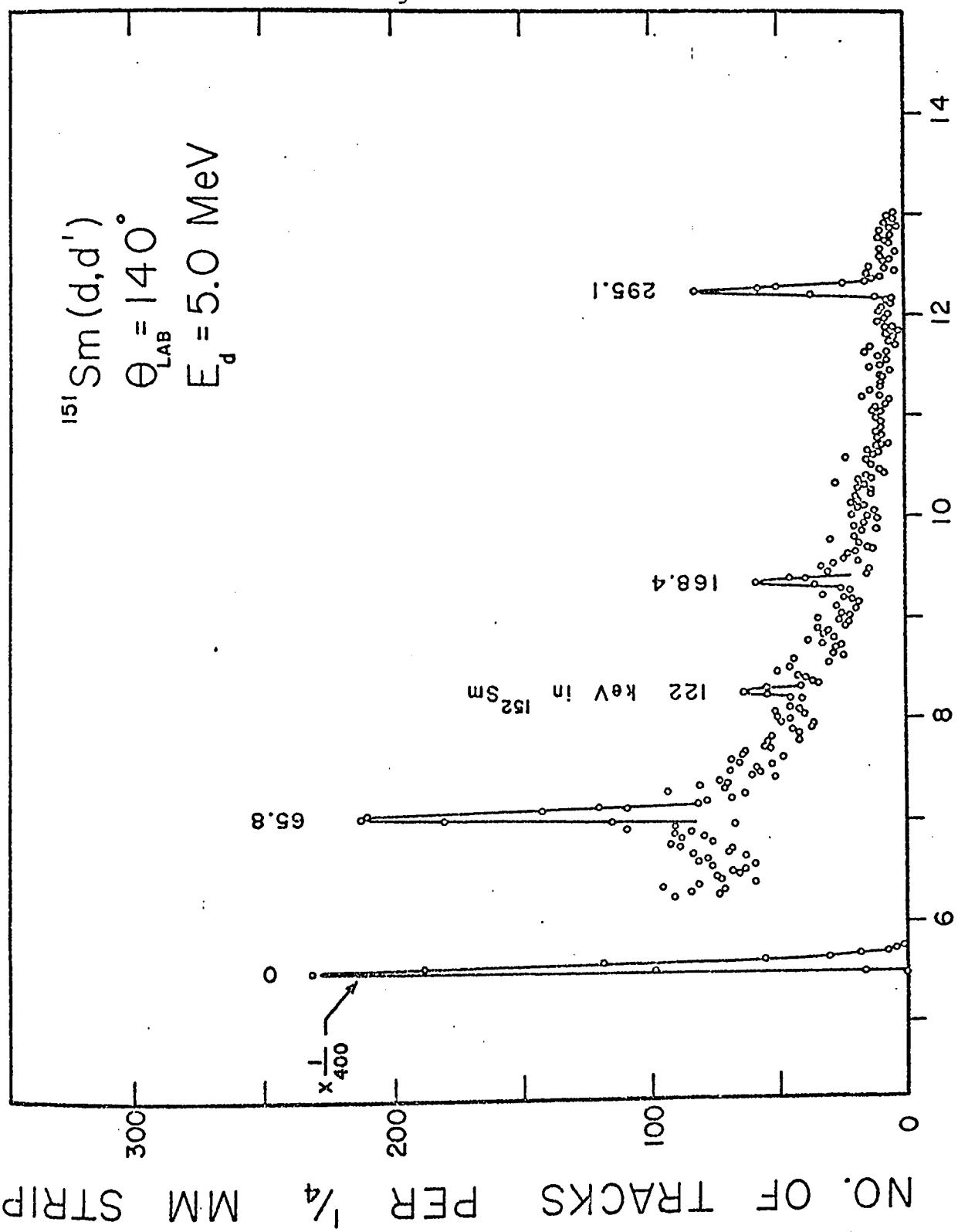

The spectrum of deuterons from the ^{151}Sm(d,d') reaction at 5 MeV. The numbers above the peaks are the excitation energies in keV. The high background is due to the tail of the large elastic peak.

Figure 21.

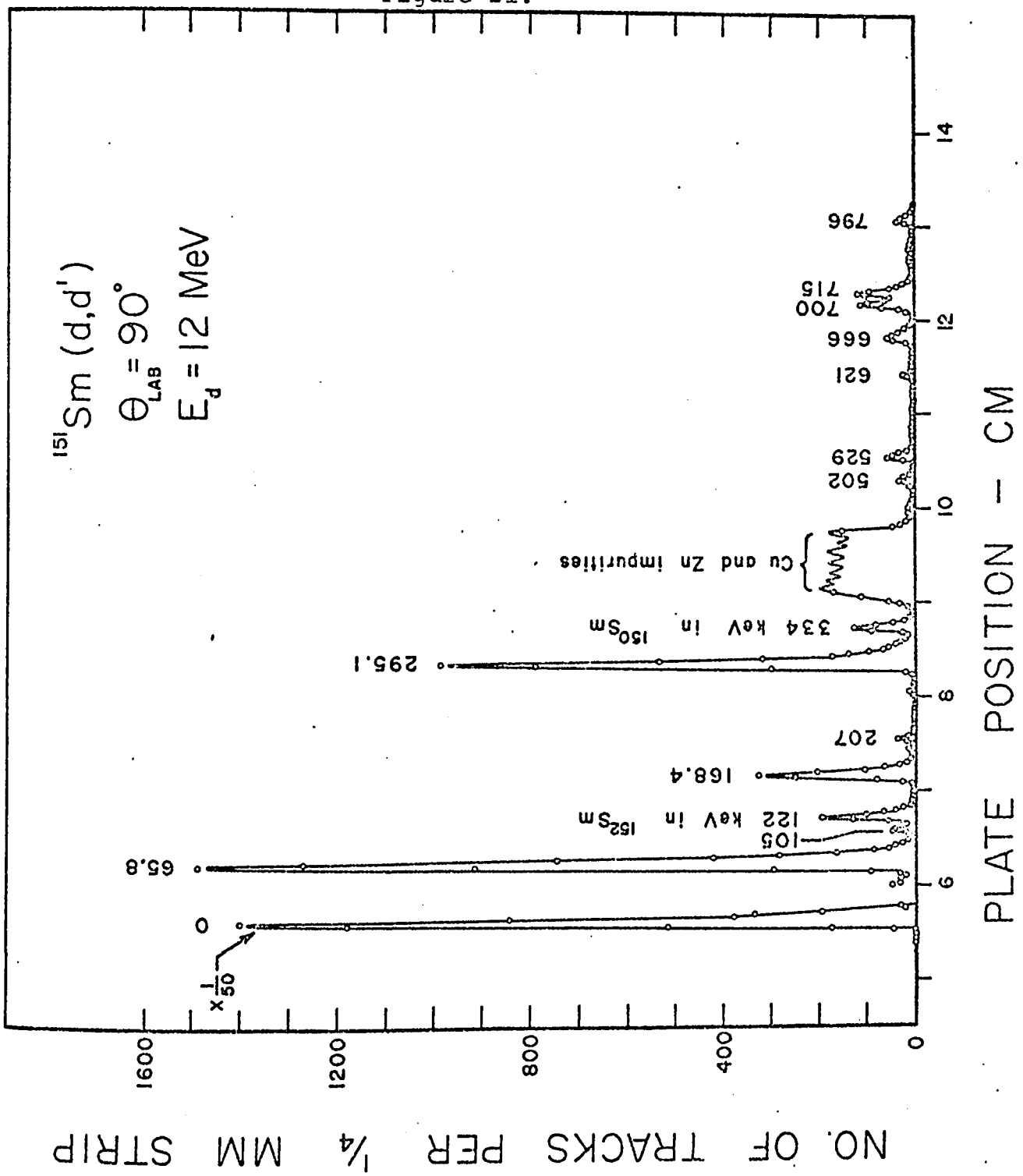

The spectrum of deuterons from the ^{151}Sm(d,d') reaction at 12 MeV. The numbers above the peaks are the excitation energies in keV.

Table 7

Inelastic scattering cross sections for states in ^{151}Sm

Energy keV	Cross section, μb/sr: 5 MeV θ = 140°	12 MeV θ = 90°	12 MeV θ = 125°	12 MeV θ = 140°	$R = \frac{d\sigma}{d\Omega}(\theta = 90°) / \frac{d\sigma}{d\Omega}(\theta = 125°)$	
0	262,000[a]	43,200[b]	9200[b]	6800[b]		
66	525 ± 50	1050	433	371	2.42	
105		20	7		~2.8	
122 (^{152}Sm)		4250(3700)[c]	1715(1820)[c]	1560	2.47	
168	85 ± 17	201	100	84	2.0	
207		13	5.9		2.2	
295	228 ± 18	655	282	236	2.32	
334 (^{150}Sm)		1990(1880)[c]	913(970)[c]	≤1020	2.18	
420		obscured	30	28		(a doublet?)
502		18	12	4	1.5	
529		31	14	10	2.2	
666		42	obscured	25		(a doublet)
700		72	obscured	50		
715		82	obscured	31		
796		21	obscured	14		

a) The elastic scattering cross-section was assumed to be the Rutherford value.

b) The elastic scattering cross-section was interpolated from the values used for ^{150}Sm and ^{152}Sm by Veje *et al.* (1968).

c) The first entry is the cross section obtained from the present results using the percentage composition stated in Table 1 for this isotopic impurity. The more reliable cross sections of Veje *et al.* (1968) are shown in brackets for comparison.

the relative cross sections is about 10-15% in this work, and one may in fact, use these ratios for transitions of known E2 multipolarity as a built-in calibration for the ^{151}Sm ratios. The relatively strong levels populated at 66 keV and 295 keV in ^{151}Sm have R values of 2.42 and 2.34, respectively, and thus the transitions leading to these states most likely have E2 multipolarity. Other levels for which the R-values indicate E2 transitions are those at 105, 168, 207 and 529 keV. In the next section, the spins and parities of the levels seen in the decay and single particle transfer studies at 104.8, 168.4, and 209.0 keV are shown to be consistent with the multipolarities assigned above.

The level seen at 502 keV is probably the 1/2+ level seen in the (d,t) reaction at 503 keV, and thus the multipolarity would have to be M2 or E3. The cross section ratio given for this level in Table 7 is similar to those measured by Veje et al. (1968) for E3 transitions. Levels at 700, 715, and 796 keV were obscured due to target impurities in the 125° spectrum, and therefore the ratios R could not be found. On the basis of the relative cross sections at 90° and 140°, one may speculate that the transition to the level at 715 keV has E2 multipolarity, while those to the 700 and 796 keV levels are of some higher order.

For the 5 MeV data, the B(E2) values for the various states populated could be directly extracted from the ratio of inelastic to elastic intensities as the excitation mechanism

at this energy will be purely due to the Coulomb field. In order to extract B(E2) values from the 12 MeV data, use has been made of the empirical conversion factors established by Veje et al. (1968) for converting inelastic scattering cross sections at 12 MeV to B(E2) values. These investigations list conversion factors at angles 90°, 125° and 155° for the nuclei ^{150}Sm and ^{152}Sm. Although there is a rather large difference (about 40%) in the conversion factors for these two nuclei, values for ^{151}Sm were obtained by simply interpolating between these values. In order to obtain a conversion factor at the angle 140°, it was necessary to make a second interpolation between the angles of 125° and 155°. In Table 8, the B(E2) values determined from the 5 MeV data are listed in the first column. The second column gives the average of the values obtained at all three angles for the 12 MeV data. In spite of the interpolations made to obtain the 12 MeV B(E2) values, the agreement between the 5 MeV and 12 MeV values is quite satisfactory for those levels observed in both experiments.

On the basis of these measurements alone it was not possible to determine which of the levels reported in the decay work had been populated in these experiments, as the best resolution obtained was about 5 keV. The strong peak at 66 keV could perhaps result from either the level reported at 65.8 keV or that at 69.7 keV, or both. Similarly, it could not be determined how the intensity observed at 168 keV

Table 8

B(E2) Values for the Population of States in ^{151}Sm

Energy	B(E2) Values in units of $e^2(barn)^2$	
	From 5 MeV data[a]	Average Value from 12 MeV data[b]
66	0.82 ± 0.08	0.75
105		0.013
168	0.14 ± 0.03	0.16
207		0.010
295	0.45 ± 0.04	0.48
529		0.023
715		0.064

a) The uncertainties indicated are standard deviations due to counting statistics only.

b) The standard deviations due to counting statistics on the values in this column are all less than 6% but there is a fairly large uncertainty in the normalization, as described in the text.

was distributed over the 167.7-168.4 keV doublet.

It was possible to clear up these ambiguities by accurately measuring the energies of the decay gamma rays resulting from the Coulomb excitation of the ^{151}Sm target. Since the only target available for these studies (that used in the previous study) was rather thin ($\sim$20 $\mu g/cm^2$) and was mounted on a carbon backing of $\sim$100 $\mu g/cm^2$, it was necessary to choose an incident beam which would minimize the interference from the carbon backing. This condition was met using a beam of ^{35}Cl ions at 50 MeV, for which the centre of mass energy on the carbon backing was too low to result in any nuclear reactions. At the same time, appreciable excitation of the ^{151}Sm target occured, and spectra could be taken. Two Ge(Li) detectors, with active volumes of 0.9 cm^3 and 50 cm^3 were positioned outside a small, thin-walled (1 mm thick) stainless steel target chamber at distances of 2 and 15 cm from the target and angles 90° and 55° respectively from the beam direction. The spectra obtained, with room background subtracted, are displayed in Figures 22 and 23. The resolution of the small detector was about 700 eV at 100 keV photon energy; however the peak widths of some of the lines were determined by Doppler broadening due to nuclei recoiling out of the thin target and decaying in flight.

Energy and efficiency calibrations for the two detectors were carried out by placing a ^{151}Pm source at the target position. The relative photon intensities in this decay are

Figure 22

The gamma-ray spectrum following Coulomb excitation of ^{151}Sm by 50 MeV $^{35}C\ell$ ions. This spectrum was taken with a 0.9 cm^3 Ge(Li) detector. The asterisks designate known impurity lines.

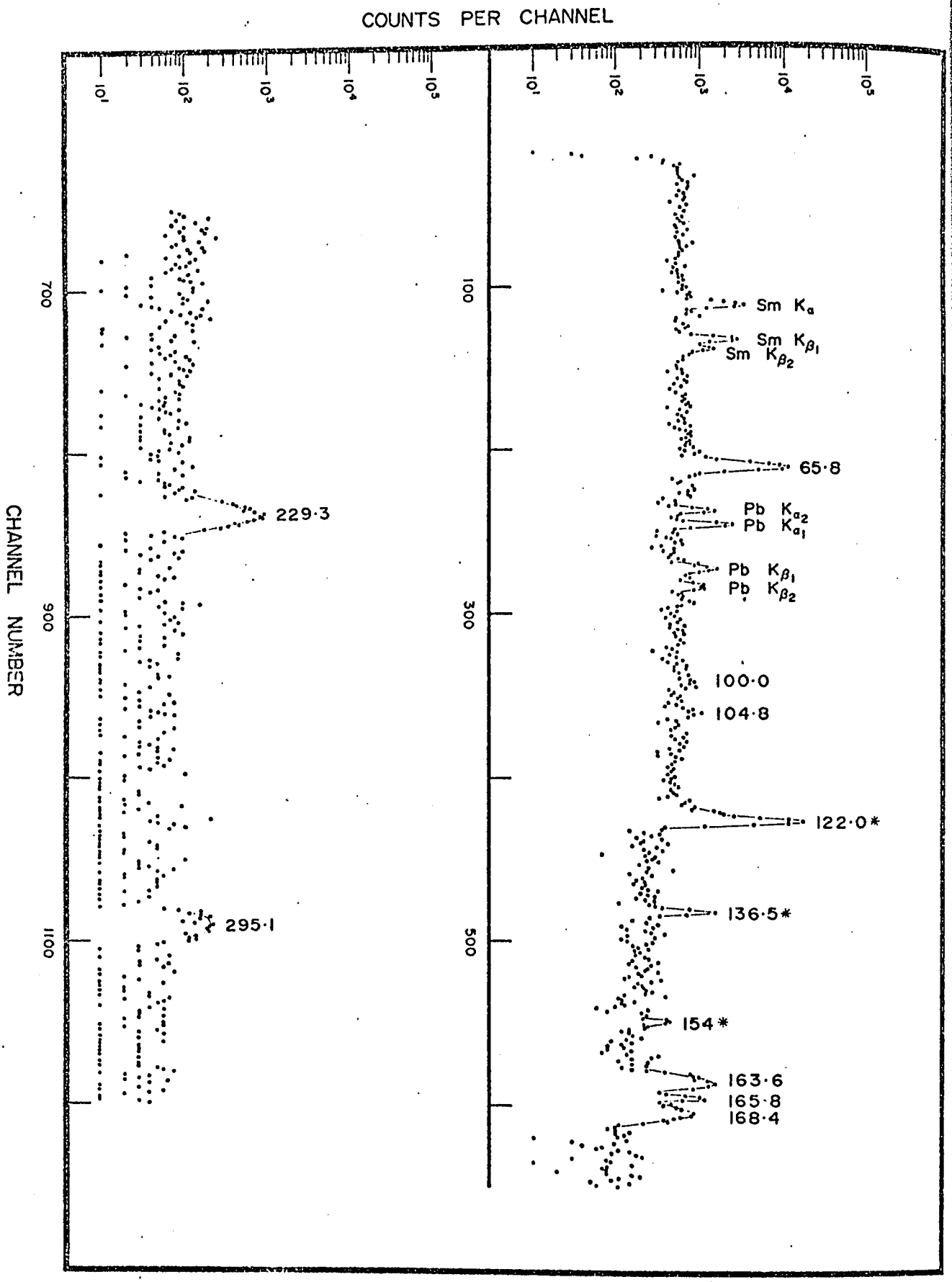
COUNTS PER CHANNEL
CHANNEL NUMBER
229·3
295·1
Sm Kα
Sm Kβ1
Sm Kβ2
65·8
Pb Kα2
Pb Kα1
Pb Kβ1
Pb Kβ2
100·0
104·8
122·0*
136·5*
154*
163·6
165·8
168·4

Figure 23

The gamma-ray spectrum following Coulomb excitation of ^{151}Sm by 50 MeV $^{35}C\ell$ ions. This spectrum was taken with the 50 cm^3 Ge(Li) detector which has a higher efficiency for the 295.1 and 229.3 keV transitions than the small detector used to obtain the spectrum in Fig. 3. The asterisks designate known impurity lines.

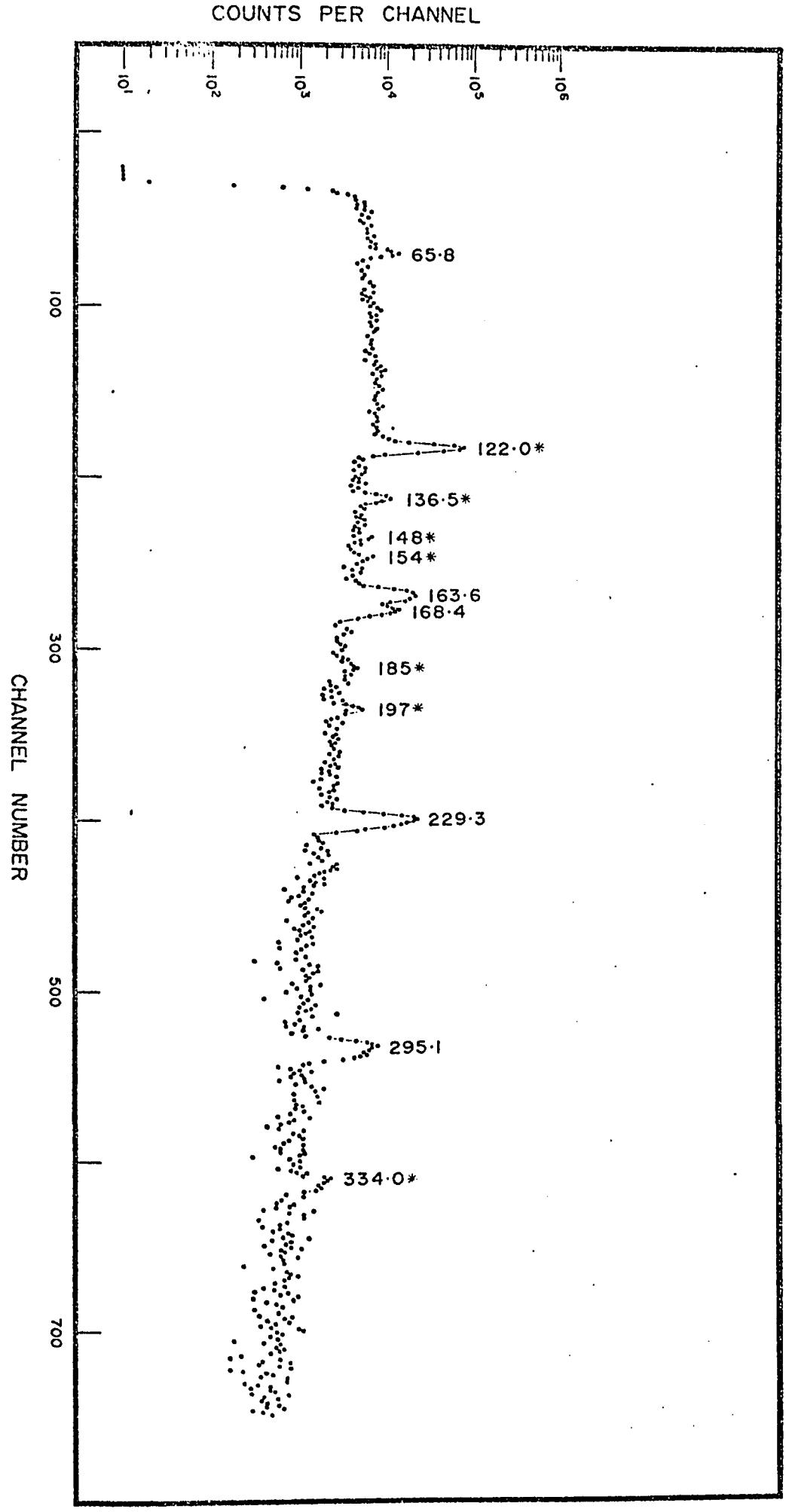
COUNTS PER CHANNEL
10¹
10²
10³
10⁴
10⁵
10⁶
CHANNEL NUMBER
1
100
300
500
700
65·8
122·0*
136·5*
148*
154*
163·6
168·4
185*
197*
229·3
295·1
334·0*

quite well known from investigations done at McMaster and from the work of Ewan et al. (1964); these were used to determine the combined energy dependence of the detector efficiency and the absorption in the target chamber. In Table 9, a list of the gamma rays seen in this experiment is given, as well as the relative photon intensities for the lines originating from ^{151}Sm. These intensities have been corrected for efficiency and absorption, but not for possible angular distribution effects. Several lines due to impurities are listed and identified in this table. No attempt was made to determine absolute gamma-ray yields, as B(E2) values could be obtained much more reliably from the inelastic scattering data.

It is clear from these measurements that the 65.8 keV level is being populated, and not the 69.7 keV level, and likewise, the 168.4 and not the 167.7 keV level is being populated. The level seen at 295 keV in the (d,d') spectra is found to have energy 295.1 keV from the gamma ray work. This level, which has not been previously reported, decays to the 65.8 and to the 0 keV levels.

Figure 24 gives a partial level scheme for ^{151}Sm showing the levels populated in these inelastic scattering and Coulomb excitation experiments and the decay transitions of these levels. The spins and parities assigned to these levels are discussed in the following section.

Table 9

Gamma Rays Observed following Coulomb Excition of ^{151}Sm by 50 MeV ^{35}Cl ions

Energy	Identification	Intensity[a]		
		0.9 cm^3	50 cm^3	Mean
65.8	^{151}Sm	106 ± 7.0		106 ± 7.0
100.0	^{151}Sm	2.4 ± 1.2		2.4 ± 1.2
104.8	^{151}Sm	3.6 ± 1.2		3.6 ± 1.2
122.0	$^{147}Sm, ^{150}Sm, ^{57}Fe$			
136.5	^{57}Fe			
148				
154				
163.6	^{151}Sm	49.3 ± 4.4	80.0 ± 6.3[b]	49.3 ± 4.4
165.8	^{139}La			
168.4	^{151}Sm	28.5 ± 3.4		28.5 ± 3.4
185	^{65}Zn			
197	$^{151}Eu, ^{147}Sm$			
229.3	^{151}Sm	100 ± 8.5	100 ± 6.7	100 ± 7.5
295.1	^{151}Sm	54.3 ± 6.0	60.2 ± 4.8	57.6 ± 4.8
334	^{150}Sm			

a) Intensities have been calculated only for those gamma rays definitely assigned to ^{151}Sm.

b) corrected for ^{139}La impurity

Figure 24

A partial level scheme for ^{151}Sm showing the levels populated in the inelastic scattering and Coulomb excitation experiments. The 12 MeV (d,d') spectra exhibited peaks corresponding to all levels shown except the 4.8 keV state. The upward pointing arrows indicate the excitations resulting from Coulomb excitation with 50 MeV ^{35}Cl ions and the downward transitions show the observed decay modes.

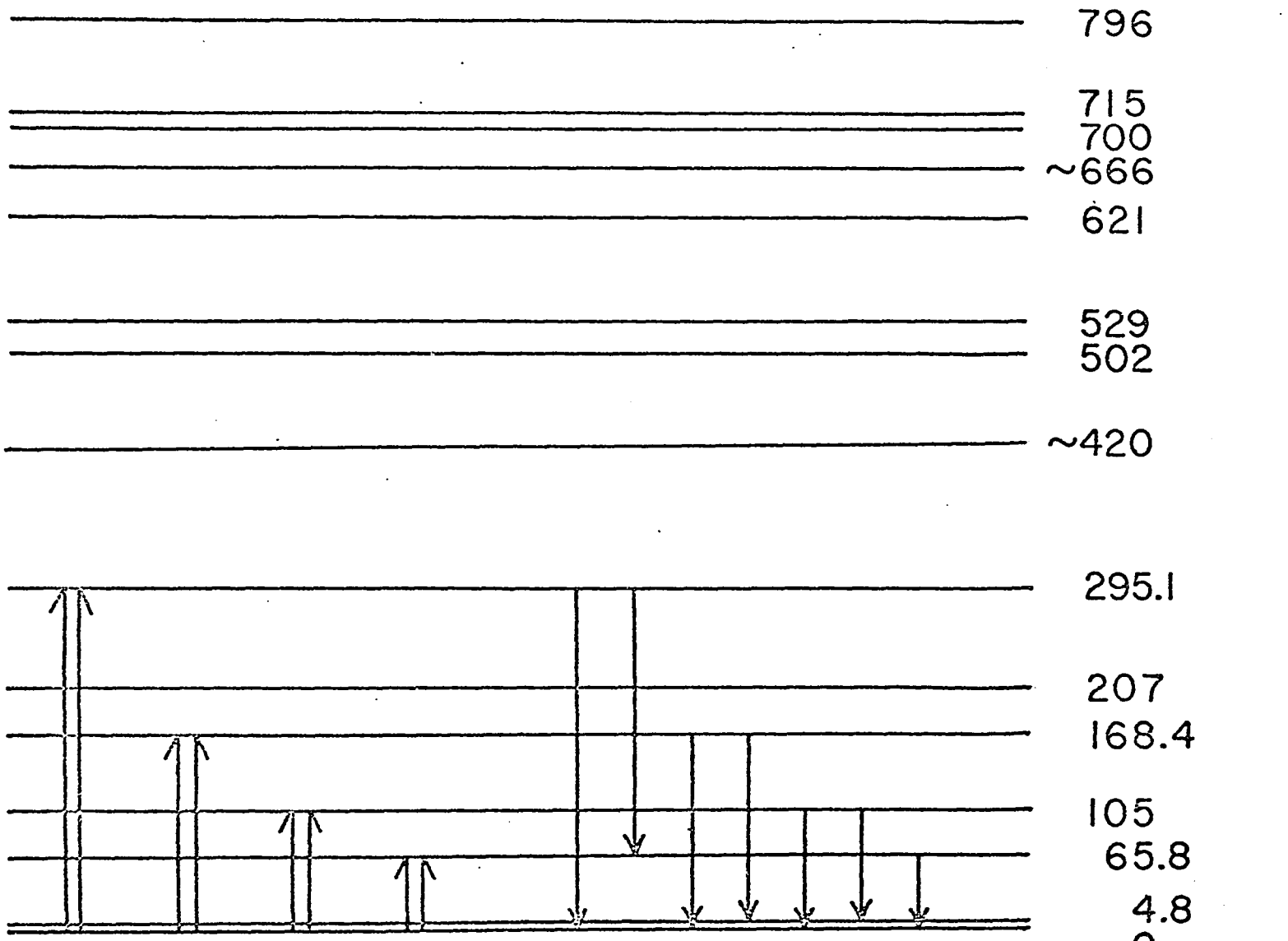
796
715
700
~666
621
529
502
~420
295.1
207
168.4
105
65.8
4.8
0
ENERGY – KEV

^{151}Sm

CHAPTER IV

DISCUSSION OF RESULTS

4.1 Assignment of spins and parities

As no spins and parities had been reliably assigned to levels in ^{151}Sm before this work was undertaken, in this section the results of the decay studies are combined with the results from the present experiments in order to determine spins and parities for as many levels as is possible. A level scheme for the low-lying states in this nucleus is given in Figure 25. The spin and parity assignments in this diagram are established below. The measured γ-ray multipolarities referred to in this section are taken from Bertelsen et al. (1964). Also, reference is made to the newer investigation of the ^{151}Pm decay that is presently under way at this laboratory (Cook et al., private communication).

In many instances, the argument will be made that transitions between levels of different parity will be of E1 multipolarity. This assumption is probably good, as M2 or E3 transitions would be several orders of magnitude slower than E1 transitions, and would not likely be seen where such decays must compete with M1 or E2 transitions.

The spins of two levels, at 148 keV and 261 keV are determined partly through model dependent arguments. These

Figure 25.

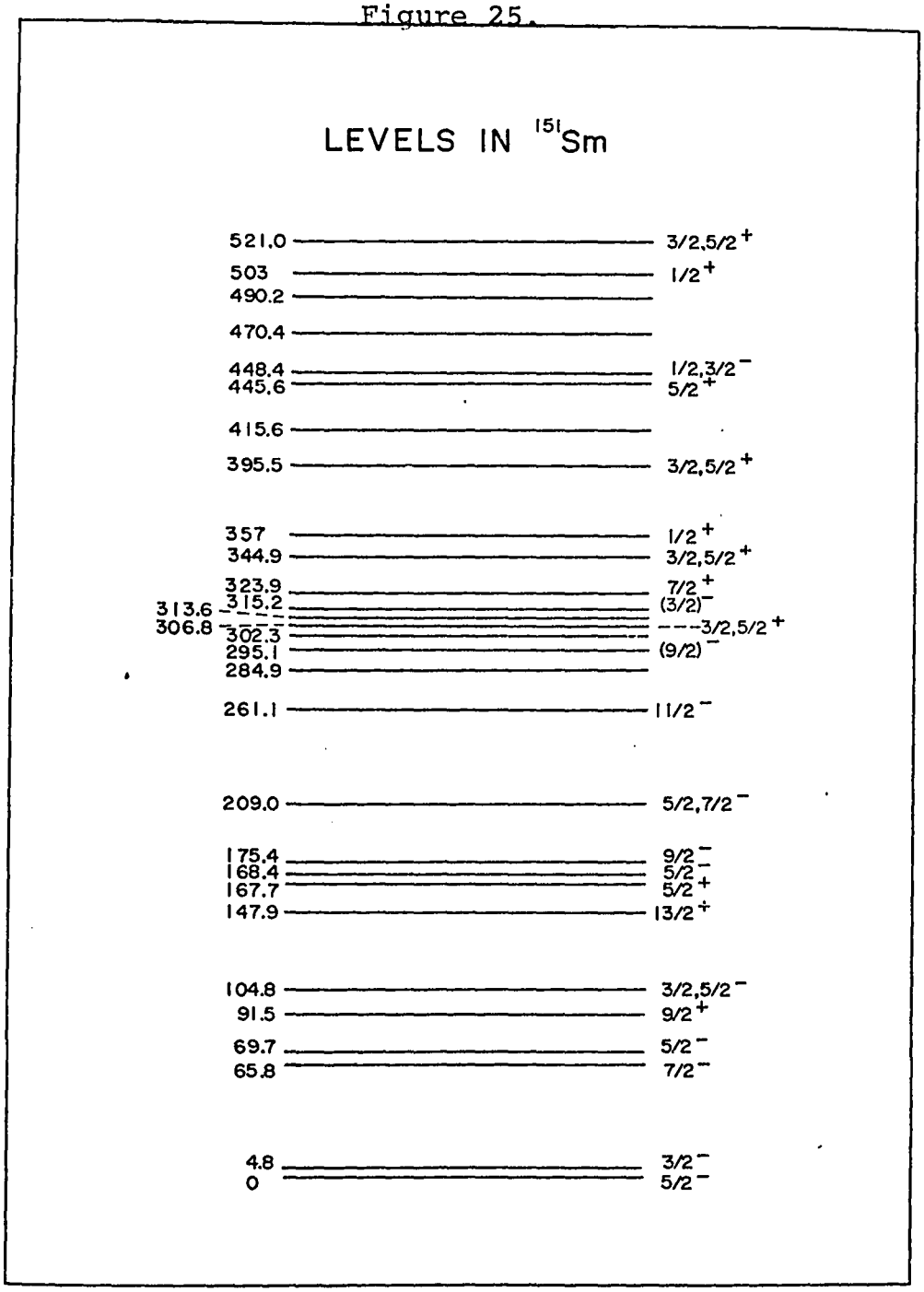

The low-lying levels in ^{151}Sm. The spins and parities given here are deduced in Section 4.1.

two levels are discussed first, and the rest in order of increasing energy.

1) The 148 keV level

A very intense peak appears in the (^{3}He,α) spectra at 150 keV and may be identified with the level seen at 148 keV in the study of an isomer in ^{151}Sm (Cook et al., private communication). The (^{3}He,α) to (d,t) cross-section ratio for this level is that for an ℓ=6 transfer (Figure 14). It is reasonable to assume that this is one of the $13/2^+$ levels stemming from the $i_{13/2}$ orbital, as observed in the studies on ^{153}Gd and ^{155}Gd. No strongly populated $11/2^+$ levels would be expected at this energy on the basis of either the spherical or deformed shell models.

2) The 261 keV level

An isomeric state at 261 keV was originally found to have a half-life of 9 ± 3 μsec (Borggreen et al. (1970)). A newer investigation of this isomer, undertaken at this laboratory (Cook et al., private communication), revealed the half-life to be somewhat shorter, about 1.4 μsec. This isomer may be identified with the level populated in the (d,t) and (^{3}He,α) reactions at 262 keV. The strong population of this level in the (^{3}He,α) reaction indicates that it has high spin. The (d,t) angular distribution was that for an ℓ=5 transfer (Figure 12), the cross section ratio for the 28 MeV (^{3}He,α) and 12 MeV

(d,t) data indicated an ℓ=5 transfer, and in fact the cross section ratio for the 24 MeV (^{3}He,α) and 12 MeV (d,t) data (Figure 14) was used as a calibration point (see section 3.11). The spin and parity must then be $9/2^-$ or $11/2^-$. Low lying $11/2^-$ isomers have been identified in several other nuclei in this region (cf Tjøm (1968)) and ascribed to the $11/2^-$[505] Nilsson orbital. It is therefore very reasonable to assume the 261 keV isomer to have spin $11/2^-$.

3) The ground state and the first excited state

The ground state is populated at most very weakly in all reactions performed, and so no direct measurement of the spin and parity of this state could be obtained from these experiments.

In contrast to this, the (d,t) angular distribution obtained for the 4.8 keV level is certainly that for an ℓ=1 transfer (Figure 7). Further evidence supporting this conclusion comes from the (^{3}He,α)/(d,t) cross section ratio obtained for the 4.8 keV state. In the (^{3}He,α) reactions only a very small peak was found in the ground state region, so small that a considerable amount of its intensity could have been due to impurities. Even so, the upper limit for the cross section ratio for this level is much lower than that required for an ℓ=2 transfer (Figure 14). Since the (d,t) angular distribution eliminates the possibility of an ℓ=0 transfer, it is

concluded that the transfer leading to the 4.8 keV state is $\ell=1$, and therefore the spin and parity of this state must be either $1/2^-$ or $3/2^-$. It has been shown in the decay studies (Geiger et al. (1963)) that the 4.8 keV level decays to the ground state via an M1 transition. Also, the ground state spin has recently been measured using a paramagnetic resonance technique (Robertson et al. (1971)) and found to be 5/2.

With this information, one may deduce that the spins and parities of the ground state and first excited state are $5/2^-$ and $3/2^-$ respectively.

4) The 65.8 keV level

The level at 65.8 keV decays to the $5/2^-$ ground state and the $3/2^-$ first excited state, and is fed by the $11/2^-$ isomer. The observed half life of the $11/2^-$ level, 1.4 μsec, is too short for transitions of multipolarity greater than M1 or E2. (Weisskopf estimates for the half-life of states decaying by M2 or E3 transitions of this energy are listed by Lederer et al. (1967) as 10^{-4} and 10^{-1} seconds respectively, while those for M1 and E2 transitions are 10^{-11} and 10^{-6} seconds.) The 65.8 keV level was strongly populated via an E2↑ transition in the inelastic scattering experiments. The spin and parity of this level must therefore be $7/2^-$. This conclusion is supported by preliminary results from the reaction $^{149}Sm(t,p)^{151}Sm$ (Burke et al., private communication). In this reaction, the 65.8 keV level was strongly populated by an

ℓ=0 transfer. Since the ground state of ^{149}Sm is known to have spin $7/2^-$, the spin and parity of the 65.8 keV level will also be $7/2^-$.

Bertelsen et al. (1964) have reported an E2, M1 admixture for the transition from the 65.8 keV level to the $3/2^-$ level at 4.8 keV. This multipolarity assignment is believed to be incorrect.

5) The 69.7 keV level

The level at 69.7 keV decays by an M1 transition to the ground state and by an E2, M1 admixture to the first excited state, and must therefore have spin $3/2^-$ or $5/2^-$. It is fed by a $7/2^+$ level at 324 keV (the spin and parity of this level are established later). The 324-69.7 keV transition is most probably E1 and therefore the spin and parity of the 69.7 keV level is $5/2^-$.

It was not possible to resolve the 65.8-69.7 keV doublet in the (d,t) experiment, but since the spins of these levels are $7/2^-$ and $5/2^-$, the ℓ-transfer to the doublet should be ℓ=3. Both the (d,t) angular distribution and the cross section ratio are in fact those for ℓ=3 transfers, (Figures 11 and 14), and thus are consistent with these assignments.

6) The 91.5 keV level

The 91.5 keV level is fed by the $13/2^+$ level at 148 keV and the $11/2^-$ level at 261 keV, and is found to decay to the

65.8 keV level via an E1 transition. If the 148-91.5 keV transition is of multipolarity no greater than E2, the spin of the 91.5 keV level will be $9/2^+$. The intensity of this level increases at forward angles in the (^{3}He,α) reaction, as does a level at 386 keV, while the level at 148 keV loses intensity A forward angle draining of $13/2^+$ strength into the 9/2 and 17/2 members of a rotational band has been seen in positive parity bands in several deformed rare earth nuclei and explained assuming a two-step reaction process. (Burke et al. (1972)). It is probable that the same process is taking place in this reaction.

The (d,t) angular distribution for the 91 keV level most closely resembles an ℓ=3 transfer, although the fit is not too good (Figure 11). Unfortunately, no angular distributions for ℓ=4 transfers have been measured, and so no comparison could be made with empirical ℓ=4 angular distributions.

The cross-section ratio for this level also indicates an ℓ=3 transfer (Figure 14). One possible explanation for these inconsistencies is that the level seen at 91 keV is in fact a doublet, namely the level at 91.5 keV seen in the decay and reaction studies and a second ℓ=1 or ℓ=2 level close nearby.

On the other hand, data which have recently been obtained on the N=89 nucleus ^{149}Nd indicate that the level in this nucleus which is most likely the $9/2^+$ state corresponding

to that seen in ^{151}Sm also has an angular distribution and cross-section ratio most closely resembling an ℓ=3 transfer. (Burke, private communication). Whether or not this similarity is of significance or is simply coincidental is not known.

7) The 104.8 keV level

A level at 104.8 keV decays via measured M1 transitions to both the ground state and first excited state and must therefore have spin $3/2^-$ or $5/2^-$. This level was not seen in the reactions performed, but was weakly populated via an E2 transition in the inelastic scattering experiment.

8) The 167.7 keV level

The 167.7 keV state decays via E1 transitions to the $5/2^-$ ground state, the $3/2^-$ first excited state, the $7/2^-$ and $5/2^-$ states at 65.8 and 69.7 keV, and via an E2 transition to the $9/2^+$ state at 91.5 keV. Its spin and parity must therefore be $5/2^+$. No measure of the intensity of this state could be made in any one of the reactions performed, as it was not possible to resolve it from the level at 168.4 keV. The (d,t) angular distribution of this doublet did appear to be some mixture of ℓ=2 and ℓ=3 , which is consistent with the decay data.

9) The 168.4 keV level

A state at 168.4 keV decays via M1 transitions to both the 0 and 4.8 keV levels, and is fed by the $7/2^+$, 324

keV level. If this last decay is assumed to be of E1 multipolarity, the spin and parity of the 168.4 keV level must be $5/2^-$. This level was weakly populated in the inelastic scattering experiment.

10) The 175 keV level

A level at 175 keV was found from the cross section ratio (Figure 14) and from the (d,t) angular distribution (Figure 12) to be populated by an $\ell=5$ transfer. Since this state is also fed by the $7/2^+$, 324 keV level, it is likely that its spin and parity will be $9/2^-$.

11) The 209 keV level

A level at 209 keV has a (d,t) angular distribution and a cross section ratio which indicate an $\ell=3$ transfer (Figures 11, 14) and therefore its spin and parity must be $5/2^-$ or $7/2^-$.

12) The 295 keV level

A level at 295.1 keV was populated via an E2 transition in the inelastic scattering and Coulomb excitation experiments, and was found to decay to the $7/2^-$, 65.8 keV level. Its spin could therefore range from $3/2^-$ to $9/2^-$. This level was not populated in any of the reactions performed.

13) The 307 keV level

A very strong peak appears in the (d,t) spectra at 307 keV. The angular distribution is that for an $\ell=2$ transfer (Figure 9). The cross section ratio is somewhere between

ℓ=2 and ℓ=3 (Figure 14) but this ratio is not very reliable due to the high density of states in this region and the limited resolution obtainable in (^{3}He,α) spectra. This level may perhaps be identified with that seen in the decay work at 306.8 keV. Since the ℓ-transfer is ℓ=2, the spin must be $3/2^+$ or $5/2^+$.

14) The 316 keV level

A level at 316 keV has an ℓ=1 angular distribution in the (d,t) reaction (Figure 8), and must therefore have spin $1/2^-$ or $3/2^-$. If this level may be identified with that seen at 314.9 keV in the decay studies, the spin may be determined, as the 314.9 keV level decays in part to the $5/2^+$ level at 167.9 keV. Since this transition would likely be of E1 multipolarity, the 316 keV level would have spin $3/2^-$.

15) The 324 keV level

The spin and parity of the level seen in decay work at 324 keV may be deduced from the measured decay multipolarities. This level decays via an E1 transition to the $5/2^-$ ground state,and via an M1 transition to the $9/2^+$ 91.5 keV keV state. The spin and parity of the 324 keV level must therefore be $7/2^+$. This state was not observed in any of the reactions performed.

16) The 346 keV level

A level populated at 346 keV in the (d,t) spectra has an ℓ=2 angular distribution (Figure 10). The cross section ratio is also that for an ℓ=2 transfer (Figure 14).

The spin and parity must therefore be $3/2^+$ or $5/2^+$. This level may be identified with the level strongly populated in the decay work at 344.8 keV. The measured multipolarities (Bertelsen et al. (1964)) of the transitions leading out of the 344.8 keV level are consistent with the assignment given above, but unfortunately do not further restrict the spin value.

17) The 357 keV level

A strong peak at 357 keV has a (d,t) angular distribution which is very definitely $\ell=0$ (Figure 7), and this level must therefore have spin and parity $1/2^+$.

18) The 386 keV level

As mentioned in the discussion of the $9/2^+$ level at 91.5 keV, a level at 386 keV appears in the (^{3}He,α) data with an increased intensity at forward angles. This may be a $17/2^+$ level formed via two-step processes.

19) The 397 keV level

A level at 397 keV has the (d,t) angular distribution for an $\ell=2$ transfer (Figure 10) and a cross section ratio (Figure 14) corresponding to an $\ell=2$ or $\ell=3$ transfer. The spin and parity of this level are therefore probably $3/2^+$ or $5/2^+$.

20) The levels at 445 and 448 keV

Burke et al, (1963) have established a level at 445 keV, and the most recent decay studies (Cook et al, private communication) indicate a second close-lying level at 448.3 keV. The 445 keV level decays via measured E1 transitions to the $5/2^-$ ground state and the $3/2^-$ first excited state, and also decays to the $7/2^-$ state at 65.8 keV. This last transition will probably be of E1 multipolarity for it to be strong enough to be seen in the decay work. The spin and parity of the 445 state would then be $5/2^+$. The level populated at 449 keV in the (d,t) reactions has an $\ell=1$ (d,t) angular distribution (Figure 8) and must therefore have spin $1/2^-$ or $3/2^-$. It is most probable that this level may be identified with the level seen at 448 keV in the newer decay studies (Cook et al, private communication), and not with the 445 keV state. The level at 448 is also strongly populated in the $^{150}Sm(d,p)^{151}Sm$ reaction.

21) The 503 keV level

Like the 357 keV level, the 503 keV level has the characteristic $\ell=0$ (d,t) angular distribution, and must then have spin $1/2^+$ (Figure 7).

22) The 523 keV level

The level at 523 keV has an $\ell=2$ angular distribution and therefore has spin $3/2^+$ or $5/2^+$ (Figure 10).

23) The 529 and 715 keV levels

Levels at 529 and 715 keV were populated via E2↑ transitions in the inelastic scattering experiment, and therefore have possible spins ranging from $1/2^-$ to $9/2^-$.

24) The 704 keV level

A level at 704 keV has a cross section ratio of either $\ell=5$ or $\ell=6$ (Figure 14). If this is the same level as that seen weakly in the (d,d') experiment at 700 keV, the spin would be $11/2^+$ or $13/2^+$, as the multipolarity of the transition was probably greater than E2.

25) The 745 keV level

A level at 745 keV has a cross section ratio of $\ell=4$ or 5 (Figure 14). The possible spin assignments are then, $7/2^+$, $9/2^+$ or $9/2^-$, $11/2^-$.

26) The 954 keV level

In the reaction $^{150}Sm(d,p)^{151}Sm$, a level at 954 keV was very strongly populated, and is therefore most likely of low spin.

27) The 1378 keV level

A level at 1378 keV has a cross section ratio of $\ell=5$, and therefore has spin $9/2^-$ or $11/2^-$ (Figure 14).

4.2 Discussion of Coulomb excitation and inelastic scattering results

Coulomb excitation and inelastic scattering studies tend to populate states of structure closely resembling the ground state, and in particular, the ground state rotational bands of deformed nuclei. It is therefore of interest to examine the results of these experiments on the ^{151}Sm target for evidence of a ground state rotational band in this nucleus. The most strongly populated peak seen was the $7/2^-$ level at 65.8 keV. The average B(E2) value found for this level was about 0.80 e^2b^2, corresponding to an E2↑ strength of ∿33 single particle units[a], and one is tempted to suggest that this is the first excited member of a ground state rotational band. If the strong coupling model holds, and if one assumes a simple, unmixed ground state band, the intrinsic quadrupole moment may be calculated from the expression

$$B(E2) = (5/16\pi)e^2Q_o^2\langle I_i 2K0 | I_f K\rangle^2$$

to be Q_o = 4.1 barns. For a homogeneous charged spheroid, the deformation corresponding to this would be β = 0.21. The assumptions involved in making these calculations become questionable, though, when the spectrum is examined for the next rotational member. For a simple rotational band, the equation above predicts that the $9/2^-$ member of the ground

[a]These single particle units are the same as those defined by Alder *et al.* (1956) and have the value 3.0 $A^{4/3}\times10^{-53}$ e^2cm^4.

state rotational band should be populated with a B(E2)↑ strength which is 7/20 times that for the $7/2^-$ member. On the basis of the I(I+1) rule, the $9/2^-$ state should appear at about 150 keV. The next level seen, with a strength of ∿20% the $7/2^-$ strength, is the one at 168.4 keV, which was shown to have spin $5/2^-$, and thus cannot be a member of this band. The $9/2^-$ level seen in the particle studies at 175 keV would appear to be a likely candidate, but is not populated in the inelastic scattering, and instead, a previously unknown level at 295.1 keV is populated with a strength about 60% larger, relative to the $7/2^-$ strength, than that expected for a $9/2^-$ level.

The 295.1 keV level decays readily to both the ground state and the 65.8 keV level. If the spin and parity of this level are $9/2^-$, then the measured ratio of the 295→66 keV photon intensity to the 295→0 photon intensity is only about half as large as that predicted by the strong coupling model for E2 transitions between band members, even if the 229.3 keV transition to the 65.8 level were assumed to be pure E2.

If this level at 295 keV were a member of a ground state rotational band, then it would certainly be necessary to invoke a great deal of configuration mixing in order to explain the departure from the I(I+1) rule. The transition rates are very sensitive to mixing effects in the nuclear structure, and any mixing large enough to explain the deviation

from a rotational energy spacing would strongly affect these rates.

It is also possible that the ^{151}Sm nucleus is not a good rotor, and might be more accurately described using some other model. These possibilities are left to be discussed in the section entitled "low-lying negative parity levels". It is most logical to proceed now to a discussion of the positive parity levels in this nucleus, as the insight gained from these levels is useful in the discussion of the negative parity levels.

4.3 Positive parity levels

The positive parity states that would be expected to appear in these reactions would be due to the $s_{1/2}$, $d_{3/2}$ and $i_{13/2}$ shell model orbitals. For a well deformed nucleus, all of the Nilsson states stemming from these orbitals could be coupled through $\Delta N=2$ and Coriolis mixing, and the level ordering further perturbed through decoupling of the K=1/2 bands. One might therefore expect the resultant spectra to be rather complex. In spite of this, studies of the positive parity levels in ^{155}Gd (Borggreen et al. (1969)) have shown that these levels are well described by the Nilsson model if the calculations include the effects of Coriolis and $\Delta N=2$ mixing, and for ^{153}Gd (Løvhøiden et al. (1972)), this theory provides at least a qualitative description of the experimental data.

The low-lying positive parity levels found in ^{151}Sm are shown in the first column of Figure 26. The spin assign-

Figure 26.

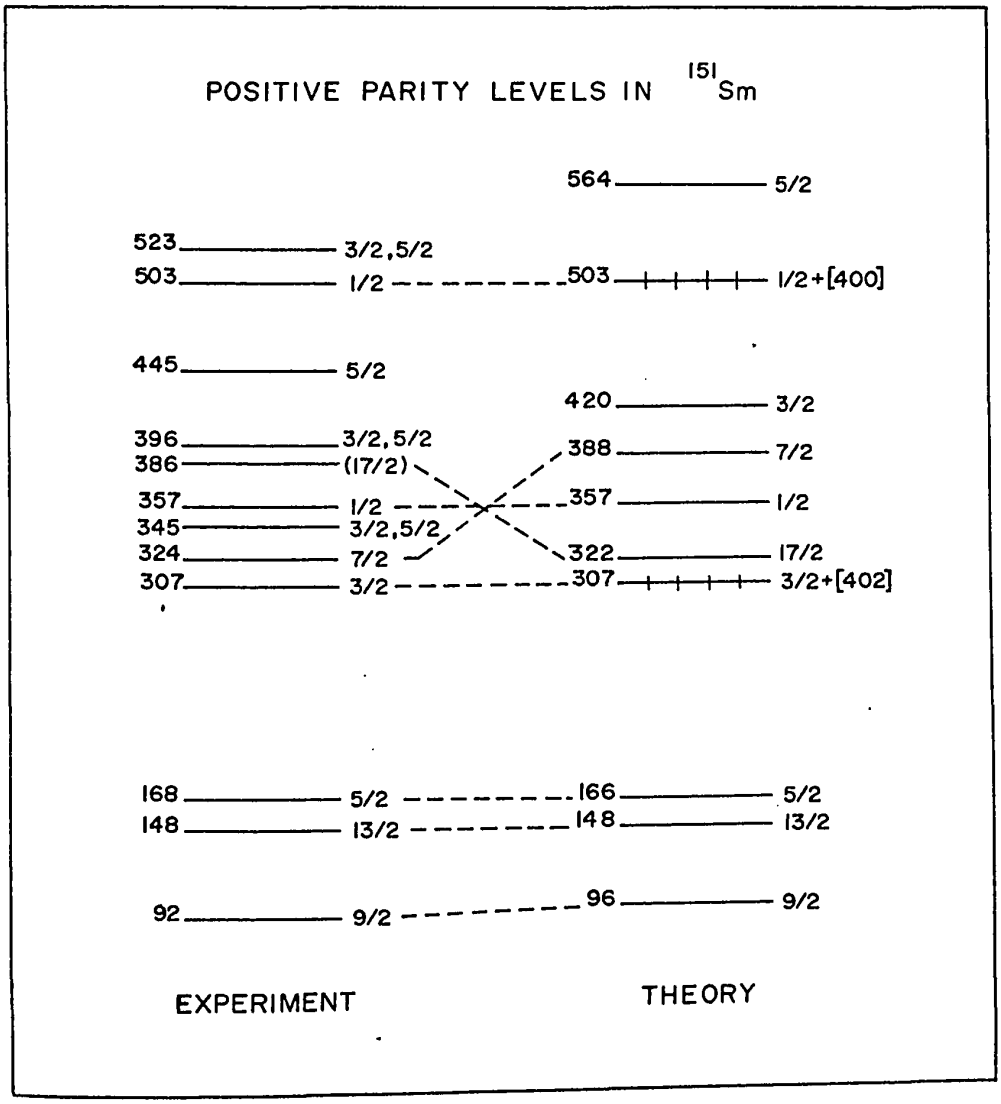

Comparison of experiment and theory for the positive parity levels in ^{151}Sm. The two N=4 levels (shown with cross-hatches) were not part of the theoretical calculation, but were put in on the basis of model systematics. See Section 4.3.

ments listed for these states were discussed in Section 4.1. If these levels do represent coupled Nilsson orbitals, as found in the nuclei ^{153}Gd and ^{155}Gd, one would expect the transition probabilities between the states to be enhanced. The lifetime of the level at 167.7 keV as measured by Andrejtscheff (1971), was found to be 0.38 nsec. The E2 transition probability for the decay from the 167.7 keV level to the 91.5 keV level may then be calcualted to be about 200 Weisskopf units, which is typical for in-band transitions for nuclei in this region of the periodic table. This transition probability corresponds to a B(E2) value of approximately 0.63 e^2b^2 and an intrinsic quadrupole moment of $Q_o \approx 3.64$ b. The inelastic scattering experiment yielded values very similar to these for the ground state "band".

The half-life of the 91.5 keV state as observed in decay has recently been reported as 78 nsec (Drost, et al, (1972)). This level decays via an E1 transition to the negative parity 65.8 keV level. The transition strength for this decay may be calculated to be about 0.6×10^{-4} Weisskopf units.

A calculation of the effect of Coriolis mixing of all the states stemming from the $i_{13/2}$ shell model orbital was carried out for ^{151}Sm. Unfortunately, the computer program used for this calculation was not sufficiently general to include $\Delta N=2$ mixing, and so the effect of the $s_{1/2}$ and $d_{3/2}$ orbitals could not be quantitatively predicted. In this program, the single particle Nilsson orbitals in a harmonic

oscillator well are calculated and adjusted to include the effects of pairing correlations. For a given rotational parameter, the rotational bands built on the intrinsic states are constructed, and the effects of Coriolis mixing calculated. In order to provide a rigorous test of the model, the only adjustable parameters allowed were:

a) the rotational parameter which was assumed to be the same for all bands

b) the position of the Fermi surface and the size of the pairing strength parameter, Δ, and

c) the empirical factor by which the Coriolis matrix elements are reduced. (The need for reducing these elements has not been explained theoretically, but has been empirically found to be necessary, for example, in the work on ^{155}Gd Borggreen et al. (1969).

The parameters describing the potential well, κ and μ, were set at 0.0637 and 0.420, respectively, as prescribed by Lamm (1969). Assuming a prolate nucleus, the deformation parameter β=0.2 was taken from the results of the inelastic scattering experiment. The Fermi level was set 100 keV below the energy calculated for the $3/2^+$[651] orbital, the parameter Δ was 1 MeV, and the Coriolis matrix elements reduced to 0.76 times as large as those calculated from the model. The second column in Figure 25 shows the predicted level spectrum, and the energies and cross sections calculated are

given in Table 10, along with the values found experimentally for the three reactions performed. The observed intensity of the 91.5 keV level (Table 10) is much larger than predicted for the 9/2 level in both the (d,p) and (d,t) reactions and only slightly larger in the (^{3}He,α) reaction. This is consistent with the suggestion made previously that the peak seen at 91.5 keV is a doublet, consisting of the $9/2^+$ level and an ℓ=1 or ℓ=2 level. The experimental intensity listed for the level at 168 keV is the total for the 167.7 - 168.4 doublet. The calculated $7/2^+$ energy is very sensitive to small changes in the input parameters (eg. the Fermi surface) and the discrepancy in the calculated and observed energies for this level is not considered to be serious. In the last section, it was shown that the level at 704 keV could have spin $11/2^-$, $11/2^+$ or $13/2^+$. This level is perhaps the second $13/2^+$ level expected at 884 keV from the calculation.

The very intensely populated $3/2^+$ level at 307 keV and the two $1/2^+$ levels strongly populated at 357 keV and 503 keV indicate that the N=4 orbitals $1/2^+$[400] and $3/2^+$[402] must be involved in this region, and a complete calculation should include the $\Delta N = 2$ mixing that would then take place between these orbitals and the N=6 orbitals. For the N=4 states to appear at this excitation energy in ^{151}Sm, the single particle energies of these orbitals would have to be about 1.5 MeV larger than those calculated from the Nilsson potential used above. Table 11 gives the cross-sections that would be expected in the (d,t)

Table 10

Predicted and observed energies and cross sections for the positive parity levels in ^{151}Sm

Level Energy (keV)		Spin		Predicted Theoretical Amplitudes				$d\sigma/d\Omega$ (d,t) at 60°		$d\sigma/d\Omega$ (^{3}He,α) at 45°		$d\sigma/d\Omega$ (d,p) at 45°	
Exp.	Theory	Exp.	Theory	$1/2^+[660]$	$3/2^+[651]$	$5/2^+[642]$	$7/2^+[633]$	Exp.	Theory	Exp.	Theory	Exp.	Theor
91.5	96	9/2	9/2	0.82	0.54	0.22	0.04	84	19	14	17	90	25
148	148	13/2	13/2	0.81	0.54	0.24	0.06	29	37	140	194	18	21
167	166	5/2	5/2	0.84	0.53	0.15	-	96	7	-	<1	76	7
306	-	3/2	3/2 $3/2^+[402]$ *				-	550		∿50		-	
324	388	7/2	7/2	0.32	0.81	0.49	-0.09	-	0.2	-	0	-	1
345		5/2	5/2 $3/2^+[402]$*				0	123		∿13	-		
357	382	1/2	1/2	1.0	0	0	0	234	0	-	0	18	-
386	322	(17/2)	17/2	0.80	0.54	0.26	-0.08	Two-step reaction process					
395	420	3/2,5/2	3/2	0.39	0.92	0	-	33		∿3		-	
445		5/2					-	-		-		-	
503	-	1/2	1/2 $1/2^+[400]$ *				-	506		-		-	
523		3/2,5/2						54		-		-	
	564		5/2	-0.50	0.62	0.61	-		0		0	-	<1
704	884	(13/2)	13/2	-0.48	0.36	+0.72	-0.33	∿6	∿1	35	15	-	∿12

*These levels possibly contain the major portion of the N=4 orbital assigned. These N=4 orbitals are not included in the mixing calculations. See text.

Table 11

Theoretical cross sections expected in the $^{152}Sm(d,t)^{151}Sm$ reaction at 60° for pure $1/2^+[400]$ and $3/2^+[402]$ orbitals

Orbital	Expected (d,t) cross-sections at 60° (μb/sr)				
	1/2	3/2	5/2	7/2	9/2
$1/2^+[400]$	850	290	68	∿4	<< 1
$3/2^+[402]$	-	962	43	∿7	<< 1

reaction for pure $3/2^+[402]$ and $1/2^+[400]$ orbitals.

For pure states, one would expect to see little $1/2^+$ intensity from the $1/2^+[660]$ orbital, but a great deal from the $1/2^+[400]$ state. Since two strong $1/2^+$ levels are seen, these two orbitals must be coupled, and the 1/2 $1/2^+[400]$ strength spread over both levels. The total cross section of these two levels in the (d,t) reaction is 740 μb/sr, which is in reasonable agreement with the total of 850 μb/sr that is predicted. If the $1/2^+[400]$ band head were at an unperturbed energy of 449 keV, and the $1/2^+[660]$ band head at 391 keV, then a $\Delta N=2$ matrix element strength of 68 keV would give the energies and relative cross-sections seen in the experiment.

The 3/2 and 5/2 members of the N=4 and N=6 orbitals will most likely be strongly mixed. Since there is some ambiguity in the assignments of the $3/2^+$ and $5/2^+$ levels in the experimental spectrum, it is difficult to sort them out. Probably the strong $3/2^+$ level at 307 keV is mainly due to the $3/2^+[402]$ orbital.

The total cross section expected in the 60° (d,t) spectrum for the I = 3/2 levels is about 1250 μb/sr, essentially all from the N=4 orbitals. The levels observed in the (d,t) reaction at 307, 346, 396 and 523 keV all have $\ell=2$ angular distributions and may therefore have spins $3/2^+$ or $5/2^+$. The experimental intensities observed are respectively 550, 123, 33 and 54 μb/sr. Perhaps the 307 and 346 keV levels are mostly due to the $3/2^+$ members of the N=4 orbitals, while the 396 and 523

are the corresponding $5/2^+$ members. Whether or not this is true, there is a discrepancy between the calculated 3/2 strength and the strength observed in the (d,t) reaction, with the predicted intensity almost a factor of two larger than the observed intensity. No large peaks other than those discussed above are seen in the (d,t) reaction up to an excitation energy of 1600 keV. This discrepancy will not be explained by making a complete mixing calculation including the $\Delta N=2$ effects and it remains unexplained. This difference was not found in similar studies on ^{153}Sm (Kanestrøm and Tjøm (1972)), where the 3/2 strength resulting from the N=4 orbitals was found to be in agreement with that predicted.

Apart from this discrepancy, the results of these calculations show that the Nilsson model including Coriolis mixing (and, qualitatively, $\Delta N=2$) mixing) does indeed provide a good description of the low-lying positive parity levels in ^{151}Sm. It should be emphasized that the parameters used in the calculation were chosen from the results of other experiments, and no wide ranging parameter variations were allowed. While it is likely possible that the predicted energies of some of the levels could be improved by slightly varying the input parameters, the results obtained are sufficient evidence of the application of the Nilsson model to ^{151}Sm. A more complete calculation, quantitatively including the effects of $\Delta N=2$ mixing, could be expected to give an even better theoretical description of the

positive parity levels. Before such a calculation is undertaken, it would be advantageous to have more experimental information on the $3/2^+$ and $5/2^+$ levels in the 300-500 keV region.

4.4 Negative Parity levels

The good agreement obtained from applying the Nilsson model, with Coriolis and $\Delta N=2$ mixing effects included, to the positive parity levels in ^{151}Sm, gives hope that the negative parity levels may also be described by this model, even though the results obtained from the inelastic scattering experiments seem rather complicated.

The existence of the $11/2^-$ isomeric state at 261 keV in ^{151}Sm tends to support the supposition that this nucleus may be described as a symmetric prolate rotor. For a prolate nucleus, the Nilsson orbital $11/2^-[505]$ is expected as a hole state in this region of the periodic table, and has been identified in neighbouring nuclei (cf Tjøm (1968)). No other $11/2^-$ levels would be expected to be strongly populated at such a low excitation energy, and it is therefore very reasonable to assume that the isomer may be assigned to the $11/2^-[505]$ orbital. The long half-life observed would result as de-excitation transitions would be K-forbidden.

The predicted and observed intensities for this level for the reactions performed are given in Table 12. The agreement between the observed and predicted values is indeed quite

Table 12

Predicted and observed $11/2^-[505]$ intensities in ^{151}Sm

	Cross Sections (μb/sr)		
	(d,t) 60°	(^{3}He,α) 45°	(d,p) 45°
Theory*	66	135	3.5
Experiment	56	117	≤ 5

* These theoretical cross sections were calculated assuming $V^2 = 0.95$, $U^2 = 0.05$.

satisfactory.

The Nilsson model in its simple form is certainly not applicable to this nucleus. The level spacings of the many $3/2^-$, $5/2^-$ and $7/2^-$ states existing in the low lying spectrum are such that these levels can not be arranged into unmixed rotational bands, and it will be necessary to invoke a great deal of mixing to explain the spectrum. The results of the inelastic scattering and Coulomb excitation experiments, as discussed in section 4.2, support this conclusion: Strong E2 transitions were observed to the level at 65.8 keV and a level at 295 keV. The wave functions for these two states must then strongly resemble that of the ground state, and if they form part of a ground state "rotational band" then strong perturbations from other bands are required to explain this level spacing.

If one accepts the deformation of $\beta=0.2$ as determined from the inelastic scattering data (this was also the deformation used to describe the positive parity levels), then filling 89 neutrons into the Nilsson diagram suggests that the orbitals $5/2^-[523]$ and $3/2^-[521]$ would be prime candidates for the $5/2^-$ ground state and $3/2^-$ first excited state. But these two orbitals alone (or any two K=3/2 and K=5/2 orbitals) even if they are highly mixed, can not give rise to the spectrum observed in inelastic scattering. This may be seen by considering the relative phases of the wave functions of states arising from two mixed bands.

Consider the following two bands which are to be Coriolis mixed;

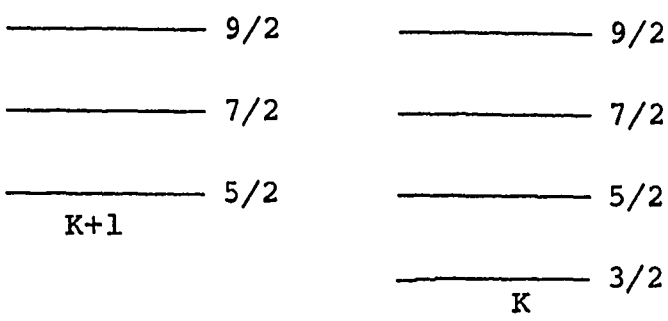

Following Kerman (1956), the state vectors for the two solutions for the mixed states of spin I may be written, arbitrarily choosing a positive relative phase, as

$$|\psi_I^L\rangle = a_I|\psi_{IK}\rangle + b_I|\psi_{I,K+1}\rangle$$

and

$$|\psi_I^H\rangle = b_I|\psi_{IK}\rangle - a_I|\psi_{I,K+1}\rangle$$

where $a_I^2 + b_I^2 = 1$ and H, L refer to the higher and lower energy solutions.

Therefore in the above problem, the lowest I = 5/2 state may be written

$$|\psi_{5/2}^L\rangle = a_{5/2}|\psi_{5/2,3/2}\rangle + b_{5/2}|\psi_{5/2,5/2}\rangle .$$

The two I=9/2 levels will then be

$$|\psi_{9/2}^L\rangle = a_{9/2}|\psi_{9/2,3/2}\rangle + b_{9/2}|\psi_{9/2,5/2}\rangle$$

and

$$|\psi_{9/2}^H\rangle = b_{9/2}|\psi_{9/2,3/2}\rangle - a_{9/2}|\psi_{9/2,5/2}\rangle$$

where the a's may be chosen to be positive, and $b_{5/2}/b_{9/2}$ will also be positive.

Then the Coulomb excitation probability between the lower I=5/2 level and the two 9/2 levels will go as

$$B(E2) \propto \{\Sigma \langle I_i\ 2\ K_i\ \Delta K | I_f K_f \rangle \langle \psi^{H,L}_{9/2} | \varepsilon 2 | \psi^{L}_{5/2} \rangle\}^2$$

where $\varepsilon 2$ is the E2 transition operator. For the upper 9/2 level this becomes

$$B^H(E2) \propto \{\langle 5/2\ 2\ 3/2\ 0 | 9/2\ 3/2 \rangle b_{9/2} a_{5/2} \langle \psi_{9/2\ 3/2} | \varepsilon 2 | \psi^{L}_{5/2\ 3/2} \rangle$$

$$- \langle 5/2\ 2\ 5/2\ 0 | 9/2\ 5/2 \rangle a_{9/2} b_{5/2} \langle \psi_{9/2\ 5/2} | \varepsilon 2 | \psi_{5/2\ 5/2} \rangle\}^2 .$$

For the lower 9/2 level

$$B^L(E2) \propto \{\langle 5/2\ 2\ 3/2\ 0 | 9/2\ 3/2 \rangle a_{9/2} a_{5/2} \langle \psi_{9/2\ 3/2} | \varepsilon 2 | \psi_{5/2\ 3/2} \rangle$$

$$+ \langle 5/2\ 2\ 5/2\ 0 | 9/2\ 5/2 \rangle b_{9/2} b_{5/2} \langle \psi_{9/2\ 5/2} | \varepsilon 2 | \psi_{5/2\ 5/2} \rangle\}^2 .$$

The cross-terms will be small and are neglected.

In these expressions, the terms $\langle \psi_{IK} | \varepsilon 2 | \psi_{KK} \rangle$ are simply the quadrupole moments Q_o of the bands. If one assumes $Q_o^{K=5/2} \approx Q_o^{K=3/2}$, these factors may be taken outside the curly brackets. Since both of the Clebsch-Gordan coefficients have the same sign, it may be seen that the lower energy I=9/2 level will tend to be more strongly populated than the upper 9/2 level, as the terms in $B^H(E2)$ tend to cancel out, while those at $B^L(E2)$ add. If one assumes that $(Q_o^{K=5/2}/Q_o^{K=3/2}) < 0$, then the highest 9/2 level would be populated, but similar calculations would show that the lowest $7/2^-$ level would not be populated. The lowest $7/2^-$ level in ^{151}Sm, at 65.8 keV, was

strongly populated in the inelastic scattering experiment, contradicting the suggestion that the two bands have quadrupole moments of different signs. In any case, it is not too clear that this whole approach is valid if these low-lying levels are described as a mixture of two bands of prolate and oblate deformation.

This argument remains valid even for two bands with different rotational parameters. The wave function for the state which has been pushed upwards in energy from its normal rotational position, as must be the case for the 295 keV level (if it is the 9/2 member of the ground state band), will have a relative phase opposite that of the ground state, and the probability for Coulomb excitation to this state will be small. Since the 295 keV level was strongly populated, one may conclude that the ground state wave function must be a mixture of more than two Nilsson orbitals, if the Nilsson model is to be applied to this nucleus.

As mentioned above, the level at 65.8 keV was strongly populated in the Coulomb excitation experiment, and thus is possibly the second member of the ground state rotational band. This level is also very strongly populated in the (d,p) experiment. One might then consider the orbital $5/2^-[512]$ for inclusion in the ground state wave function, since this orbital has a large spin 7/2 component and would lie above the Fermi surface, and therefore contribute strongly to the observed (d,p) cross-section.

The results from the experiment $^{151}Sm(d,p)^{152}Sm$ should give additional information on the ground state in ^{151}Sm, as the relative intensities of the ground state rotational band in ^{152}Sm will characterize the ground state of ^{151}Sm. The observed intensities are listed in column 2 of Table 13. A computer program was written to calculate the predicted intensities for the ^{152}Sm band for all possible mixtures of the three orbitals, $3/2^-[521]$, $5/2^-[523]$ and $5/2^-[512]$ as components of the ^{151}Sm ground state. Of these mixtures, only two gave good relative agreement with the experiment. These were:

1) $\psi = 0.98(5/2^-[523]) + 0.15(3/2^-[521])$

and

2) $\psi = 0.65(5/2^-[523]) + 0.61(5/2^-[512]) - 0.42(3/2^-[521])$.

For the first of these solutions to be considered, it must contain at least small admixtures of other states, since, as previously explained, a simple mixture of two Nilsson rotational bands would not yield the inelastic scattering results. The calculated relative values for the intensities of the ^{152}Sm rotational band are in reasonable agreement with the observed values (Column 3, Table 13). The second solution gives even better relative values. (Column 4, Table 13). The predicted absolute values are all somewhat larger than those observed. One might expect this, as it is probable that there is a shape difference between the initial and final nuclei, which would tend to hinder the transfer process. The calcu-

Table 13

Population of the ground state band in the reaction $^{151}Sm(d,p)^{152}Sm$: Experimental cross sections and intensities predicted for the three wave functions considered for the ground state of ^{151}Sm .

Level	Cross sections (μb/sr)			
	Experiment	Empirical Solutions (1)	(2)	Oblate nucleus
0^+	1.3	1.6	1.6	11
2^+	8.4	28	17	66
4^+	4.5	15	8.6	15
6^+	1.1	2.8	2.2	0.6

The last three columns are the intensities predicted assuming the following wave functions for the ground state of ^{151}Sm

Empirical solution 1) $\psi = 0.15(3/2^-[521]) + 0.98(5/2^-[523])$

2) $\psi = 0.65(5/2^-[523] + 0.61(5/2-[512]) - 0.42(3/2^-[521])$

Oblate nucleus $\psi = 0.90(5/2^-[523]) - 0.44(3/2^-[532])$

lations included no such shape factors. Both solutions predict that the ground state populations of all (d,p) and (d,t) reactions leading into and out of ^{151}Sm will be small, as is observed in these reactions.

Unfortunately, these semi-empirical determinations of possible wave functions for the ground state of ^{151}Sm do not yield information on the nature of the other members of a possible ground state band, and so no further comparison can be made with the other low lying negative parity levels.

A Nilsson model calculation including Coriolis mixing was made for the negative parity levels in ^{151}Sm using the computer program described in the previous section.

This calculation was made using the well parameters κ = 0.0637 and μ = 0.42 to describe the deformed harmonic oscillator potential. The deformation parameter β = 0.2 and rotational parameter A=15 keV were chosen as they gave good results in describing the positive parity states. These parameters were kept constant from band to band. The Fermi level was set 250 keV above the energy calculated for the $3/2^-$[521] orbital. The first 82 neutrons were considered inert; the calculation included all the Nilsson states stemming from the $h_{9/2}$ and $f_{7/2}$ orbitals. The resulting spectrum is given in column 1 of Figure 27.

The cross-sections for these levels are calculated from the equation

Figure 27.

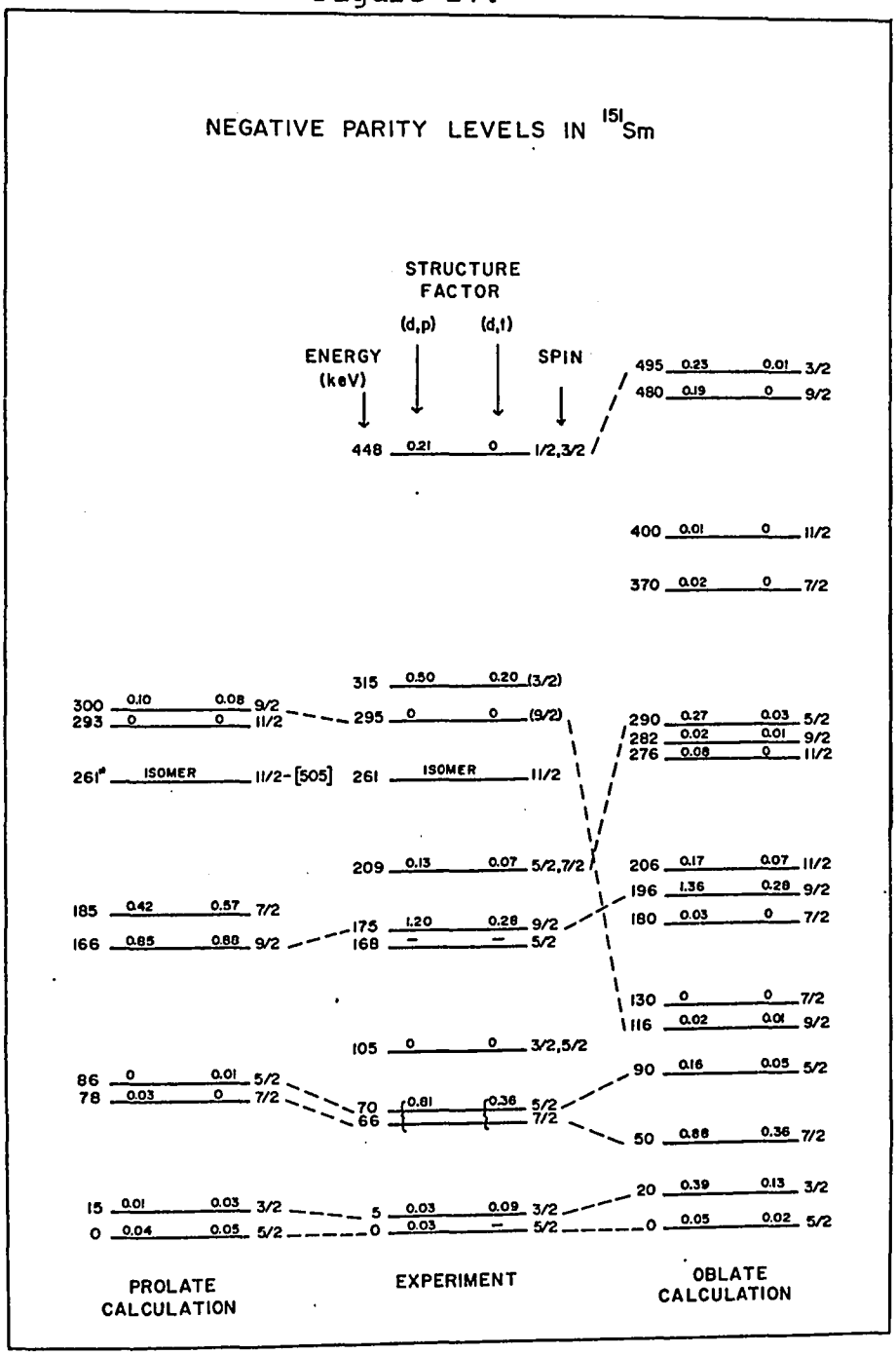

Comparison of experiment and theory for the negative parity levels in ^{151}Sm. The numbers above the level bars give an indication of the strength of the level for (d,p) and (d,t) reactions, as explained in Section 4.4.

$$\frac{d\sigma}{d\Omega} = 2 \sum_n \left(a_n C_{j\ell}^{(n)} \begin{matrix} U_n \\ or \\ V_n \end{matrix}\right)^2 \sigma_\ell(\theta)$$

where the index n includes all the orbitals mixed into a level and $\sigma_\ell(\theta)$ is the DWBA cross section. It is useful to use the structure factor

$$\sum_n \left(a_n C_{j\ell}^{(n)} \begin{matrix} U_n \\ or \\ V_n \end{matrix}\right)^2$$

calculated from the model as a basis of comparison with experiment, as an effective empirical value for this structure factor may be obtained by dividing observed intensities by twice the appropriate DWBA cross section.

In Figure 27, the numbers drawn above each level are these structure factors calculated from the model for the (d,p) reaction (on the left) and for the (d,t) reaction (on the right). The second column in this figure gives the experimental spectrum and the empirical structure factors. It is interesting to note that the wave function calculated for the ground state was

$$\psi = 0.90(5/2^-[523]) + 0.42(3/2^-[521])$$

which is somewhat similar to the first of the "empirical" solutions. The wave functions of the higher states are such that the first 7/2 and first 9/2 levels would be populated in inelastic scattering; no mechanism is predicted which would explain the observed inelastic scattering spectrum. Furthermore, the structure factors predicted do not agree too well

with those observed. Reasonable variations of the Fermi level, the rotational parameter and deformation have not produced a spectrum which more closely resembles the observed spectrum than that given here.

The deformation parameter used above was that for a prolate nucleus. Since this parameter was extracted from the inelastic scattering data, which gives only the absolute magnitude of the deformation, and not the sign, it is interesting to perform the same Nilsson calculation for an oblate nucleus, that is for $\beta = -0.2$, The results obtained using a rotational parameter of A=10 keV and putting the Fermi level 200 keV below the $5/2^-[523]$ orbital are given in column 3 of Figure 27. This spectrum shows some correspondence to the observed spectrum, not only in the level ordering but of more importance, in the predicted structure factors for some of the levels. The wave function calculated for the ground state was

$$\psi = 0.90(5/2^-[523]) - 0.44\,(3/2-[532]) + \text{small terms}\ .$$

This function yields the cross section pattern for the ^{152}Sm ground state rotational band for the reaction $^{151}Sm(d,p)^{152}Sm$ as given in the last column of Table 13. The absolute magnitudes of the values predicted are much larger than those observed (again this might be explained as due to a large difference in initial and final shapes) and the relative intensities are not as good as those predicted from the prolate

calculation, but the discrepancy is not too large.

Further evidence tending to support these oblate calculations comes from the experiments $^{151}Sm(^{3}He,\alpha)^{150}Sm$ and $^{151}Sm(d,t)^{150}Sm$. The cross-section ratios for the levels populated in ^{150}Sm give an indication of the transferred ℓ value. For such experiments on odd A targets, the transfer involves a mixture of ℓ-values,and the empirical ratios may not identify these ℓ-values, but the empirical ratios must be consistent with those calculated from any theories that are being considered.

Figure 19 shows the empirical ratios found for the first 2^+ and 4^+ states in ^{150}Sm, as well as the ratios predicted from the oblate calculations and those from the prolate calculation involving the $3/2^-[521]$, $5/2^-[523]$ and $5/2^-[512]$ orbitals. In these calculations, the 2^+ level at 334 keV and the 4^+ level at 774 keV in ^{150}Sm were treated as members of a ground state "band". It is seen that the oblate ratios (which have a large ℓ=3 component in the ^{151}Sm ground state wave function) are quite similar to the empirical ratios, while those for the prolate ground state differ by a great deal. It is difficult to say how meaningful these calculated results may be, in view of the assumptions made on the nature of the two levels in ^{150}Sm.

The oblate nucleus calculations, like those of the prolate nucleus, also predict that the lowest lying $7/2^-$ level would be

strongly populated in an inelastic scattering experiment. In the (d,d') and Coulomb excitation experiments, the lowest lying $7/2^-$ level at 65.8 keV was indeed intensely populated. Furthermore the (d,p) and (d,t) structure factors predicted in the oblate calculations for the first $7/2^-$ level and the second $5/2^-$ level very closely resemble those found from the (d,p) and (d,t) experiments.

Three low-lying $9/2^-$ levels are predicted in the calculated oblate spectrum at 116, 196 and 282 keV. Of these, the 196 keV level has (d,p) and (d,t) structure factors closely resembling those of the $9/2^-$ level seen at 175 keV in the experimental spectra. The predicted $9/2^-$ level at 196 keV would not be expected to be populated in the (d,d') or Coulomb excitation experiments; the spectra for these experiments revealed no trace of the $9/2^-$ level at 175 keV.

The calculated oblate $9/2^-$ levels at 116 and 282 keV both have very small predicted structure factors, and it would be satisfying if the 282 keV level could be identified with the level seen in the (d,d') experiments at 295 keV. But the wave function of the predicted level at 282 keV is such that it would be populated very weakly in an inelastic scattering or Coulomb excitation experiment, while the predicted level at 116 keV should be intensely populated. In this respect, the oblate calculation does not seem any more capable of describing the inelastic scattering spectra than does the prolate calculation. Further-

more, the oblate nucleus calculations do not explain two other facts: 1) the negative parity, high spin isomer seen at 261 keV in this nucleus. None of the predicted oblate levels should be isomeric. As previously discussed, this isomer would appear in the prolate spectrum. 2) The predicted spectrum of oblate positive parity states shows little resemblance to the observed spectrum. These states were well described assuming a prolate nucleus.

Recent calculations of deformed single particle orbitals have included a second deformation term in the nuclear shape, ie $r = r_o (1+\beta_2 Y_{20}+\beta_4 Y_{40})$. The effect of this term is being investigated for various forms of potential. (eg. Nilsson (1969). It would appear that in some cases, the addition of this term has the effect of rearranging the Nilsson orbitals, and perhaps this extension of the model could provide a better description of the negative parity levels of ^{151}Sm. Calculations of nuclear shapes are also being made by various methods (eg. Kumar and Baranger, (1968)), the results of which indicate that the equipotential surfaces may contain more than one minimum and therefore one may expect to observe co-existing states corresponding to different deformations in the same nuclear spectrum. A semi-empirical calculation of this sort (Takemasa et al. (1972)), describes the ground states of ^{150}Sm and ^{152}Sm as containing both spherical and deformed structure, and suggests that both nuclei contain levels of "foreign" deformation. These conclusions were based on the results of two-neutron transfer reactions between ^{150}Sm and ^{152}Sm.

Considerations of this sort must also be related to the fundamental assumption made at the outset in adopting the rotational model; that the rotational and intrinsic motions are adiabatic. The extremely high number of low-lying negative parity levels in ^{151}Sm may be an indication that for this nucleus, the adiabatic assumption is poor. Furthermore, application of the variable moment of inertia model to ^{150}Sm, ^{152}Sm and ^{154}Sm yields "softness" parameters σ of 33.5, 0.229 and 0.0024 respectively, for these nuclei (Mariscotti et al. (1969)). This indicates that even in ^{152}Sm the adiabatic approximation is not completely valid. Unfortunately, this model gives no details of the intrinsic states of the nucleus.

The theoretical problems involved in solving the non-adiabatic rotor problem are rather subtle and certainly beyond the scope of this thesis, but one further point can be made. The positive parity levels in ^{151}Sm are reasonably well described assuming an adiabatic prolate rotor model. Whatever nuclear models are applied to this nucleus, they must explain why this prolate model works for the positive parity levels, but seemingly not for the negative parity levels.

4.5 Conclusions

A considerable amount of new information has been gained about the nuclear structure of ^{151}Sm, and the spins and parities of many of the low lying levels have been established, yet no nuclear model seems capable of simultaneously explaining all the observed properties of this nucleus. Earlier investigators

suggested that both spherical and deformed states could co-exist in the low lying level structure of ^{151}Sm, and that it might be possible to experimentally sort out these levels by performing single particle transfer reactions (leading into ^{151}Sm) on the "spherical" target nucleus ^{150}Sm and on the "deformed" target nucleus ^{152}Sm (Kenefick et al. (1965)). As was seen in these studies, the $^{150}Sm(d,p)^{151}Sm$ and $^{152}Sm(d,t)^{151}Sm$ in general tended to populate the same low lying levels, and no classification of levels as spherical, or deformed, could be made on this basis. This becomes understandable in the light of recent experiments and calculations on the shapes of nuclei in this transition region: some authors consider that the ground states of ^{150}Sm and ^{152}Sm contain both spherical and deformed components. In other words, the transition of nuclear shape does not occur abruptly as neutrons are added to the nucleus in these nuclei, but is a somewhat more gradual process than that previously imagined.

As might be expected, attempts to describe all the levels in ^{151}Sm using a simple nuclear model have not yet met any success. Assuming a prolate deformation, the Nilsson model gave a good description of the positive parity levels, and predicted the existence of the low-lying isomer, and yet did not seem capable of describing most of the negative parity levels in this nucleus. These levels seemed, at first glance, to be more closely described assuming an oblate nucleus. Neither the positive parity level spectrum observed nor the isomer are pre-

dicted for an oblate nucleus in this region. Although no complete parameter search was carried out for the oblate nuclear level calculations, no means were found to explain the strange "rotational" band populated in the Coulomb excitation and inelastic scattering experiments.

Further theoretical considerations on this nucleus should include speculations as to whether the adiabatic assumption inherent in the Nilsson model holds true in this case. Or it might be that the spectrum of an adiabatic asymmetric rotor would more closely describe the experimental results.

The most pressing piece of information that must be experimentally obtained is the exact spin of the level at 295 keV that was populated so strongly in the Coulomb excitation work. This may perhaps be accomplished by studying the angular distributions of the decay γ rays from this level in a Coulomb excitation experiment. Also, it would be of interest to have more information on the 3/2 and 5/2 positive parity levels in the 300-500 keV region, so that a more complete positive parity calculation could be undertaken.

$(\alpha, {}^3He)$ experiment

An interesting experimental investigation of nuclear shapes in this region of the periodic table could be made by studying the positive parity levels in these nuclei. The positive parity levels in ^{151}Sm, ^{153}Gd and ^{155}Gd have been shown to be due to the few valence neutrons which occupy the lowest-lying Nilsson orbitals stemming from the $i_{13/2}$ shell

model orbital.

In a deformed nucleus, the total strength of the spherical $i_{13/2}$ orbital is about evenly divided among the $13/2^+$ rotational levels based on the Nilsson orbitals stemming from the $i_{13/2}$ orbital. One could say that the onset of deformation lifts the degeneracy of the shell model orbital. These deformed levels are split farther apart as the deformation increases.

A measurement of the relative positions of the $13/2^+$ levels in these nuclei would then be essentially equivalent to a measure of the deformation of the nucleus.

In this study, information on these positive parity levels in ^{151}Sm was gained using the (d,t) and (^{3}He,α) reactions. Since there are only a few neutrons in the lowest $i_{13/2}$ Nilsson orbitals, only one $13/2^+$ level was positively identified. A stripping reaction, which would put neutrons into the empty $i_{13/2}$ orbitals, would populate many more of these orbitals. Since the strength of these orbitals is all concentrated in the $13/2^+$ members, it would be necessary to use a reaction which preferentially transfers high angular momentum. The reaction (α,^{3}He) would be excellent, and could be complemented by the corresponding (d,p) reactions.

The rare earths Nd, Sm and Gd all have stable, even A isotopes in the spherical region, the transition region and the strongly deformed region. The (α,^{3}He) reaction would strongly populate the $13/2^+$ levels in all these nuclei, and one could

perhaps follow the splitting of the $i_{13/2}$ orbital as it is brought about by the increasing deformation. Unfortunately, the large negative Q-value of $(\alpha, {}^{3}He)$ reactions puts them beyond the range of the McMaster accelerator.

APPENDIX

TARGET CONSTRUCTION

The separated isotopes of Sm that were used to make the targets for this experimental program were obtained in oxide form from the Oak Ridge National Laboratory. A list of the isotopic purities of these materials as supplied by ORNL is given in Table 1. Following the procedure outlined by Westgaard and Bjørnholm (1966), these oxides were reduced using La metal;

$$Sm_2O_3 + 2La \rightarrow La_2O_3 + 2\ Sm\uparrow.$$

This chemical reaction goes quickly at about 1200°C, and at this temperature the vapour pressure of the free Sm is sufficiently great that it may be collected above the crucible on the target backing, while the vapour pressure of the La is not great enough to get much La deposited on the target.

For the stable Sm isotopes used in these studies, about 15-20 mg of Sm_2O_3 was weighed out and intimately mixed with $\sim$ 20 mg of fresh La metal filings. This mixture was placed in a tantalum crucible made by drilling a 1/8" diameter hole into a 1" length of 3/16" Ta rod to a depth of 3/4". A tight fitting Ta lid with a 1/16" hole in the centre was placed on the crucible. The crucible was then put in a vacuum chamber and very carefully warmed up to about 300° or 400°C to drive off any gases trapped or adsorbed in the mixture. If this was not done, there was a tendency for the mixture to be "burped" out of the crucible.

This initial heating was carried out by wrapping tungsten strips around the crucible and passing a high current through these strips. When the "out-gassing" was completed (this could be monitored on the vacuum guage), the crucible was transferred to an electron bombardment heating apparatus and held at 1200°C for about 5 minutes. Carbon foils of thickness $\sim$ 30 $\mu g/cm^2$ which had been evaporated onto glass microscope slides were in position about 3-1/2" above the crucible lid. If the pressure in the chamber was kept below $\sim 10^{-5}$ Torr, a layer of Sm of thickness ranging from $\sim$ 20 $\mu g/cm^2$ to $\sim$ 70 $\mu g/cm^2$ was collected on the carbon foil. As the carbon foil was attached to the glass slide with a soluble "glue", sections of the carbon and Sm film could be floated off the slide by gently immersing it at an angle into a bowl of distilled water. These sections were then picked up on an aluminum frame 1" square with a 3/8" hole in the centre. This could then be mounted in the target chamber and used for the experiment.

Making targets of ^{151}Sm was considerably more difficult, as this isotope is radioactive with a 90 year half-life. One mg of this material has a β activity of $\sim$ 27 mCi, and it therefore had to be handled in a "hot lab" specifically equipped for handling radioactive substances. A small evaporator was constructed in a glove box in the hot lab. This evaporator was very cheaply constructed, mostly of old vacuum parts, as it would become completely contaminated and would have to be dis-

posed of. Instead of using electron beam bombardment heating, a very small Ta crucible was made by drilling a 1/16" diameter hole in a 1" length of 1/8" Ta rod. This crucible was heated by passing a high current through it. This heating method could be controlled accurately enough that both the outgassing of the contents and the reduction process could be done with the single heating system. A 100 $\mu g/cm^2$ C foil already floated off onto a target frame was placed about 3 cm above the mouth of the crucible. This foil was shielded from all but the crucible top by placing a tungsten plate with a 1/8" hole in it directly over the crucible.

Due to the radioactivity involved and the relatively high cost of the separated isotope, only about 1 mg of Sm_2O_3 could be used per target. Several trial runs were made using natural Sm and inexpensive separated isotopes of Sm (both natural Sm and the separated isotopes were tried in case of differences in the chemical production of the Sm oxides). During these trials, it was discovered that Carbon backings less than 50-60 $\mu g/cm^2$ were not always strong enough to stand the heat generated during the evaporation; for this reason the 100 $\mu g/cm^2$ backings were used. Heating to approximately 1100-1200°C yielded targets about 20-25 $\mu g/cm^2$ thick. These targets were then mounted in a special container (a modified Squirrel brand† peanut butter jar) which could be placed in the target chamber of the spectrograph. In anticipation of possible target breakage, the target chamber had been carefully lined with Al foil. The container top was

†Mention of a manufacturer's brand name does not necessarily imply endorsement by the author.

then removed, exposing the target, the chamber pumped down carefully, and the spectra taken.

Three targets were made; for the first, the inelastic scattering spectrum (Figure 21) revealed impurities of La and other isotopes of Sm in the target, and also peaks due to Cu and Zn. The La and isotopic impurities were expected but the Cu and Zn were a puzzle. It was later found that the accelerator beam had been improperly focussed, and part of the beam had struck a brass support post in the spectrograph target chamber, thus evaporating a thin layer of brass onto the target. Fortunately, the exposures were not ruined, as these impurities did not obscure the peaks of primary interest in the inelastic spectra. For subsequent experiments, one of the other targets was used.

References

Alder, K., Bohr, A., Huus, T., Mottelson, B. and Winther, A. Rev. Mod. Phys. 28 (1956) 432.

Andrejtscheff, W., Schilling, K.D., Stacy, F. and Dubbers, F. Nucl. Phys. A168 (1971) 513.

Bertelsen, V., Ewan, G.T. and Nielsen, H.L. Nucl. Phys. A50 (1964) 657.

Borggreen, J., Løvhøiden, G. and Waddington, J.C. Nucl. Phys. A131 (1969) 241.

Borggreen, J. and Sletten, G., Nucl. Phys. A143 No. 2 (1970) 255.

Burke, D.G., Law, M.E. and Johns, M.W. Can. J. Phys 41 (1963) 57.

Burke, D.G., Zeidman, B., Elbek, B., Herskind, B. and Olesen, M. K. Danske Vidensk. Selsk. Mat.-Fys. 35 No. 2 (1966).

Burke, D.G., Alford, W.P. and O'Neil, R.A. Nucl. Phys. A161 (1971) 129.

Burke, D.G. and Waddington, J.C. Can. J. Phys. 59 (1972) 700.

Chi, B.E. State University of New York, Department of Physics, preprint. (1967).

Christensen, P.R., Berinde, A., Neamu, I. and Scintei, N. Nucl. Phys. A129 (1969) 337.

Drost, H., Weiss, W. and Weyer, G. Nucl. Phys. A172 (1971) 348.

Elbek, B. Determination of Nuclear Transition Probabilities by Coulomb Excitation (1963) (E. Munksgaard Press, Copenhagen).

Enge, H.A. Introduction to Nuclear Physics Addision-Wesley (Canada) Ltd., Don Mills, Ontario (1966).

Ewan, G.T. and Tavendale, A.J. Can. J. Phys. 42 (1964) 2286.

Jaskola, M., Nybø, K., Tjøm, P.O. and Elbek, B. Nucl. Phys. A96 (1967) 52.

Kanestrøm, I., Tjøm, P.O. and Bang, J. Nucl. Phys. A164 (1971) 664.

Kanestrøm, I. and Tjøm, P.O. Nucl. Phys. A179 (1972) 305.

Kenefick, R.A. and Sheline, R.K. Phys. Rev. 139 (1965) B1479.

Kerman, A.K. K. Danske Vindensk. Selsk. Mat.-Fys. 30 No. 15 (1956).

Kumar, K. and Baranger, M. Nucl. Phys. A110 (1968) 490.

Lederer, C.M., Hollander, J.M. and Perlman, I. Table of Isotopes 6th ed., John Wiley and Sons, New York. (1968)

Løvhøiden, G., Hjorth, S.A., Ryde, H. and Harms-Ringdahl, L. Nucl. Phys. A181 (1972) 589.

Mariscotti, M.A.J., Scharff-Goldhaber, G. and Buck, B. Phys. Rev. 178 No. 4 (1969) 1864.

MacFarlane, M.H. and French, J.B. Rev. Mod. Phys. 32 (1960) 567.

Nathan, O. and Nilsson, S.G. Alpha-, Beta-, and Gamma-Ray Spectroscopy, edited by K. Seigbohn, Vol. 1 (1965) 603 North Holland Publishing Co., Amsterdam.

Nilsson, S.G. K. Danske Vidensk. Selsk. Mat-Fys. 29 No. 16 (1955).

Nilsson et al. (1969) Nucl. Phys. A131 (1969) 1.

Robertson, R.G.H., Choh, S.H., Summers-Gill, R.G. and Stager, C.V. Can. J. Phys. 49, (1971) 766.

Satchler, G.R. Ann. Phys. (N.Y.) 3, (1958) 275.

Satchler, G.R. Nucl. Phys. 55 (1964) 1.

Spencer, J.E. and Enge, H.E. Nucl. Inst. 49 (1967) 181.

Takemasa, T., Sakagami, M. and Sano, M. Phys. Lett. 37 No. 5 (1971) 473.

Tjøm, P.O. Thesis, University of Oslo (1968).

Veje, E., Elbek, Herskind, B. and Olesen, M. Nucl. Phys. A109 (1968) 489.

Wapstra, A.H. Nucl. Phys. 57 (1964) 48.

Westgaard, L. and Bjørnholm. S. Nucl. Inst. and Meth. 42 (1966) 77.

Zeidman, B. Elbek, B., Herskind, B. and Olesen, M.C. Nucl. Phys. A86 (1966) 471.